Development of a Biomimetic Scaffold for Ligament Tissue Engineering

by

JAMES HAYAMI

A thesis submitted to the Department of Chemical Engineering in conformity with the requirements for the degree of Master of Science (Engineering)

Queen's University

Kingston, Ontario, Canada

November 2006

Abstract

The focus of this thesis was to design a scaffold for *in vitro* culture that would mimic the structure of the native ligament in order to influence primary ligament cells towards the production of ligament-specific tissue. A major part of this project was material selection and subsequent testing to determine if the chosen materials were suitable for the scaffold design. A 20:80 (CL:DLLA) poly(ε-caprolactone-co-D,L-lactide) copolymer (PCLDLLA) was synthesized and electrospun with sub-cellular fibre diameters. The fibres were manufactured into aligned arrays to mimic the collagen fibrils of the ligament. To enhance cell and protein adhesion properties, the PCLDLLA polymer surface was modified using a base catalyzed etching technique. A photocrosslinked methacrylated glycol chitosan (M-GC) hydrogel was used to deliver encapsulated ligament cells to the biomimetic scaffold and mimic the hydrated proteoglycan matrix portion of the ligament. The scaffolds were cultured *in vitro* for a 4 week period and characterized using immunohistochemistry to identify and localize ligament specific proteins produced within the scaffolds. Cell culture results indicated that the M-GC hydrogel was an effective method of delivering viable cells evenly throughout the biomimetic scaffold. Compared to the unmodified PCLDLLA surfaces, the base-etched electrospun PCLDLLA fibre surfaces increased cell adhesion and acted as new tissue growth guides in the biomimetic scaffold. The biomimetic scaffolds produced and accumulated ligament specific proteins: collagens type I and III. The biomimetic scaffold design was determined to be a viable alternative to the current designs of ligament tissue engineering scaffolds.

Acknowledgements

I would like to thank my family and friends for their support and understanding during this epic process. I would also like to thank my supervisors Dr. Brian Amsden and Dr. Stephen Waldman as well as my co-workers for their help and patience throughout this project. Special thanks to Charlie Cooney for the SEM images, Matt Gordon and Jeff Mewburn for the confocal images, Stephen Shapka for assistance with the NMR, Verna Norkum for the cryo-sections, Dr. Herbert Shurvell for help with the ATR-FTIR processing and analysis, Andrea Liskova for the GPC work and Dr. Yat Tse for technical advice and assistance with the histology and immunohistochemistry work.

Table of Contents

List of Figures

List of Tables

List of Abbreviations

^{1}H NMR	Proton nuclear magnetic resonance
20:80 blended polymer	Final 20:80 CL:DLLA ratio after blending 70:30 mass ratio of 10:90 and 40:60 copolymers
ACL	Anterior cruciate ligament
ATR-FTIR	Attenuated total internal reflectance infrared
BMSC	Bone marrow stromal cell
DMEM	Dulbecco's modified eagle's medium
DMF	N,N-dimethylformamide
DMSO	Dimethyl sulfoxide
DSC	Differential scanning calorimetry
ECM	Extracellular matrix
EthD-1	Ethidium homodimer-1
FDA	Food and drug administration
FBS	Fetal bovine serum
FITC	Fluorescein isothiocyanate
FGF	Fibroblast growth factor
GAG	glycosaminoglycan
GC	Glycol chitosan
GPC	Gel permeation chromatography
HA	Hyaluronic acid
I2959	Irgacure 2959
IHC	Immunohistochemistry
LS	Light scattering
DCM	Dichloromethane
M-GC	Methacylated glycol chitosan
NaCL	Sodium chloride
NaOH	Sodium hydroxide
PBS	Phosphate buffered saline
PCLDLLA	Poly(ε-caprolactone-co-DL-lactide)
PCL	Poly(ε-caprolactone)
PDLLA	Poly(DL-lactide)
PEO	Poly(ethylene oxide)
PEG	Poly(ethylene glycol)
PG	Proteoglycan
PLA	Poly(lactide)
RI	Refractive index
SEM	Scanning electron microscope
TCP	Tissue culture polystyrene
TFA	Trifluoroacetic acid
TGF	Transforming growth factor
Wt%	Weight percentage
X:Y copolymer	X:Y CL:DLLA synthesised copolymer

Chapter 1. Introduction

1.1 Ligament Structure and Function

Ligaments play a crucial role in the biomechanics and stability of joints. The ligament has a proposed hierarchal structure (Figure 1), with a fibrous collagen molecule being the main structural unit. On a dry mass basis, 80±10% of the extra-cellular matrix (ECM) of the ligament is made up of collagen, the majority being collagen type I (88±2%) and the remainder composed of collagen type III (12±2%)[1]. The remainder of the ligament ECM consists of proteoglycan (PG) and glycosaminoglycan (GAG) molecules.

The collagen molecule is the largest molecule in the body with a rod like appearance and is approximately 300 nm in length and 1.5 nm in diameter[1]. The collagen molecule is made from the tight winding of three collagen α-chains into a triple helix. Assembly of collagen into a three dimensional array in the ECM is influenced by environmental stresses and additional biological factors. The sum of these factors affects the orientation and size of the fibrils that are assembled from the collagen molecules[2,3].

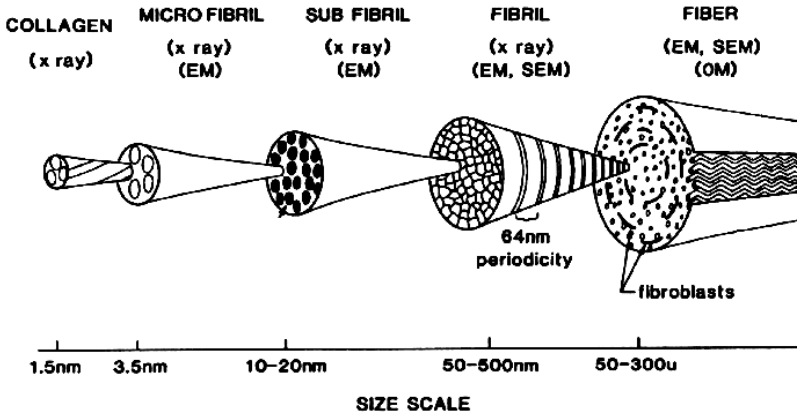

Figure 1: Hierarchical structure of the ligament
Image modified from Kastelic *et al.*[4]

Assembly is typically patterned in a quarter stagger, which is seen as the characteristic 64 nm sub-bonding on transmission electron micrographs (Figure 2). Covalent intra- and inter-collagen molecular crosslinks, mainly from peptide bound lysine and hydroxylysine groups, give the fibrils additional stability. The crosslinks form between lysyl oxidase generated aldehyde groups (aldol condensation) or the enzyme derived aldehyde group and the unmodified amino group (Schiff-base reaction)[1].

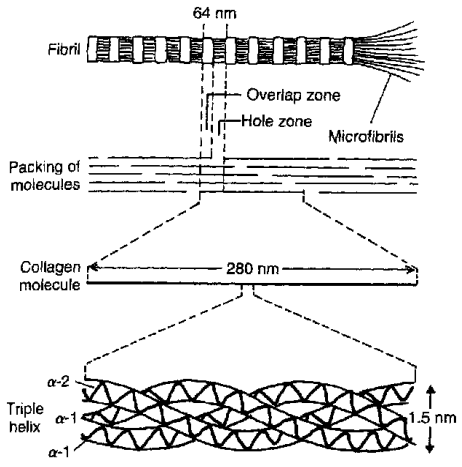

Figure 2: Organization and structure of collagen molecule
Image taken from Sellaro[5]

The collagen fibrils impart a structural characteristic in the ligament known as crimp. The crimp pattern is a regular sinusoidal pattern parallel with the long axis of the ligament, which can be seen in Figure 3. The periodicity and amplitude of the crimp appears to be a structure specific feature for different ligaments and tendons. Ligaments generally range from 45-60 μm for the crimp wavelength and 5-10 μm for the crimp amplitude[1]. This crimp gives the ligament a nonlinear stress strain relationship that allows longitudinal elongation of the ligament without damage to the collagen fibrils.

The crimp feature also acts as a mechanism for the control of tension and acts as a shock absorber along the length of the tissue. The typical stress-strain curve for the ligament shows a toe region where individual crimped fibrils start to straighten. Once the majority of fibrils have uncrimped, a linear region is observed until the failure region (Figure 4).

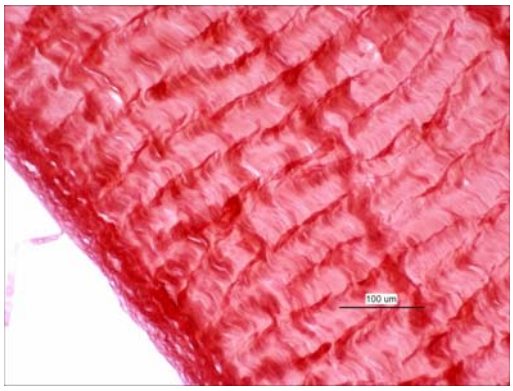

Figure 3: Ligament crimp pattern
Intra-synovial ligament stained with Picrosirius Red to show characteristic crimp pattern of the ligament

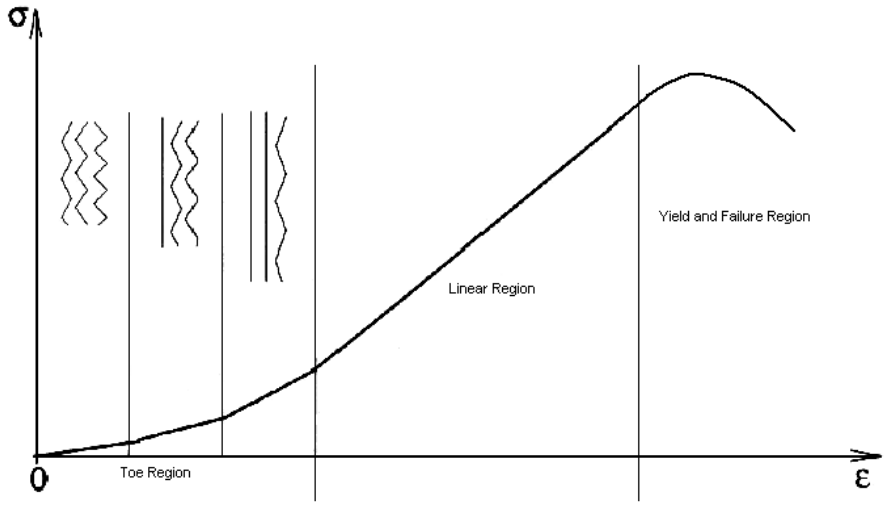

Figure 4: Theoretical stress strain curve of the ligament
Chart showing the characteristic toe region (fibrils starting to uncrimp) and linear region (all fibrils uncrimped) of the ligament. Modified diagram from Hirokawa[6]

The main PG present in the other matrix molecules of the ligament is decorin (80%) with chondroitin, keratan and dermatan sulfate GAG chains[7]. Decorin has been shown to play a role in the structural organization of the ligament during development and tissue maintenance[3,8]. The other 20% of the PGs are composed of a large chondroitin sulphate PG that may be a versican-like PG[9]. Aside from the main ligament components some other minor components that are characteristic to the ligament ECM are; tenacin-C, biglycan, versican and aggrecan[10]. Water, which makes up 60-80 % of total wet weight of the ligament, is entrapped within the ligament between these large highly charged PG molecules[1]. The water and PGs provide the lubrication and spacing that is crucial to the gliding function at the fibril interception points in the ligament tissue matrices. The other matrix molecules also confer some viscoelastic properties to the ligament[11,12].

Located within the ligament are fibroblast cells which are responsible for the maintenance of the ligament ECM[13]. They are round to ovoid in shape, 5-8 μm in diameter and 12-15 μm in length and are arranged longitudinally in a column between layers of compact parallel bundles of collagen fibrils (~20 μm)[1]. Fibroblasts have abundant cellular organelles, indicating a high cellular activity. The cells have multiple small cellular processes, or microvilli, which project into the surrounding areas of the amorphous PG-water portion of the ligament ECM.

1.2 Ligament Injuries

It is estimated that in North America, approximately 100,000-200,000 patients require total reconstructive ligament surgery per year[14,15]. The ligament that is usually injured

and after which most of the current repair methods are modeled, is the anterior cruciate ligament (ACL) of the knee joint. Figure 5 shows the main ligaments present in the knee.

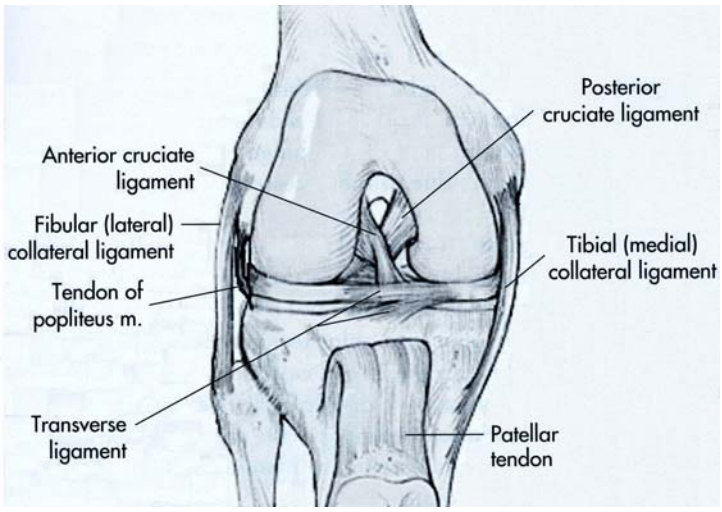

Figure 5: The main ligaments of the knee
Image modified from Fritz *et al*. [16]

Partial tears or complete rupture of the ACL occurs mainly from hyperextension and/or excessive rotational forces on the knee joint[17]. The main cause of ligament injury is a result of competitive athletes pushing their body to the limit or novices attempting a new sport/activity and putting their body in unfamiliar situations. Guidoin *et al*.[18] investigated causes of ACL injury and found that the majority of ligament failures occurred in individuals aged between 20-25 from activities such as soccer (34.7) and alpine skiing (27.8%). In another study conducted by Johnson *et al*.[19] the main activity to cause ligament injury was alpine skiing, resulting in 20,000 ACL surgeries per year.

It has been demonstrated that current surgical techniques for the repair of ACL ruptures have a more positive outcome than non-operative treatments in terms of relative speed of recovery and strength of the ligament and joint[17,20]. Non-operative treatments can cause the injured joint to become unstable, which can lead to cartilage degeneration, meniscus lesions and/or osteoarthritis[21,22,23]. Therefore, sports medicine for ligament repair/reconstruction is an essential field of study since active people require an efficient method of repair to allow them to return to their activities as soon as possible.

1.3 Ligament Reconstruction

When considering the repair of an injured ligament, the ligament environment is an important factor for the method of repair. The two main environments of the ligament are the intra-synovial (anterior and posterior cruciate ligaments) and extra-synovial (medial and lateral collateral ligaments)[24]. Extra-synovial ligaments derive their nutrients and blood supply from arteries and osseous attachments[1]. They are also known to exhibit a wound healing response, which usually results in the majority of their initial strength being restored[26]. However, the severity of the ligament injury dictates the length of the remodelling phase. Major complete-gap injuries usually require a 1-2 year remodelling phase in order to regain the majority of initial strength[25] whereas minor non-gap injuries have been shown to heal rapidly and return to normal within 6 weeks[26]. On the other hand, intra-synovial ligaments typically have a limited healing capacity and require a total replacement when completely torn. Studies have shown that intact intra-synovial ligaments are capable of deriving nutrition from the diffusion of nutrients in the synovial fluid[27]. However, in injured intra-synovial ligaments it has been shown that the synovial

fluid is detrimental to exposed fibroblasts and causes resorption of damaged ligament tissue within 1-2 months[28]. Also, increases in active collagenase levels in the ligament have been detected in studies with the injured ACL compared to the latent collagenase levels in the intact ACL[28]. These findings could potentially explain the rapid resorption and poor healing observed in intra-synovial ligaments. For these reasons, injured intra-synovial ligaments typically require total reconstruction for repair. Therefore, much of the ligament repair research has focused on these ligaments.

Currently the gold standard for ACL reconstruction involves the use of tendon autografts[29,30]. The major disadvantages of this approach include donor site morbidity and long periods of time for the graft to change into ligament tissue with respect to crosslink density and architecture (ligamentization[31])[32,33,34]. Long ligamentization periods result in poor mechanical properties of the graft and inefficient stability of the joint due to a mismatch in the tendon tissue properties[35,36,37,38]. One possible alternative is to use allografts, which eliminates donor site morbidity. However, with these grafts there are additional concerns, such as: alteration to structural and mechanical properties due to processing and sterilizing techniques, slower and incomplete ligamentization periods, an immune response, and/or disease transmission[39,40,41,42]. Another problem for both auto- and allografts is the poor integration of the graft into the bone attachment sites (tunnels that are drilled to incorporate the graft into the joint)[43]. This problem also leads to joint instability due to laxity of the graft. In the early 1970s, attempts to overcome problems with auto- and allografts involved permanent ligament prosthetics made from synthetic materials. Examples of the materials used in these fibrous devices were

polyester, polypropylene, ultra-high molecular weight polyethylene, polyarylamide and polytetrafluoroethylene. However, high occurrences of material fatigue and creep with eventual graft failure lead to poor acceptability of these grafts as permanent ligament replacements[18].

1.4 Ligament Tissue Engineering

In general, tissue engineering, or the fabrication of living tissue substitutes, has provided an alternative approach to current tissue repair methods by allowing tissue to be produced *in vitro* or *in vivo*. Tissue engineering has also allowed for a more complete understanding of cell behaviour in regard to the physical and chemical environment. Tissue engineering consists of three main components: scaffold material and design, cell type and cell signals. These three components make up what is known as the "tissue engineering triad[44]". There are many questions that have to be considered before initiating the design of a tissue engineering scaffold based on the triad. These considerations include: cellular or acellular scaffolds, rate of scaffold degradation and tissue ingrowth rates, culturing the construct *in vitro* or *in vivo*, when to implant the device, and whether to design the scaffold to maximize tissue ingrowth or mechanical strength. However, tissue engineering of the simpler tissues (e.g. connective tissues) to minimize the number of these considerations will be the ground-breaking work in this field of research.

Ligament tissue engineering aims to produce ligament tissue to replace damaged ligaments in place of the current surgical procedures involving the use of auto- or allografts. Moreover, a better understanding of cell behaviour for tissue production *in vitro* is required to produce more functional tissues. Current ligament tissue engineering attempts have so far been unsuccessful in producing functional tissue replacements and these failures will be further elaborated in the following chapter. It was proposed that a scaffold constructed to mimic the structure of the ligament would be required to accomplish the goals of ligament tissue engineering.

Chapter 2. Literature Review

Currently there is fairly limited research being conducted on ligament tissue engineering. It is possible that because ligament injury is rarely life-threatening and is more related to sports medicine, it is not receiving as much attention as other tissues. However, ligament tissue engineering is still an important field of study since a better understanding of cell behaviour in these simpler connective tissues can be applied to more complex tissue engineering structures. This chapter is an overview of the current literature based on ligament tissue engineering. From this review, shortcomings of ligament tissue engineering will be highlighted. Methods to overcome these problems will be provided in the later sections.

2.1 Fibrous Scaffolds

Early reports on ligament tissue engineering were very similar in design to the prosthetics used in the 1970s. However, bioabsorbable scaffold materials were used in place of the non-degradable synthetic materials previously used. The primary goal of these scaffolds was to provide initial mechanical support to the joint by having similar mechanical properties of the native ligament[48,51,52,56]. The fibrous scaffold design was used to mimic the behaviour of the native ligament when in use. In some of these scaffolds, knitting or braiding of the fibres was used to match the mechanical properties of ligament tissue. The secondary role of these scaffolds was to promote tissue ingrowth to eventually take over function of the native tissue. In order to tailor the cellular response, degradation rates and mechanical properties of the scaffold, different materials have been used to produce the scaffolds. Both natural (hyaluronan[45], chitin[46], silk[47] and collagen[48,49,50]) and

biodegradable synthetic (poly(desamino tyrosyl-tyrosine ethyl ester carbonate))[51], (poly(ε-caprolactone) (PCL) and poly(lactic acid) (PLA))[46], poly(L-lactic acid) (PLLA)[52,53], poly(lactide-co-glycolide) (PLGA)[54,55,56,57], poly(glycolic acid) (PGA)[58],) polymers have been used to produce fibrous ligament scaffolds. However, the polymer fibres used in these scaffolds had diameters ranging from 10s to 100s of μm, which were well above the diameters of the ligament fibroblasts (~10 μm). The use of fibre diameters of this scale resulted in the cells interacting with a planar surface as opposed to a three dimensional matrix. In addition, the large fibre diameters and the braided design used in these scaffolds limited cell seeding to the outside of the scaffolds and poor tissue integration into the scaffolds[46,45,47,53,55,64].

Modification to these fibre material surfaces were used to improve their cell adhesion and tissue integration properties. Ide *et al*.[59] studied PLLA fibres coated with type I collagen and demonstrated that cellular adhesion and proliferation was much greater on the collagen-modified scaffold than the unmodified PLLA scaffolds both *in vitro* as well as *in vivo*. Fibronectin, a protein up-regulated during ligament wound healing, was shown to increase cellular attachment and matrix production on PGA, PLLA and PLGA fibre scaffolds by Lu *et al*.[60]. Funakoshi *et al*.[61] coated chitosan fibres with hyaluronan (HA) and found that HA increased fibroblast adhesion, proliferation and extracellular matrix (ECM) production. A similar report by Majima *et al*.[62] used chitosan, a cationic polysaccharide similar to GAGs found in the body, to coat alginate fibres and found that the hybrid scaffold had improved the cellular response as well as the mechanical properties of the fibres. Other groups have used an arginine-glycine-aspartic acid (RGD)

peptide sequence known to promote cell binding on silk matrices to improve bone marrow stromal cell (BMSC) attachment and differentiation into fibroblast cells[63,64]. Surface modification of these fibrous scaffolds showed improvements in cellular adhesion, proliferation and ECM production over the unmodified scaffolds. However, the surface modified scaffolds were still plagued with many of the same problems as the unmodified fibre scaffolds (poor cell seeding and tissue integration) since similar fibre diameters and fibre braiding techniques were used to manufacture them.

2.2 Hydrogel Scaffold

There are a limited number of ligament constructs based on hydrogel systems due to their limited mechanical properties for immediate implantation; a design criteria on which most of the current research has focused. Altman *et al*.[65] used a collagen type I hydrogel to differentiate BMSCs into fibroblast-like cells and to act as a structural template for tissue development. The cells and scaffolds were cultured in a bioreactor under static and dynamic conditions which allowed the cells to differentiate into fibroblast-like cells. However, the tissue that was produced was not comparable to native ligament tissue in terms of histology and mechanical properties. A similar study was conducted by Noh *et al*.[66] that examined a collagen type I hydrogel with mesenchymal stem cells for ligament tissue engineering. The constructs were also cultured in a bioreactor under static and dynamic conditions. Fibroblast-like cells along with ligament-like ECM were produced in the dynamically loaded constructs but, the constructs were again too weak for animal or clinical applications. Therefore, hydrogels are capable of supporting and maintaining ligament cells and producing ligament-like

ECM during culture. However, these hydrogel scaffolds by themselves were too weak to be used as a scaffold for ligament tissue engineering.

2.3 Composite Scaffolds

Other attempts to fabricate bioresorbable ligament scaffolds have used a matrix to encapsulate fibres and make a composite. The main purpose of this design was to mimic the structure and mechanical property of the native ligament. Dunn *et al*.[67] used extruded collagen fibres (dry diameter 50-70μm) in a poly(lactic acid) solvent extracted matrix for rabbit ACL reconstruction. Neo-tissue was observed after 4 weeks in 88% of the implanted scaffolds. Davis *et al*.[68] constructed an artificial tendon using a poly(2-hydroxyethyl methacrylate)/poly(ε-carprolactone) hydrogel to encapsulate a commercially available poly(lactic acid) fibre (Davis and Geck 5-0 Dexon Plus fibre) for Achilles tendon reconstruction in rabbits. Fibre/matrix degradation and tissue ingrowth was noticed after 45 days. Also, Gentleman *et al*.[69] developed a collagen fibre scaffold embedded in a cell seeded collagen hydrogel to create a scaffold to mimic the mechanical and viscoelastic properties of the ACL. Common to all these scaffolds was that large fibre diameters were used to meet the design criteria of ligament-like mechanical properties. Therefore, these scaffolds failed to provide adequate space for *de novo* tissue integration. Therefore, the tissue produced in these scaffolds was not comparable to native ligament tissue in terms of structure or function.

2.4 Cell Types

An important component of ligament tissue engineering is the cell type used to produce tissue within the scaffolds. Eijk *et al*.[55] conducted a study using goat BMSCs, primary ACL cells, and primary skin fibroblast cells. These cells were grown on a resorbable poly(L-lactide-co-glycolide) suture material and it was determined that the BSMCs and primary skin fibroblasts cells showed the most promise for ligament tissue engineering based on cell proliferation, collagen content and specific ECM results. Another study conducted by Cooper *et al*.[53] examined primary ACL, MCL, Achilles tendon and patellar tendon rabbit cells as possible sources for ligament tissue engineering. Based on cell morphology as well as the type and amount of ECM production, it was found that the primary ACL fibroblasts were better suited for ligament tissue engineering compared to the other cell types investigated.

When conducting ligament tissue engineering research with primary cells, the main concern is that the cells do not change (de-differentiate) into other cell lineages. Cell differentiation can be monitored by analyzing for specific cell or protein markers during or after the culturing period. Culturing BMSC cells, on the other hand, is a much more complicated process since the cells must first be differentiated towards the desired lineage and then maintained throughout the rest of the culture period. The results reported above indicated similar findings for both BMSCs and primary cells. Therefore, it appears that for preliminary studies the cell choice depends mainly on the expertise and resources available to the researcher.

2.5 Cell Signals

2.5.1 Mechanical Signals

Residential ligamentum fibroblasts are subject to many different forces during normal daily activities. The effects of mechanical stimulation on planar *in vitro* culture systems have been studied by many groups to better understand and improve on results seen in non-stimulated cultures (Table 1).

Table 1: Effects of mechanical strain on cell behavior in 2-D culture

Type of Mechanical Load	Cell Type	Culture System	Effect of Mechanical Stimulation	Reference
Cyclic tensile load	Rabbit ACL	Monolayer on FLEX-I culture plates	Cells aligned perpendicular to direction of load with an increase in collagen type I synthesis	Takashi *et al.*[70]
Cyclic tensile load	Human ligament	Monolayer cultures on random and aligned polyurethane films	Increase in matrix production with no effect on tissue histology	Lee *et al.*[71]
Uniaxial cyclic tensile load	Human ACL	Monolayer culture on silicon membrane	Increase in mRNA expression of collagen type I and III and TGF-β1.	Kim *et al.*[72]
Cyclic tensile load	Bovine periodontal ligament	Monolayer on flexible culture plates	Increase of collagen type I and decorin mRNA expression and decrease in ALP activity	Ozaki *et al.*[73]
Cyclic tensile load	Human ACL	Monolayer on flexible culture plates	Increase of collagen type I and decrease in decorin expression through ERK pathway	Miyaki *et al.*[74]
Constant tensile load	Rat tendon	Monolayer on laminin coated silicon membrane (rolled) anchored at both ends	Self assembled aligned collagen fibrils, which increased in diameter from 20-80 to 200-300 nm after 16 weeks in culture	Calve *et al.*[75]

Table 1 indicates that mechanical stimulation for ligament cells grown on a planar surface was beneficial for the production of ligament-like ECM *in vitro*. These findings have also been applied to three dimensional hydrogel ligament scaffolds. Altman *et al.*[65] and Noth *et al.*[66] in separate studies used BMSC and type I collagen gels anchored at both ends with a cyclic translational and rotational strain. The results showed that there was

an up-regulation of collagen type I and III, tenascin-C, fibronectin and elastin compared to unloaded gels. The cells appeared to align in the direction of load, however, the tissue produced within the collagen matrix was poorly organized and far from the histology or mechanical properties of the native ligament. The end results were well below the criteria for an implantable ligament augmentation device. Therefore, more work is required to determine the effectiveness of mechanical stimulation for ligament tissue engineering

2.5.2 Chemical Signals

Many studies have been performed to determine the effects of growth factors specific to ligament tissue engineering. A table constructed by Goh *et al.*[76] is reproduced here to summarize some of the findings in the literature (Table 2). Another study by Murray *et al.*[77] looked at the effects of transforming growth factor (TGF) on a cell outgrowth study and found that it had an inhibitory affect on cell outgrowth from a ruptured ligament *in vitro*. Hankemeier *et al.*[78] also examined the effects of fibroblast growth factor (FGF) on the differentiation and proliferation of human bone marrow stromal cells into fibroblast-like cells and found that a low dose (3ng/mL) of FGF was the most effective.

Table 2: Ligament/tendon growth factors
The table was taken and modified from Goh *et al.*[76]

Growth factor	*Model*	*Animal*	*Subject*	*Effect*
Transforming growth factor (TGF)	*In vivo*	Rabbit	ACL	TGF-β induced cell proliferation response
	Ex vivo		MCL fibroblasts	Increased collagen and total protein synthesis
			MCL scar explants	Collagen synthesis increased, especially type I collagen
		Canine	ACL and MCL cells	Increased collagen and noncollagen protein synthesis
			ACL fibroblasts	Increased collagen and proteoglycan synthesis
Platelet-derived growth factor (PDGF)	*In vivo*	Rabbit	MCL	Increased structural properties
			Patellar tendon	Induced cell proliferation response
			Ligaments	Increased stiffness of ligaments
		Rat	MCL	Increased structural properties
	Ex vivo	Rabbit	ACL and MCL fibroblasts	Increased cell proliferation (age and cell origin affect response)
		Canine	ACL fibroblasts	Increased cell proliferation
		Avian	Tendon fibroblasts	Stimulated mitogenic response in dose-dependent manner
		Rabbit	Flexor tendon fibroblasts	Increased cell proliferation and matrix synthesis in dose-dependent manner
				Response different in various types and regions of tendons
Epidermal growth factor (EGF)	*Ex vivo*	Rabbit	ACL and MCL fibroblasts	Increased cell proliferation
			Flexor tendon cells	Increased matrix synthesis and cell proliferation at 100 ng/mL
		Canine	ACL and MCL cells	No effect
			ACL cells	Increased cell proliferation and proteoglycan synthesis
Fibroblast growth factor (FGF)	*In vivo*	Canine	ACL	Enhanced neovascularization and formation of granulation tissue
		Rabbit	Ligaments	Increased stiffness of ligament
		Rat	Patellar tendon	Increased cell proliferation and type III collagen synthesis
	Ex vivo	Rabbit	ACL and MCL cells	Increased cell proliferation
Insulin-like growth factor (IGF)	*In vivo*	Rat	Achilles tendon	Accelerated functional recovery of tendon
	Ex vivo	Rabbit	Tendon segments	Increased matrix synthesis
		Canine	Flexor tendon cells	Increased cell proliferation and matrix synthesis
		Avian	MCL scar explants	Increased collagen type I and III synthesis
			ACL cells	Increased collagen synthesis

Delivery of growth factors to an *in vitro* culture system is simplified because the cells and tissues have been singled out and delivery can be modified by adjusting its concentration in the culture media. *In vivo* studies are more difficult with respect to growth factor delivery to the injured ligament. The method of delivery, how often and where to introduce the growth factors must all be considered. This is especially important in hostile environments such as the intra-synovial ligaments, where the presence of synovial fluid may interfere with delivery. However, conflicting results from the literature indicate that the conditions under which the growth factors are examined could alter their effect on the cells. Therefore, the use of growth factors must be individually tailored to each specific culture system to obtain the desired effects.

2.6 Gene Therapy

One possible method to help with the *in vivo* delivery of growth factors for ligament tissue engineering is gene therapy. Gene therapy is the introduction of specific sequences of nucleic acid that carry the desired gene, usually in the form of viral vectors (retro- or adeno- virus), into cells to express (or over-express) the gene of interest[25]. Hildebrand and Woo reported the expression of a marker gene, LacZ, in the MCL and ACL of rabbits using an adenovirus vector[79]. The results indicated that this technique could possibly be used for many known therapeutic growth factors. Pascher *et al*.[80] found that a collagen hydrogel seeded with an adenovirus transfected with the TGF-β1 gene promoted the migration of cells into the gel *in vitro*. Results indicated that this could assist in the healing process of augmented ligaments.

Antisense gene therapy is another method that utilizes oligonucleotides to bind to the target genes and inhibit their expression. Woo *et al*.[25] demonstrated that antisense gene therapy could down-regulate collagen type III and V production, which has been shown to be overproduced compared to collagen type I during the ligament healing process. Nakamura *et al*.[81] also demonstrated that antisense gene therapy could be used to down-regulate the production of decorin in healing rabbit ligaments, resulting in the increased diameter and strength of the collagen fibrils.

Current gene therapy techniques have shown that there is a decrease in the expression of the delivered gene within several weeks[82,83]. These limited gene expression periods have been utilized for ligament tissue engineering since growth factors are mainly required to accelerate the initial healing response[84]. However, the use of gene-based therapeutics raises a major concern, especially for ligament tissue engineering where the injury is non-life threatening. There are also some safety concerns with the use of gene therapy, including: possible immune response, toxicity effects of the gene product and gene delivery system, and non-specific insertion of the gene vectors[85]. Therefore, more research into this area is required before it is considered an option for ligament tissue engineering applications.

2.7 Summary

For a successful tissue engineered ligament the scaffold must allow for adequate cell and tissue integration evenly throughout the scaffold during the culture period. There must be adequate spacing between the fibres to allow for sufficient tissue to be produced between

the fibres. The fibers should have dimensions that allow the cells to interact with the fibres as a three dimensional matrix. The alignment of the fibres is also important to guide *de novo* tissue growth into more functional ligament-like tissue during the culture period. Disregarding biocompatibility issues, these design criteria are important for producing a final tissue in an engineered environment that mimics the native ligament tissue.

From the literature it was obvious that the previous research in ligament tissue engineering has concentrated on the mechanical properties necessary for immediate implantation of the scaffolds. This major design criterion resulted in the use of fibre diameters that were larger then the dimensions of the seeded cells and acted as a planar culture surface. The design of these scaffolds along with conventional cell seeding techniques (adding cells to scaffold in culture media) did not allow for adequate distribution of the cells throughout the scaffold. During the culture period these same design flaws did not allow for sufficient tissue integration into the center of the scaffolds. Therefore, the final tissues that would likely be produced in these scaffolds would not have the functional properties necessary to act as tissue graft replacements once the scaffold degraded

To improve on previous ligament tissue engineering attempts a biomimetic scaffold approach was suggested for this thesis. The biomimetic scaffold could also be used as a tool to gain insight into the cell behaviour for the purposes of improving the tissues produced within the scaffold.

Chapter 3. Scope of Project

3.1 Proposed Scaffold Design

To improve upon previous ligament tissue engineering attempts it was determined that a biomimetic scaffold design was required. Biomimetics is the field of study which takes concepts from biology and implements them in another field, such as biomaterials or tissue engineering[86]. Therefore, it was proposed that a fibrous design was required to mimic the collagen fibrils of the native ligament as well as to act as a *de novo* tissue guide in the scaffolds. The ability to produce fibre diameters at the sub-cellular level (<10 μm) is very important in making a biomimetic scaffold for ligament tissue engineering[87]. Electrospinning is a technique that allows for the production of aligned fibres within the required diameter range (see Table 3). Since the design criteria for the scaffold was to mimic the parallel collagen fibrils in the ligament the scaffold could be designed without reinforcing braids. This design would allow for sufficient space in the scaffold for cell seeding and tissue integration during *in vitro* culture.

It was also proposed that a hydrogel was required to mimic the hydrated portion of the ligament ECM to entrap water and provide lubrication between collagen fibrils as well as to deliver and distribute cells evenly throughout the scaffold. The hydrogel would also act as a support to maintain the shape of the very thin electrospun fibres. A schematic diagram of the proposed biomimetic scaffold is shown in Figure 6.

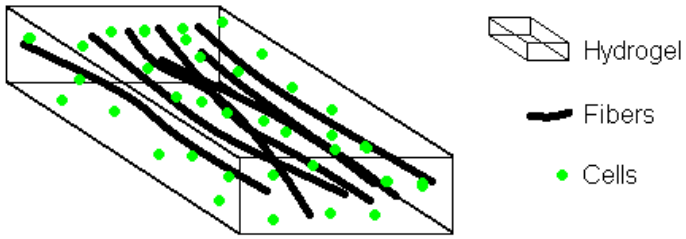

Figure 6: Diagram of proposed scaffold design

3.2 Fibres

3.2.1 Electrospinning

Electrospinning is the material processing technique[88] that has recently been used as a means of producing fibres in the micron to sub-micron range for tissue engineering applications. The process of electrospinning requires the use of a high voltage generator to produce an electrical field (Figure 7) between a charged needle and a grounded collecting mat.

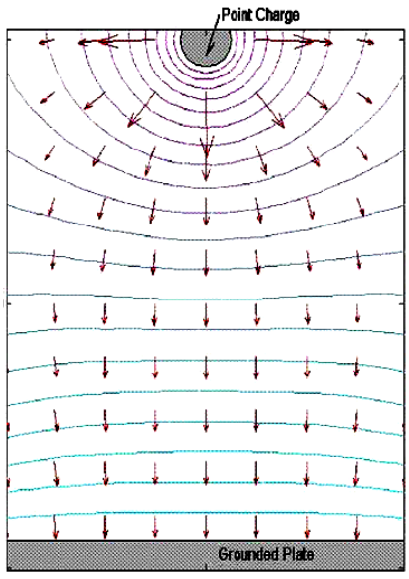

Figure 7: Equipotential lines created during electrospinning
Image taken and modified from Theron *et al.* [89]

The electrospinning process works as follows. A working solution is pumped through the needle until a droplet is formed at the tip. When the electrical field is generated it causes the droplet to be pulled toward the collecting mat creating what is known as a Taylor cone[90]. As the electrical field is increased, the pull of the field eventually breaks the surface tension of the droplet (Taylor cone) and a continuous fibre is formed in the air gap (the space between the needle and collection mat), which is attracted to the grounded collecting mat. Depending on the solvent properties of the solution, the length of the air gap will allow most of the solvent to evaporate from the fibre. This creates a dry, randomly orientated fibrous mat on the grounded collecting mat. These fibres can also be aligned if a rotating drum or mandrel is used to collect the fibres.

3.2.1.1 Parameters Affecting Electrospinning

Many studies have been conducted to understand the process of electrospinning. A report by Baumgarten[91] found that a minimum weight percent of material was required for electrospinning poly(acrylonitrile) in dimethylformamide (DMF). Below this limit, a droplet spray resulted whereas above this limit, fibre diameters were found to increase. This increase in fibre diameter continued until an upper weight percent limit was reached, which was identified by a discontinuous flow from the Taylor cone. The solution flow rate was found to be important for producing a continuous fibre with consistent diameters. Discontinuous fibre production was observed when the solution flow rate was faster than the electrospinning system could produce the fibres. It was also noted that the optimal solution flow rate increased proportionately with the electric field strength. Ambient spinning conditions were also investigated and were found to have an effect on

the evaporation rate of the solvent. In dry air (<5% relative humidity) the evaporation rate of DMF was found to be too high. The high evaporation rate caused the Taylor cone to dry out and block the flow of the spinning solution, which disrupted the production of continuous fibres.

Another study conducted by Son *et al.*[98] found that the minimum spinning concentration of poly(ethylene oxide) was dependent on the solvent used (chloroform, ethanol, DMF and water) and the dielectric constant of the solutions. Higher dielectric constants or higher polarity of the solvents were found to decrease the diameter of the fibres produced. The higher dielectric constants of the solutions resulted in a higher charge density and greater elongation force on the fibres that improved the solution's spinability. The addition of polyelectrolytes (poly(allylamine hydrochloride) and poly(acrylic acid sodium salt)) to the spinning solution resulted in further reduction in fibre diameters and a lower minimum weight percent required for electrospinning. The size of the salt ion (NaCl, NaH_2PO_4 and KH_2PO_4) on the electrospinning process with poly(lactic acid) was also investigated by Zong *et al.*[99]. It was determined that ions with smaller atomic radius have a higher charge density and therefore are more mobile under an electric field. Greater elongation forces of the polymer molecules were observed when ions with smaller atomic radius were used in the spinning solutions, which allowed for the production of smaller diameter fibres. McKee *et al.*[92] studied the addition of different amounts of NaCl to a cationic polyelectrolyte, poly(2-(dimethylamino)ethyl methacrylate) solution. The results indicated that the minimum electrospinning weight percent decreased as the salt concentration increased.

A study conducted by Um *et al.*[93] showed that when conventional electrospinning methods were unable to spin fibres of hyaluronic acid (HA) in an aqueous HCl solution, the use of a heated co-axial air stream could be used to produce fibres. The heated co-axial air stream helped to produce HA nanofibres by decreasing the viscosity and increasing the evaporation rate of the aqueous-based spinning solution.

Similar findings to those mentioned above have also been reported. Minimum and upper limit weight percentage has been reported with a variety of other electrospinning systems[94,95,96,97,98,99]. Fibre defects (bead on fibres) have been observed by other groups to be related to an increase in voltage[96,100], lower weight percent polymer solutions[97,98,99] and molecular weight[101] for a variety of polymers. Reductions in bead on fibre defects have been made using (co-solvents[102],[103] and surfactants)[104].

3.2.1.2 Cellular Response to Electrospun Fibres

Table 3 summarizes the results of previous studies on how cells have responded to different polymers electrospun into either random or aligned fibres. From Table 3 it appeared that when the electrospun fibres were aligned, cells orientated themselves in the same direction as the fibres. Therefore, the influence of the fibres on the cells could also be beneficial to affect the orientation of the *de novo* tissue produced in a scaffold. The cells were also observed to grow with multipoint attachments into the fibre mats. The overall results indicate that electrospinning was an acceptable method for producing fibres of sub-cellular diameters.

Table 3: Cellular response to random and aligned electrospun fibre mats

Material	Fibre Orientation	Fibre Diameter (nm)	Cell Type	Effect on Cells	Reference
Poly(DLLA-co-GA)	Random	500-800	Mouse BALB/c C7 fibroblasts	-Normal cell phenotype -Attachment and proliferation on and into fibres	Li *et al.* [105]
Poly(p-dioxanone-co-L-lactide)-block-PEG	Random	380 (avg.)	NIH 3T3 fibroblasts	-Normal cell phenotype -Attachment and proliferation on and into fibres	Bhattarai *et al.* [103]
Gelatin and elastin	Random	200-500 (gelatin), 0.6-7 μm (elastin)	Human mesenchymal cells	-Attachment and proliferation until confluent	Li *et al.*[94]
PCL	Random	700 (avg.)	Fetal bovine chondrocytes	-Attachment and proliferation into fibres -Cell morphology: flattened; on planar surface and rounded; in fibres	Li *et al.*[106]
PLA	Random	140-2000	MC3T3-E1 osteo-progenitor cells	-Larger cells with higher aspect ratios on larger diameter fibres (similar to planar culture surfaces) -Proliferation into fibres	Badami *et al.*[107]
Poly(LLA-co-CL)	Aligned	~500	Human artery smooth muscle cells	-Attachment and alignment of cytoskeletal proteins along fibres -Higher proliferation rate on fibres than on thin films	Xu *et al.*[108]
Chitosan-PEG blend	Random	~40	MG-63 osteoblasts and HTB-94 chondrocytes	-Normal cell phenotype -Attachment with filopodia and multiple long micovilli within fibres	Bhattarai *et al.*[104]
Polyurethane	Aligned	~700	Human ACL fibroblast	-Cell attachment and proliferation with tissue orientation along fibres -More collagen production on aligned than random fibres	Lee *et al.*[71]

3.2.2 Fibre Material Selection Criteria

When choosing the material to use for the fibres certain criteria had to be met. First, the material had to have acceptable cell biocompatibility since the cells where required to adhere and produce ECM on this fibre material. Secondly, the material had to be biodegradable. Biodegradation was one of the important aspects considered for the fibre material. For tissue engineering applications it is required that the *de novo* tissue

produced within the scaffold will take the place of the biodegradable scaffold once degraded. The material and its degradation products, therefore, must not be cytotoxic or elicit a foreign body response. Finally, it was important that the material could be easily manufactured into sub-cellular diameter fibres by conventional electrospinning techniques.

3.2.3 Fibre Material Selection

A wide variety of natural and synthetic materials along with their blends can be electrospun and cellular responses to the fibres have been determined (Table 3). However, one material that stood out from the rest was chitosan. Chitosan is a cationic random polysaccharide of (1-4)-linked 2-amino-2-deoxy-β-D-glucopyranose and (1-4)-linked 2-acetamido-2-deoxy-β-D-glucopyranose and is soluble in dilute aqueous acidic solutions. Chitosan is produced from chitin (Figure 8); which is derived mainly from crab shells, certain fungi, and squid pens. Therefore, it is plentiful and economical to obtain. Although chitosan is similar to chitin, it is generally accepted that chitosan has a degree of *N*-de-acetylation greater than 50% (Figure 9).

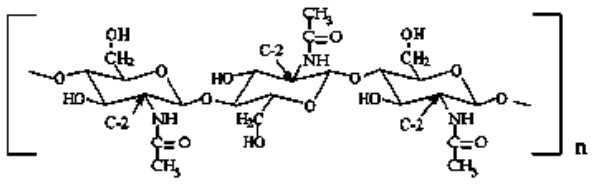

Figure 8: Chitin

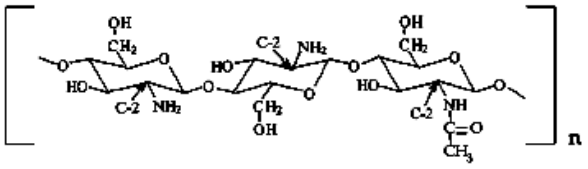

Figure 9: Chitosan
Images from Knaul *et al*.[109]

Chitosan has functional characteristics that are very close to that of glycosaminoglycans (GAGs) found in the body[110]. It is believed that GAGs may be involved in cell-cell and cell-matrix interactions in the body, which influence cellular proliferation and tissue organization. Chitosan has also been shown to similarly affect these same cellular processes *in vitro* and *in vivo* and could possibly be involved as a biological catalyst for these behaviours[110,111]. Chitosan has positive effects on fibroblast attachment and proliferation when the cells are grown on chitosan thin films[112] or on tissue culture polystyrene (TCP) surfaces with chitosan supplemented media[113]. Since chitosan is similar to GAGs found in the ligament ECM, its degradation products should not elicit a major foreign body response. It is believed that the main mechanism of chitosan degradation in the body is via lysozyme[114,115,116].

Although chitosan was the initial choice for the scaffold fibres, the low volatility of the dilute aqueous acid solutions used to dissolve chitosan could hamper the electrospinning process making it difficult to produce continuous sub-cellular sized fibres. Therefore, there was some uncertainty associated with producing the scaffold fibres with chitosan. Alternatively, a poly(ε-caprolactone-co-D,L-lactide) (PCLDLLA) polymer system was investigated. Biomaterials constructed from poly(ε-caprolactone) (PCL) and

poly(lactide) (PLA), separately or as copolymers, have been previously used with widespread acceptability and FDA approval history[117,118]. PCL is a semi-crystalline polymer with a glass transition temperature (T_g) of -60°C and an *in vivo* degradation rate of approximately 2 years[119]. Poly(D,L-lactide) (PDLLA) on the other hand is an amorphous polymer that has a T_g between 50-60°C and an *in vivo* degradation rate of less than a year[119]. These materials are also well established for producing fibres using electrospinning[99,103,105,106,107,108,120]. Even though the polymers are not chemically similar to the constituents of the native ligament, both polymers can be broken down by hydrolysis of the ester bonds into relatively harmless by-products[121] (shorter polymer segments with carboxylic acid and alcohol terminal groups).

The problem with PCL and PDLLA is that they have been shown to elicit lower cellular adherence and proliferation rates when compared to other polymers such as poly(lactide-co-glycolide) (PLGA)[122]. However, certain physico-chemical surface modifications have been used to improve their surface chemistry for better cellular recognition. These techniques include: etching, coating, blending, ion implantation and graft polymerization[123] all of which are attractive as they do not change the bulk properties of the material. One of the most convenient methods for physicochemical surface modification is base-catalysed hydrolysis. This method improves the hydrophilicity of aliphatic polyester materials by producing carboxyl and hydroxyl groups on the surface. Base-etched polymer surfaces have been shown to improve protein adsorption, cellular adhesion and cellular proliferation[124,125,126,127]. The treatment is conducted in an aqueous

solution and only requires a simple washing step with water to stop the reaction and remove the excess reagents thereby making it ideal for tissue culture work.

3.3 Hydrogels

3.3.1 Hydrogel Material Selection Criteria

Hydrogels used for cell encapsulation act as an artificial three dimensional environment that can mimic most native extracellular matrices. Some of the most important considerations in choosing a hydrogel system for encapsulating cells for tissue engineering are that the pre-gel solution, crosslinking method and final hydrogel are cytocompatible. The hydrogel must provide an environment conducive for the cells to grow in and re-organize as new tissue is produced as well as not impede the diffusion of nutrients or metabolic waste products[128]. Sufficient mechanical properties of the gel were also required to allow for handling and manipulation during culture.

3.3.2 Hydrogel Material Selection

Many synthetic and natural materials have been used to construct hydrogels. A material that is commonly used for cell encapsulation is poly(ethylene glycol) (PEG)[129,130,131,132,133]. PEG has been shown to be fairly inert in terms of cell adhesion and protein adsorption[134]. However, PEG has poor biodegradation properties as it is not very susceptible to hydrolysis or enzymatic degradation[135]. Another problem is that low molecular weight components of PEG diacrylates have been shown to be cytotoxic at low concentration[136]. Alginate is another material that is commonly used to construct hydrogels. However, alginate cannot be efficiently broken down by enzymes present *in*

vivo, which could result in unpredictably long degradation times[137]. Alginate has also been shown to have poor cell adhesion properties[138]. Alternatively, chitosan and hyaluronic acid (HA) are attractive as they are both structurally similar to the GAGs found in the native ligament. Compared to HA, chitosan is more economical to obtain in large quantities and has a readily modifiable amine group. In addition, cationic polymer hydrogels have been shown to promote fibroblast migration, proliferation and ECM production[139]. Therefore, the positive charge of chitosan, compared to the negative charge of HA[140], could be beneficial for the encapsulated fibroblasts. For these reasons, chitosan was chosen as the hydrogel material. Specifically, a water soluble glycol chitosan was selected so that pre- and post-gelation work could be conducted at physiological conditions.

3.3.3 Crosslinking System

A table of previously used cell encapsulating chitosan hydrogels is shown in Table 4.

Table 4: Cell encapsulation in chitosan hydrogels

Hydrogel Materials	Crosslinking Method	Cell Type and Density	Results	Reference
Chitosan, Glycero-phosphate and hydroxyethyl cellulose	Heat induced ionic crosslinking	-Bovine chondrocytes -10000 cells/μL	-Cartilage and proteoglycan accumulation after 20 day *in vitro* and *in vivo*	Chenite *et al.*[141]
Protasan (chitosan chloride and glutamate salts)	Genipin crosslinking at 37°C for 2hrs	-Bovine interverebral disk cells -2440 cells/μL	-Cell viability decreased with higher protasan concentrations - chitosan as glutamate salts had better viability then as chloride salts	Mwale *et al.*[142] and Roughley *et al.*[143]
High molecular weight Chitosan	NaCl ionic crosslinking and precipitation	-R208F & R208N.8 fibroblasts and PC12 cells -8000 cells/μL	-Cells were viable up to 4 weeks in precipitated chitosan -Poor viability in tripolyphosphate crosslinked chitosan controls at 1-2 weeks	Zielinski *et al.*[144]

The various crosslinking methods used in the literature that involved a reversible ionic crosslinking or precipitation approach for cell encapsulation did not seem suitable for this project. Variations in pH during cell culture could affect the physical properties of these reversible hydrogels[145]. Therefore, a permanent crosslinking method would be more suitable for this application. A variety of covalent crosslinking systems were examined due to the uncertainty in physical gel properties as well as cellular compatibility with the gelation system using the different crosslinking agents.

For all crosslinking systems investigated, the water soluble glycol chitosan (GC) was used either in an unmodified form or in a modified methacrylated form (M-GC) for photocrosslinking. The structures of both are shown below in Figure 10.

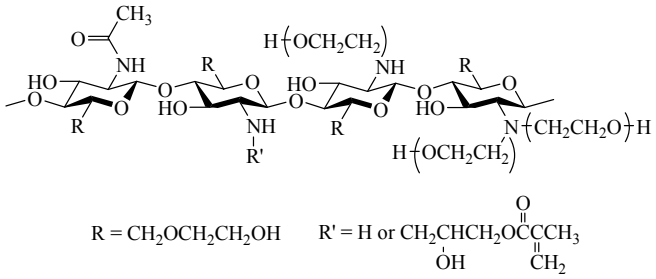

Figure 10: Structure of glycol chitosan and methacrylated chitosan prepared at pH 9.

Genipin was first investigated as it has been shown to be cytocompatible[146] with little or no effect on cell viability (90% after 20 days)[142,143]. Mi *et al.*[147] stated that the genipin crosslinking reaction has two possible mechanisms depending on the pH of the system (Figure 11).

Acidic and Neutral Conditions

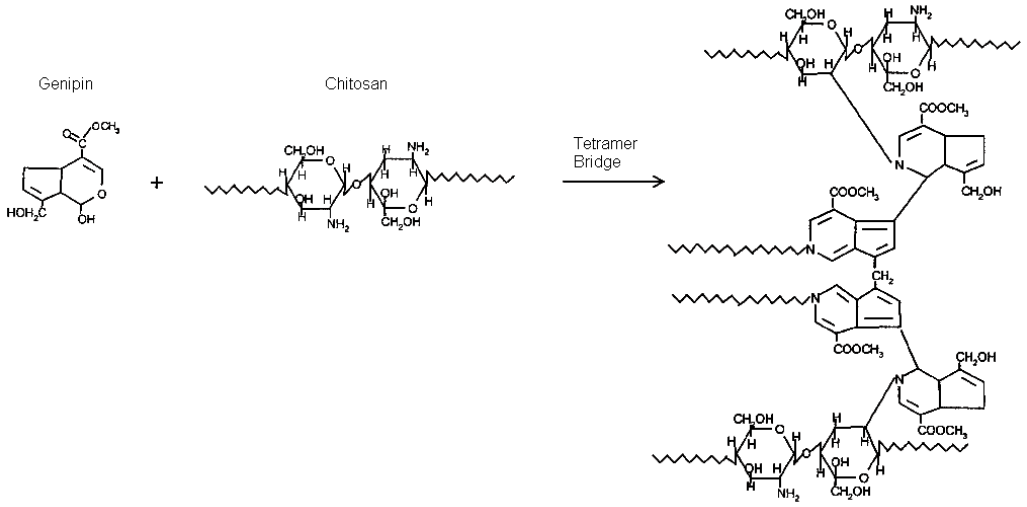

Basic Conditions

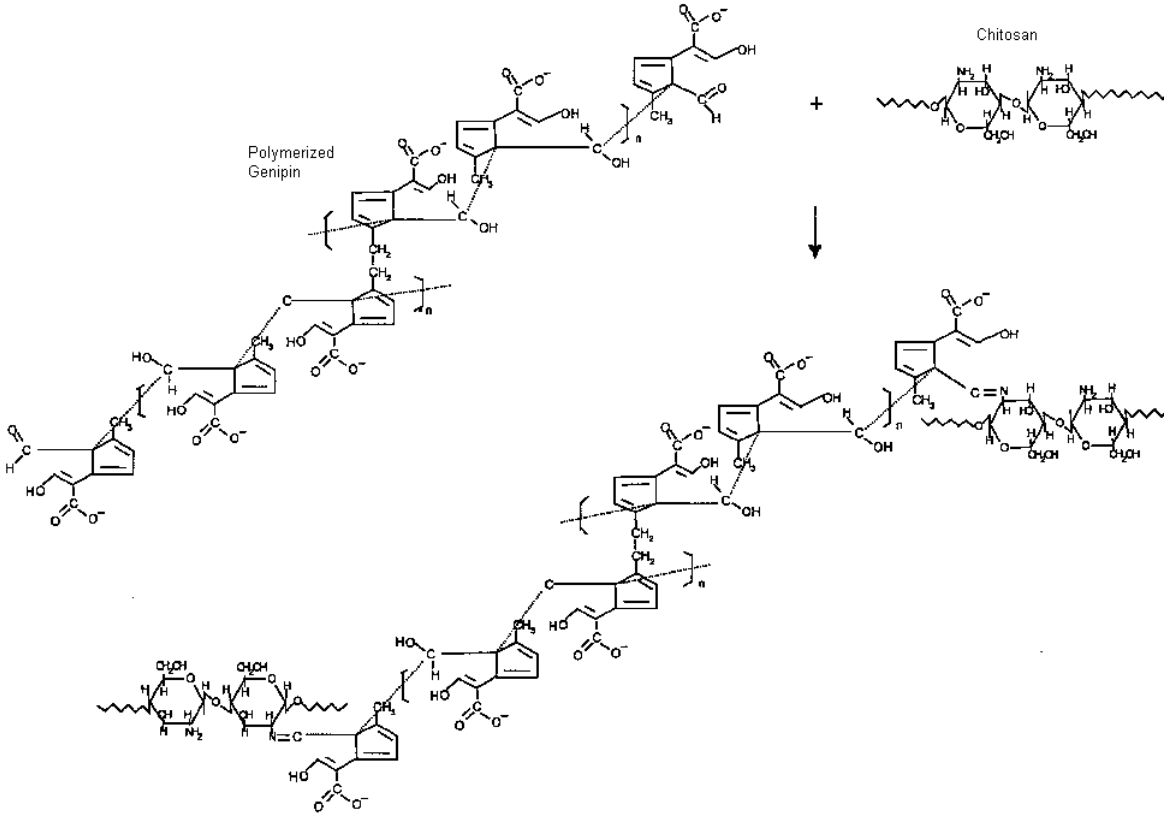

Figure 11: Reaction mechanisms of genipin with chitosan at different pH conditions Images taken and modified from Mi *et al.*[147]

At neutral and acidic conditions, the crosslinking reaction occurs by nucleophilic attack of the amino groups on the chitosan backbone to open the dihydropyran ring of genipin to form a heterocyclic amine. These heterocyclic amines can then form either dimer, trimer or tetramer bridges with chitosan to create a tightly crosslinked network. Alternatively at strongly basic conditions, nucleophilic attack on the hydroxyl group of the genipin molecule by OH^- ions in the solution results in a ring-opening reaction to form an aldehyde group. The aldehyde groups on the ring-opened genipin molecules undergo an aldol condensation polymerization reaction. The terminal aldehyde groups on the polymerized genipin react with the amino groups on the chitosan backbone via a Schiff-base reaction to form a loosely crosslinked network.

A PEGD crosslinker system was also examined since it has been used as a hydrogel material itself or as a crosslinker for a variety of cell encapsulation methods with acceptable results[129,135,148]. PEGD reacts with GC through a 1-4 Michael-type reaction (Figure 12). The 1-4 Michael-type reaction occurs between the free amine group on the chitosan backbone which acts as a nucleophile and attacks the carbon-carbon double bond on the acrylate groups present on the PEGD crosslinker molecule to form the covalent bond.

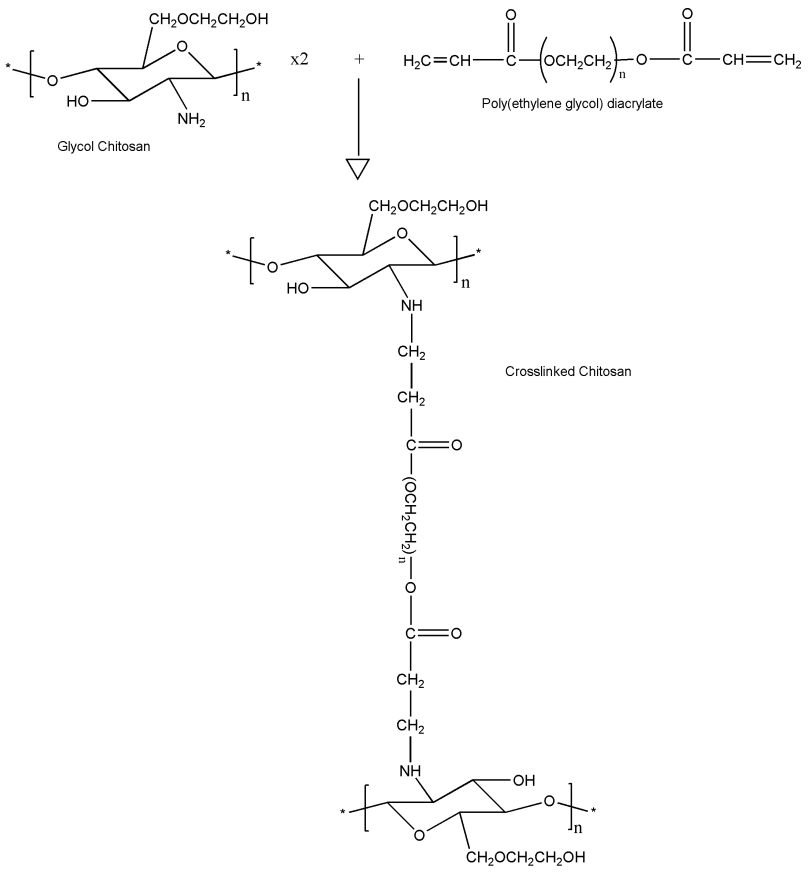

Figure 12: 1-4 Michael-type addition reactions between GC and PEGD700
Reaction occurs between free amine group on chitosan and reacts the C=C bond on PEGD700

Finally, M-GC was examined as a photocrosslinkable hydrogel. Photocrosslinking is a rapid gelation system commonly used to encapsulate cells with acceptable cytocompatibility levels, which has been demonstrated with a variety of different cell types[129,130,131,148,149,150,151]. The photoinitiator I2959 has been commonly used for cell encapsulation work with acceptable cytotoxicity levels[149,152] and so was chosen to initiate gelation of the M-GC. A possible reaction mechanism for this system is shown below (Figure 13).

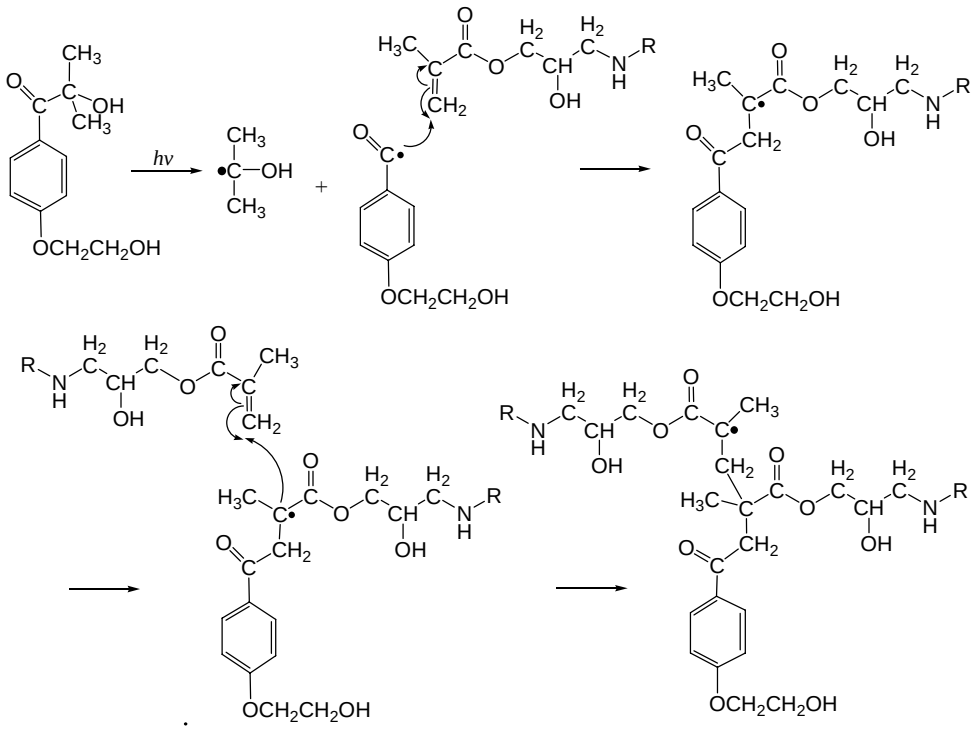

Figure 13: Photocrosslinking reaction with M-GC and I2959
R = glycol chitosan backbone, image taken and modified from Knight *et al.*[153]

3.4 Cell Selection

For ligament tissue engineering purposes the main choice of cells was either mesenchymal stem cells (MSC) or primary ligamentum fibroblasts. One of the main disadvantages of using MSCs is that they have to be influenced to differentiate into the desired cell type. This requires an in-depth knowledge of stem cell biology and differentiation pathways[154]. Primary cells, on the other hand, are present in the tissue and are actively producing and maintaining the ligament ECM. Another consideration for cell choice was the use of passaged cells. However, Zimmermann *et al.*[155] has shown that cultured passaged fibroblasts quickly lose their phenotype and cell markers even by the fourth passage. Cell lines are also very similar to passaged cells since they are

established only to proliferate. Thus, it was proposed that primary ligamentum fibroblasts would be an ideal and economical choice for this study.

3.5 Objective

The primary objective of this thesis was to engineer ligament tissue by designing an artificial biomimetic environment to encourage cultured cells to function and produce tissue as if present in a native ligament. More specifically, the objectives were to investigate a variety of materials to produce fibres of sub-cellular diameters and a variety of chitosan crosslinking methods to produce a cytocompatible hydrogel. The final objective was to characterize the tissue produced within the scaffold to confirm that the cells were behaving as expected, by producing ligament-like tissue.

Chapter 4. Materials and Methods

4.1 Fibres

4.1.1 Reagents

Trifluoroacetic acid (TFA), chitosan (high M_r ~ 2000 kDa, medium M_v ~ 200 kDa and low M_v ~ 50 kDa), stannous octoate, 99+% anhydrous 1-octanol, 99.8% anhydrous N, N-dimethylformamide (DMF), poly(ethylene glycol) (Mv~900kDa) and ≥99.9% dimethyl sulfoxide (DMSO) were purchased from Sigma-Aldrich (Canada). Dichloromethane (DCM), methanol and glacial acetic acid (all reagent grade) were purchased from Fisher Scientific (Canada). Triton X-100 was purchased from VWR (Canada). Anhydrous ethanol was obtained from Commercial Alcohols Inc (Canada). Purasorb D,L-lactide (DLLA) was obtained from Purac (Holland) and was used as received. 99% ε-caprolactone (CL) was purchased from Lancaster (Canada) and was dried over calcium hydride and distilled under reduced pressure before use. Dimethyl sulfoxide D-6 (99.9%) for ^{1}H NMR was obtained from Cambridge Isotope Labs (USA).

4.1.2 Material Preparation

4.1.2.1 Chitosan

All chitosan for electrospinning was purified before use by first dissolving in 1% v/v aqueous acetic acid and then filtering with Fisher Brand coarse/fast filter paper. The filtered chitosan was then precipitated using 1 M NaOH to bring the pH up past the pK_a of chitosan (6.5)[156]. The precipitated chitosan was filtered, collected and air dried under vacuum at room temperature. Chitosan was also freeze dried by re-dissolving the

precipitated chitosan, freezing the solution overnight at -20°C and then placing on the lyophilizer for 2-3 days or until completely dry.

4.1.2.2 PCLDLLA

To synthesize the linear PCLDLLA copolymer, a ring opening polymerization reaction of ε-caprolactone and D,L-lactide was performed (Figure 14). The monomers were added to a flame dried ampoule along with the required amount of initiator (1-octanol). It was then purged with nitrogen gas, covered and placed in a 140°C oven. Once the monomers were completely melted and a homogeneous liquid, a single drop of the catalyst (stannous octoate) was added. The ampoule was purged with nitrogen gas and placed on a vacuum line and vortexed. After being flame-sealed, the ampoule was placed back into the 140°C oven and allowed to polymerize for 48hrs.

After polymerization, a methanol purification process was used to remove any impurities or unreacted monomers from the polymers. The ampoule containing the polymer was crushed and the polymer dissolved in DCM. Once the polymer was dissolved the solution was filtered to remove any glass debris. The excess solvent was evaporated off by forcing air over the top of the beaker (adiabatic cooling). This was done until approximately half of the DCM was evaporated. Methanol was then added in excess and the solution was placed in a -20°C freezer and left overnight. After removing the mixture from the freezer, the top solution was discarded and the remaining polymer slurry was placed on a Teflon™ sheet (to facilitate removal of the polymer once dry) which was then placed in a 70-80°C heated vacuum oven with a vent and H_2O trap for 24 hours.

PCLDLLA copolymer blends were produced using either a solvent or high temperature blending technique. For the solvent blending method, DCM was added to the desired copolymer ratio and vortexed until completely dissolved (~1 hr). After mixing the DCM was evaporated off and DSC analysis was performed to obtain the blended polymers T_g. For high temperature blending, the desired copolymer ratio was added to a glass vial and heated at 140-150°C for 4-5 hrs. DSC analysis was performed once the PCLDLLA blend had cooled down to room temperature.

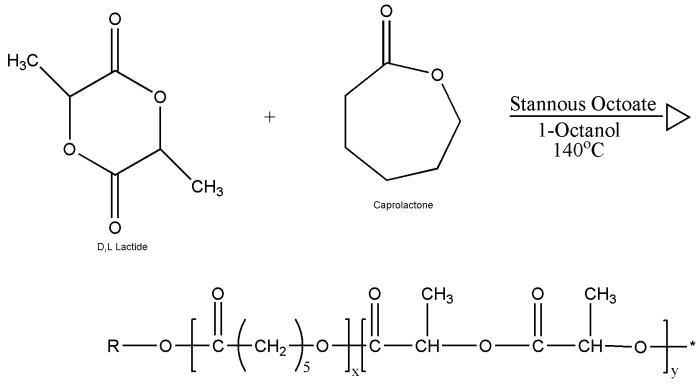

Figure 14: Ring Opening Polymerization of CL and DLLA

The Flory-Fox equation (Equation 1) was used to determine the copolymer CL:DLLA mass ratios, where (m_i) and (T_{gi}) represents the mass fraction and glass transition temperature for the two monomers, respectively. T_g represents the glass transition temperature of the copolymer.

$$\frac{1}{T_g} = \frac{m_1}{T_{g1}} + \frac{m_2}{T_{g2}} \qquad \textbf{Equation 1}$$

A pre-determined final mass of the copolymer along with the calculated CL:DLLA mass ratio was used to determine the actual amount of each monomer required for the

polymerization reaction. To calculate the amount of initiator required it was assumed that one mol of initiator was required for every mol of polymer (1 mol initiator = 1 mol copolymer). Therefore, to determine the amount of initiator required, the total starting mass of both monomers used was divided by the desired molecular weight of PCLDLLA to be synthesized. This resulted in the mol of polymer that would be produced from the given reactants which in turn equaled the mol of initiator required.

4.1.3 Electrospinning

4.1.3.1 Chitosan

The chitosan electrospinning apparatus consisted of a syringe pump, high voltage generator, heated co-axial air flow and a grounded copper collecting mat (Figure 15). A conventional electrospinning setup was also used when a heated co-axial air flow was not required. The heated co-axial air flow apparatus was constructed from a "T" type air process heater (model AHP-3741) and a 1/32 DIN autotune temperature process controller (model CN 8590) with a T-type thermocouple (model TMQSS) (Omega). Swagelok™ fittings were used to construct an apparatus to flow the heated air around a 1/16" O.D. stainless steel spinning solution feed tube. To control the co-axial air flow a Matheson flow meter (model 7630T with a #605 tube) was used to limit the air flow rate between 0.8-3 SLPM with an air temperature from 60-80°C. A glass insulator tube was used to isolate the other electrical equipment from the high voltage power supply (Bertan Associates Inc. Series 230-30R). A syringe pump (Sage Instruments Model 220) was used to control the feed rate of solution at the needle tip with either a 5 mL disposable syringe for the aqueous based solutions or a 5 mL glass and Teflon™ syringe (SGE) for

the corrosive solutions. To connect the syringe to the charged syringe needle (18 ga.), 1/16" I.D. PharMed™ tubing was used with the appropriate Tefzel™ luer lock fittings (Cole-Parmer). For all trials, a solution flow rate of less then 1 mL/min was used. The air gap ranged from 5-15 cm with the electrical field between 15-30 kV.

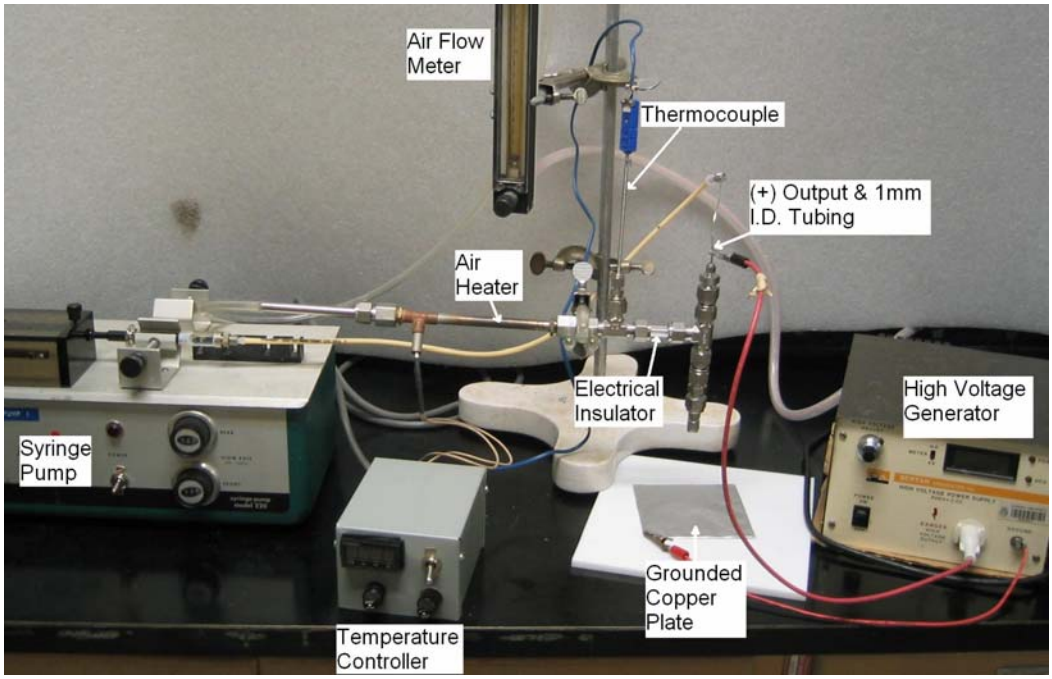

Figure 15: Electrospinning apparatus for chitosan solutions with heated co-axial air flow.

Chitosan fibres were either electrospun with or without the aid of a 1M NaOH precipitation bath that was contained in a 10 cm Petri dish. The fibres electrospun with the precipitation bath were chemically dried using a graded series of methanol solutions to approximately 100% methanol. After chemically drying, the fibres were removed from solution and air dried overnight at room temperature in a fume hood. Fibres that did not require the aid of a 1 M NaOH precipitation bath were removed from the collecting

mat and soaked in a 1 M NaOH for 30 min with agitation (600 rpm) at room temperature. After the 1 M NaOH treatment, the samples were rinsed three times in 70% ethanol for 10 min (600 rpm) each. The fibres were then dried overnight in a room temperature vacuum with a vent and H_2O trap.

4.1.3.2 PCLDLLA

The PCLDLLA electrospinning apparatus utilized the same syringe pump and high voltage generator from the conventional chitosan electrospinning apparatus (Figure 16). Alternatively, a 3 mL disposable syringe with a 21 ga. blunt tip needle was used. In addition, a wire mandrel was constructed from aluminium wire by using two end pieces (~5 cm in diameter) and four 10 cm parallel rods connecting everything together (Figure 17). The wire mandrel was then attached to a horizontally mounted in-line mixer (Barnant, series 20). A contact tachometer (Extech) was used to measure the rotational speed of the mandrel.

A set flow rate of 0.03 mL/min, 13.5 cm air gap, positive 2 kV/cm electric field and a mandrel rotation speed of 1000 rpm were used to electrospin the PCLDLLA copolymer. The fibres, while still on the mandrel, were removed from the in-line mixer and stored in a fume hood for 0.5 – 1 hr to dry. Further drying of the fibres was completed in a room temperature vacuum desiccator with a vent and water trap for 1-2 days. For long-term storage, the fibres were kept on the mandrels in a vacuum desiccator at room temperature.

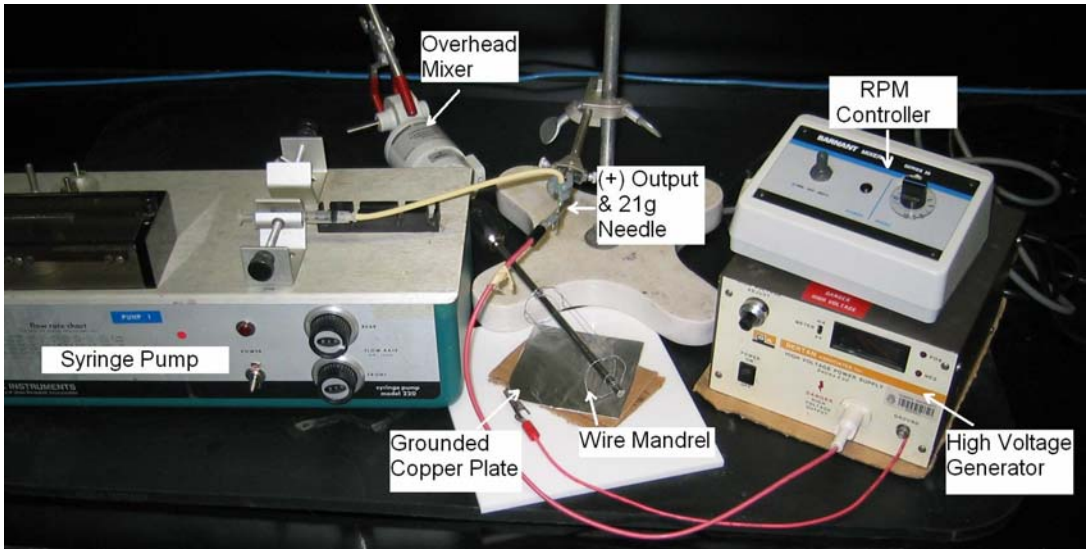

Figure 16: Electrospinning apparatus for PCLDLLA fibres with rotating wire mandrel

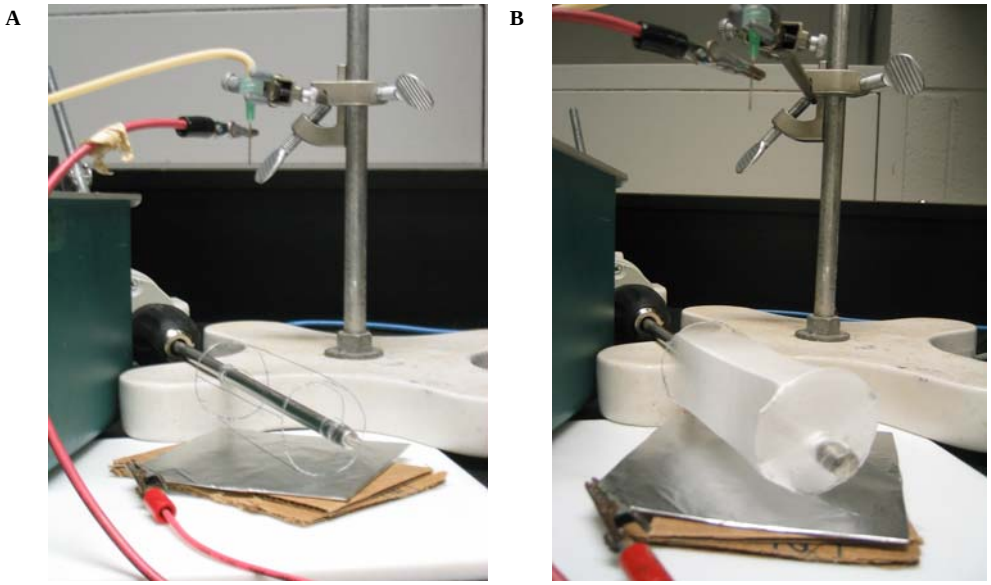

Figure 17: Wire mandrel used to collect electrospun PCLDLLA fibres
Wire mandrel mounted on modified overhead mixer, A – before spinning and B – after spinning with collected fibres

Base-etching of the PCLDLLA copolymer was used to enhance the surface properties for culture work. To facilitate certain surface analysis techniques on the copolymer after the base-etching procedure, thin films of the same composition were prepared by solvent evaporation on a Teflon™ surface. It was assumed that there would be no difference in surface chemistry between the base-etched thin films and fibres. However, shorter etching times were used on the fibres due to their finer dimensions. To construct the PCLDLLA thin films, a 75 μL droplet of 5 wt% polymer solution in DCM was placed on a Teflon™ mold and allowed to evaporate overnight in the fume hood. This method produced a thin film of ~1 cm in diameter similar to the 24-well plates used for the cell culture experiments. Afterwards, the thin films were transferred to a vacuum desiccator for further drying for 1-2 days.

Base etching of all samples was performed in 1.5 mL poly(propylene) micro-centrifuge tubes with 1 mL of 0.5-1.0 M NaOH per sample for the required time (5 min – 3 hr) at room temperature with constant agitation (600 rpm on an Eppendorf Thermomixer*R). The samples were then rinsed at least 3 times (600 rpm) or until the solution tested neutral (using pH sensitive paper strips) with 1 mL ddH_2O for 10 min each. The base-etched copolymers were then air-dried at room temperature in a vacuum desiccator with a vent and H_20 trap overnight. After drying, the collapsed fibres were spread out to their original shape to ensure the majority of the base-etched fibres were aligned before incorporation into the scaffold. No further work was required for the dried PCLDLLA thin films.

4.1.4 Analysis

Glass transition temperatures (T_g) of the PCLDLLA copolymer for various CL:DLLA compositions were measured with a Seiko Instruments DSC 220U. Samples of ~10 mg in crimped aluminium sample pans were used, and the data were taken from the second heating cycle to ensure a common thermal history. The cycles used were as follows: (1^{st}) room temperature to 100°C, (2^{nd}) 100°C to -100°C and (3^{rd}) -100°C to 100°C (data taken). A 15°C/min heating rate with a 10min hold time at each set point was utilized.

Proton nuclear magnetic resonance (^{1}H NMR) was used to confirm the molar ratios of CL:DLLA in the synthesized PCLDLLA polymers. ^{1}H NMR was also used to detect changes in surface chemistry on 5 min – 3 hr, 0.5 M NaOH, base-etched PCLDLLA electrospun fibres. PCLDLLA samples of 10 mg/mL were dissolved in dimethyl sulfoxide-D6. ^{1}H NMR was performed on a Bruker Avance-600 MHz and an Avance-400MHz with automatic sampler. Samples were analysed at room temperature. An external reference was not used for any of the spectra.

Attenuated total reflectance Fourier transform infra-red spectroscopy (ATR-FTIR) was performed to determine surface carboxyl groups after 0.5-1.5 hr and 0.5-1.0 M NaOH hydrolysis of the PCLDLLA thin films. ATR-FTIR was performed on an Avatar 320 Fourier Transform Infrared Spectrometer using a single pass diamond with a 45° incident angle. Spectra were collected at atmospheric conditions using 32 scans with a resolution of 4cm^{-1}. Grams/32 AI software (Galactic Industries Corporation) was used to analyse the spectra.

Static water contact angle measurements (n=3) were conducted on the PCLDLLA thin films to determine the effect of alkaline hydrolysis on surface chemistry. Water contact angles of original and 1.5 hr, 0.5 M NaOH, base-etched PCLDLLA thin films were measured with an AST Products Inc. VCA Optima goniometer along with VCA Optima XE v1.90.0.2 software. A 1 μL droplet of distilled water was used and pictures were taken immediately after contact.

To determine the molecular weight of the PCLDLLA polymers, gel permeation chromatography (GPC) was performed. Samples were analyzed on a Waters 2960 separation module with a Waters 410 refractive index (RI) detector and a Wyatt Technology light scattering (LS) system (690 nm and angles 62-110° with a 2^{nd} order molar mass vs. volume polynomial fit), which was equipped with 5 Waters Styragel columns in series (High Resolution, 5E, 4, 3, 1 and 0.5 at a size of 300x5 mm and an effective molecular weight range of 0-4000 kDa). Samples were made up at 5 mg/mL in THF distilled over calcium hydride under a nitrogen atmosphere and 0.45 μm filtered. A 100 μL injection volume was used with a flow rate of 1 mL/min at 40°C. Results were analyzed and fitted in Astra v4.90.07 (Wyatt Technology) using either a polystyrene/THF universal calibration curve with for RI values or a PCLDLLA/THF dn/dc value[157] of 0.067 for LS values.

A molecular weight degradation study, based on viscosity, was conducted with a purified and lyophilized 6 wt% chitosan solution in 70:30 TFA:DCM. A #400 capillary viscometer (Fisher Scientific) was used to measure the viscosity. The time required for

the solution to move the through the viscometer, which was proportional to the molecular weight of the solution, was recorded until the readings were constant.

PCLDLLA fibres were mechanically tested at 37°C using a Mach-1™ micromechanical tester (Bio Syntech, Canada) (n=4 for stress strain measurements, n=1 for residual stress tests). Sections of fibres, while still on the collecting mandrel, were mounted within a cardboard window using double sided adhesive tape at both ends. The cardboard windows were approximately 2.5 cm by 2.5 cm with an average gauge length of 1.4±0.1 cm. The average mass of the fibre mats alone was 5.3±0.5 g. The cardboard windows were then mounted in the tensile tester grips with the gauge length of fibers exposed. The sides of the window were cut and the residual forces in the fibres were measured. The fibres were then stretched until failure at a rate of 1 %/s. Respective density values of 1.094 and 1.248 g/mL for amorphous poly(ε-caprolactone)[158] and poly(D,L-lactide)[159] were used for an approximate PCLDLLA density based on the mass ratio of CL:DLLA. For the true stress-strain measurements, the cross-sectional area of the fibre mats was determined from the calculated density and the gauge length. The calculated cross-sectional area along with the fibre diameter distribution was used to determine the number of individual fibres per mat and thereby the individual fibre mechanical properties.

$$\varepsilon_T = \ln\left(\frac{l_f}{l_o}\right) \qquad \textbf{Equation 2}$$

$$\sigma_T = \sigma(1+\varepsilon) \qquad \textbf{Equation 3}$$

Equation 2 was used to calculate the true strain for the fibre mats and the individual fibres, where l_f and l_o are the final and intial lengths, respectively. In addition, Equation 3 was used to calculate the true stress, where σ and ε are the engineering stress and engineering strain values, respectively.

Brightfield images of the electrospun chitosan (aqueous acetic acid solvent) fibres were taken while the fibres were still in solution (~100% methanol). All other brightfield images were taken on glass slides. A Leica camera (model DFC320) mounted on a Hund Wetzlar inverted microscope (model Wilovert S) was used to take the pictures. Images were captured using Leica IM50 software.

SEM images for the electrospun fibres were taken on a JSM-840 Scanning Microscope with a 10 kV electric field and a tungsten filament. Specimens were removed from the collecting mat or mandrel and mounted on an aluminium stub using a double sided adhesive tape. The samples were then gold coated prior to SEM imaging using a Hummer VI-A pulse - sputter coating system (Anatech Ltd.) under a 60 mtorr vacuum.

Brightfield and SEM images were used to determine the diameter and crimp parameters of the electrospun fibres. Random diameter measurements were taken using Iconico Screen Calipers version 3.3. For the crimp measurements single wavelengths were randomly chosen and measured along with their amplitude. Pixel readings were converted either using the scale present on the SEM images or a 0.01 mm division micrometer image taken using the same microscope at the same magnification. SEM

images were also used to visualize the effects of base etching on the electrospun PCLDLLA fibres in 0.5 M NaOH for a variety of time points from 5min-3hrs.

4.2 Hydrogels

4.2.1 Reagents

Glycol chitosan (GC) (M_n = 180 kDa), poly(ethylene glycol) diacrylate (M_n = 700) (PEGD700) and 2-hydroxy-4'-(2-hydroxyethoxy)-2-methylpropiophenone (I2929) were purchased from Sigma-Aldrich (Canada). Genipin was purchased from Wako Chemicals (Japan). Dubecco's Modified Eagle Medium (DMEM) and 1X phosphate buffered saline (PBS) were purchased from Invitrogen (Canada). Methacrylated glycol chitosan (M-GC) was manufactured in our lab.

4.2.2 Material Preparation

Glycol chitosan (GC) was purified by making a 2 wt% solution in ddH_2O until dissolved (overnight). The solution was vacuum filtered using Fisher brand coarse/fast filter paper. The solution was dialyzed in 1 L of ddH_2O using Spectra/Por 7 regenerated cellulose 50 kDa MWCO dialysis tubing (Spectrum Labs) twice for 4hrs each. The dialyzed GC was then frozen at -20°C overnight and placed on the lyophilizer until dry. GC was redissolved in either 1X PBS or culture media prior to making the gels.

4.2.3 Crosslinking

For gelation of the biomimetic scaffold and controls, a custom designed Teflon™ mold (Figure 18) was constructed with a base and raised platform of 4x7 mm and a separable

top section that fit around the platform forming a well 2x4x7 mm. This design allowed for easy removal with minimal stress on the gel/scaffold. Once the top was removed, the scaffold could be easily transferred into the culture vessel.

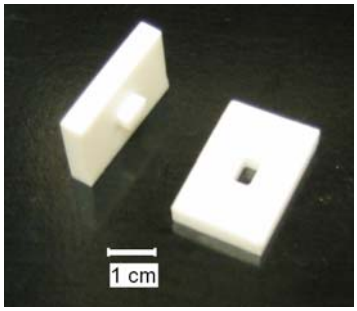

Figure 18: Two piece Teflon™ mold used for gelation work

Work done by Mwale *et al.*[142] was used as a guide for the genipin and GC hydrogel work. The chitosan chloride/glutamate salts previously used were replaced with GC. A 2.5 wt% solution of GC in DMEM with 5% w/w genipin/GC was used as the working gel solution. Gelation studies were conducted at 37°C in consideration for future cell culture work. A change in color from yellow to a dark blue throughout the whole gel was used to indicate when the hydrogels were formed[142,143].

GC and PEGD700 gelation studies were also conducted at 37°C. A variety of molar ratios were used to test the 6 wt% GC:PEGD700 gelation system to determine the lowest possible concentration with an acceptable crosslinking time. The shortest possible gelation time was used in order to minimize the time the cells would be in contact with

the unreacted PEGD crosslinker. Molar ratios of 6 wt% GC:PEGD700 (1:15, 1:30, 1:45, 1:60 and 1:80) were examined. Gelation was competed in 1 dram glass vials to facilitate the analysis techniques after gelation. Because of the small amount of the PEGD700 crosslinker required for the gel solution, a stock solution was made using a higher concentration diluted in 1X PBS. 3.5 μL of this solution was added to the appropriate amount of 6 wt% GC. To determine when the pre-gel solution was visually gelled, a simple flow test was performed where the gelation vial was tilted. If the solution did not flow, a basic mechanical poke test was conducted with a glass pipette tip until the solution/gel was resistant. At this point the solutions were considered gelled and the gel properties were analyzed.

For the photoinitiated hydrogel solution a 3.4 wt% M-GC stock solution in 1X PBS was initially prepared. The photoinitiator, 2-hydroxy-4'-(2-hydroxyethoxy)-2-methylpropiophenone (I2959), was dissolved in ddH_2O at its maximum solubility limit of 0.8 wt%. The I2959 solution was vortexed and then heated at 60°C for ~30 min to facilitate mixing. A 1 mL 3 wt% stock gel solution was prepared by mixing 880 μL of 3.4 wt% methacrylated glycol chitosan (M-GC) with 120 μl 1XPBS and 20 μL of I2959. To photocrosslink the gel solution, 50 μL was placed in custom designed Teflon™ molds (Figure 18) and the lowest possible UV intensity and exposure times. Photocrosslinking was performed with an EXFO Lite lamp with a 320-480 nm (UV/Visible range) filter and a dual leg liquid light guide (length = 100 cm and active output diameter of 5 mm). Energy output was determined with an EXFO R5000 radiometer.

4.2.4 Analysis

To estimate how the gels would perform in an aqueous culture environment, their sol contents were measured (n=3). After crosslinking, the gels were air dried at room temperature in a vacuum desiccator with a vent and H_2O trap for 48 hrs. Gels were then swollen at 37°C in 1X PBS and placed on a rotating mixer at a low speed. The water was changed 5 times within a 48 hr period and then re-dried under the same conditions. Weights were recorded after each step to calculate the water equilibrium content and sol fraction of the gels. Water equilibrium content was calculated using the following equation (Equation 4) where m_s is equal to the re-swollen gel mass and m_{d1} is the first dry mass of the gel.

$$Equilibrium\ Water\ Content = \frac{m_s - m_{d1}}{m_s} \qquad \textbf{Equation 4}$$

Sol fractions were calculated using the following equation (Equation 5) where m_{d2} is the second dry mass of the gel after 48hr swelling period in 1X PBS.

$$Sol\ Fraction = \frac{m_{d1} - m_{d2}}{m_{d1}} \qquad \textbf{Equation 5}$$

For the GC and PEGD700 hydrogels it was assumed that the gels were not completely gelled due to the relatively short gelation period. Therefore, a degradation study was conducted to determine the stability of the hydrogels in an aqueous environment. Immediately after it was determined that the solution had gelled, the vial was filled with 1X PBS and placed on a low speed rotating mixer at 37°C. The vials were checked daily until the gels no longer had a defined shape at which time the gel was considered completely degraded.

4.3 Cell Culture

4.3.1 Reagents

Dulbecco's Modified Eagle Medium (DMEM) with 4.5 g/L of glucose and L-glutamine without sodium pyruvate, 100X antibiotics with 10000 units/mL of penicillin G sodium and streptomycin sulphate and 25μg/mL amphotericin B (fungizone) in 85% saline, 1X phosphate buffered saline (PBS) pH 7.4 without calcium chloride and magnesium chloride, 10X Trypsin-EDTA (0.5% trypsin with EDTA 4Na), trypan blue and the Live/Dead™ viability/cytotoxicity kit for mammalian cells were purchased from Invitrogen (Canada). Sodium bicarbonate, L-ascorbic acid and fetal bovine serum (FBS) (Canadian origin) were obtained from Sigma-Aldrich (Canada). Collagenase A (from *Clostridium histolyticum*, 0.228 units/mg lyophilized) was obtained from Roche Diagnostics (Germany). 100% ethanol was obtained from Botterell Stores at Queen's University. All culture media and regents were sterile filtered using Nalgene Supor Mach V filtration flasks with a PES 0.2 μm membrane prior to use. Polyclonal rabbit anti-bovine collagen type I was obtained from Biodesign Inc. (USA) and collagen type III from Karlan (USA). Both antibodies were received as a lyophilized powder and reconstituted in 0.5 mL of ddH_2O. 10 μL of each antibody were aliquot into 0.5 mL Eppendorf tubes and stored at -70°C for later use. Fluorescein isothiocyanate (FITC) and Texas Red conjugated goat secondary anti-rabbit antibodies, normal goat serum and vectashield™ aqueous mounting medium with 4,6-diamidino-2-phenylindole (DAPI) were obtained from Vector Labs, Canada. A 4 wt% paraformaldehyde solution, Picrosirius Red stain (0.5 g Sirius red, 500 mL aqueous saturated picric acid solution) and

0.5% v/v aqueous glacial acetic acid were obtained and used as received from the Department of Anatomy and Cell Biology at Queen's University.

4.3.2 Cell Preparation

The lower metacarpal joints from ~18 month old cows were obtained from Brian Quinn's Meats (Yarker, ON.) the day of dissection. Legs were cleaned and then submerged in 70% ethanol for 1 hr to sterilize the outer surface. The central ligament from the lower metacarpal joint was dissected under sterile conditions in a laminar flow hood. The ligament section was first placed in a 10X antibiotic/DMEM solution and trimmed of all adipose tissue. The trimmed ligament was then transferred to a 0.25% collagenase /DMEM solution and minced using surgical scissors into < 2 mm pieces in a 10 cm Petri dish. The digest solution was then placed in an incubator (5% CO^2 and 37°C with 95% relative humidity) for ~36 hrs with mixing twice a day to aid in digestion. After the digestion was complete, the cell digest solution was filtered with a stainless steel cell dissociation sieve with a 140 μm pore opening (Sigma, Canada) to remove large undigested tissue pieces. The cell suspensions were centrifuged at 800 g for 8 min. Media was aspirated and the cells were resuspended in fresh DMEM. On the third centrifugation cycle, the cells were counted using a trypan blue dye exclusion assay. Passaged cells (in 75 cm^2 flasks) were used in all preliminary cytotoxicity studies whereas primary (unpassaged) cells were used in the biomimetic scaffold studies. To culture the cells, the cell pellet obtained from the ligament digest was resuspended in DMEM containing 5% FBS to a concentration of $5x10^5$ cells/3mL media. To facilitate cell attachment to the surface of the flask a low seeding volume (3 mL) was used. Once a

sufficient number of the cells had attached (2-3 days), the flask was topped up with 12 mL for a total volume of 15 mL. The flasks were fed every 2-3 days until the cells reached confluence (80-90% coverage). To passage the cells, the media was aspirated and the culture surface was trypsinized using 3 mL of a 0.5% Trypsin/EDTA solution for ~5 mins. After the cells were completely lifted off the culture surface, the trypsin/cell solution was neutralized using 3mL DMEM. The flasks were then rinsed with DMEM to remove any additional cells and added to the rest of the cell suspension. The cell solution was centrifuged and a similar washing/spinning protocol described previously was used.

4.3.3 Culturing

A cell attachment assay (n=5) was performed on the 1.5 hrs 0.5 M NaOH base-etched PCLDLLA thin films to determine the effect of the modified surface on cell behavior. First passage (P1) cells were used for this study. Thin films (original and base-etched) were placed in 24-well culture plates (Costar) and pre-wetted with 5% FBS/DMEM culture media. The tissue culture polystyrene (TCP) surfaces were used as a control. A low volume (20 μL) of a high cell density solution (750 cells/μL) was used to ensure that the cells attached to the surfaces in an even manner. This solution was pipetted onto the thin films and control surface followed by a 30 min cell attachment period. After seeding, the wells were then topped up to 2 mL with 5% FBS/DMEM culture media. Media was changed every 2-3 days. Cells were cultured for 2 weeks or until the TCP surface became confluent. A Live/Dead™ assay was performed on the cultures to determine cell viability as well as to help visualize the number of cells attached to the thin films and their morphologies.

A nutrient deprivation study (n=3) was conducted since the long crosslinking times (4-6 hrs) of some of the gelation systems, could deprive the cells of nutrients. P1 cells were cultured until confluent after which the culture media was replaced with 1X PBS for the appropriate time. Viability was assessed using a Live/Dead™ assay.

Another assay was conducted to determine cytocompatibility of the hydrogel materials as well as the viability of the cells encapsulated in the hydrogels after the gelation process (n=3). Confluent cells were cultured with the individual hydrogel components in the culture media for 24 hours to examine any possible adverse affects on the cells. If any toxic effects were detected from these exposure tests then culture work with the gelation system was not conducted. To determine if the gelation process and hydrogels were cytocompatible, cell viability was analysed after a 24 hr culture period. For the hydrogel viability testing passaged fibroblasts (P1) were used at a seeding density of $6x10^5$ cells per gel.

To manufacture the biomimetic scaffolds, strips from the mat (sections between each parallel wire on the collecting mandrel ~2-3 cm in length) were cut to the width of the Teflon mold (~ 4 mm) and base-etched. Approximately 4mg of the base-etched PCLDLLA fibre strips (2-3 strips/4 mg) were sterilized using UV light in a laminar flow hood for 30 min on each side prior to use in the scaffolds. The base-etched strips were then individually folded into thirds at 1/3 and 2/3 the length of the strip. The same materials and gelation procedures were used for the biomimetic scaffold as in the photoinitiated hydrogel work in the previous section (§4.2.3). To make the cell seeding

gel solution, a 1 mL stock solution was prepared by mixing 880 μL of 3.4 wt% M-GC (lyophilized and autoclaved) in 1X PBS with 20 μL of the I2959 and vortexed. The primary ligament cell pellet was re-suspended in 120 μL 1X PBS at a cell density of 8000 cells/μL ($4x10^5$ cell/construct) and then added to the M-GC/I2959 solution and gently mixed to disperse the cells using a 1000 μL pipette. A 50 μL aliquot of the stock cell solution was used for each biomimetic scaffold. To seed the biomimetic scaffold a fraction of the cell solution was added to the Teflon™ mold (Figure 18) along with a single PCLDLLA fibre strip. This process was continued for each scaffold until all of the cell solution and fibre strips were used. Due to the hydrophobic nature of the dried base-etched PCLDLLA fibres, each mat had to be tamped down with a syringe needle until completely wetted. After all the fibres were wetted with the cell seeding gel solution, the construct was photocrosslinked and then immediately removed from the Teflon™ mold and placed into the culture media. A gel-only control was prepared with the same volume of cell seeding gel solution but without the PCLDLLA fibres. A PCLDLLA fibre-only control was also prepared using a conventional cell seeding method with the same number of cells as the other scaffolds. To seed the fibre-only scaffold, a low volume and high cell density seeding solution was used ($4x10^5$ cells/20 μL). Half of the seeding solution was added to each side with a 30 min incubation time per side. After the initial seeding was completed, the total volume of culture media was added to the well. In total, 27 constructs were made with three samples for each of the fibre-only, gel-only and fibre-gel scaffolds and for each of the three time points studied (1, 2 and 4 weeks). Cells were cultured in 800 μL of 5% FBS in DMEM supplemented with 25 ug/mL L-ascorbic acid and 1X antibiotics. Ascorbic acid is an important factor in the production

of collagen by fibroblasts[160,161,162]. Biomimetic scaffolds and controls were cultured for 1, 2 and 4 weeks with media changes every 2-3 days.

4.3.4 Analysis

To visually investigate cell viability, a Live/Dead™ assay was used. The kit is a two colour fluorescence assay consisting of calcein AM and ethidium homodimer-1 (EthD-1). Live cells take up and convert calcein AM to calcein via esterase. Calcein produces a green fluorescence with excitation and emission intensities of 494 and 517 nm, respectively. EthD-1 enters through the damaged membrane of dead (or dying) cells and produces a 40 times amplification of fluorescence in the red region upon binding to nucleic acid (495 nm excitation and 635 nm emission). Both dyes do not fluoresce unless they interact with cells. A working solution of 4 μM EthD-1 and 2 μM calcein AM in 1X PBS was prepared 2-3 hours before imaging. Samples in 48 well plates were incubated with 800 μL of the working solution and incubated on an orbital shaker for 45 min – 1 hr at room temperature to ensure sufficient staining.

To calculate the ratio of live/dead cells (viability) in the hydrogels, a 9 x 9 grid was placed on the red/green channel overlay picture. Four of the 9 grids were randomly chosen and counted for the number of live and dead cells. The number of live cells was then divided by the total number of cells to determine the percent cell viability.

To observe and characterize the tissue being produced in the scaffolds immunohistochemistry (IHC) of fresh frozen sections was used. To prepare the cultured

scaffolds for embedding in the CryoMatrix™ (Thermo Shandon) medium, the culture media was aspirated and scaffolds were rinsed in 1X PBS. An aluminum foil mold was constructed and partially filled with CryoMatrix and placed in a methanol bath cooled with dry ice until it was partially frozen. The sample was positioned in the unfrozen matrix close to the bottom of the mold and then placed back into the methanol bath until completely frozen. The frozen samples were sent to the Department of Anatomy and Cell Biology for cryo-sectioning. Sections 10-20 μm thick were cut on a cryostat at -25°C and mounted on Superfrost Plus™ slides (Fisherbrand). Slides were stored in a -20°C freezer until needed.

For IHC staining, the slides were taken out of the freezer and allowed to warm up to room temperature for 30 min - 1 hr. Sections on the same slide were isolated from each other using a diamond etching pen and hydrophobic grease marker to prevent mixing of staining solutions during incubations. Slides were rinsed in 1X PBS twice for 5 min each. Sections were blocked with a 1.5% v/v normal goat blocking serum in 1X PBS for 30 min. After blotting off the excess goat serum, sections were incubated for 3 hrs with their respective primary antibodies at a 1:100 dilutions in goat serum. Slides were rinsed twice with 1X PBS for 5 min each. Incubation with secondary antibodies was performed in the dark to prevent photobleaching of the fluorescent secondary antibodies. Secondary antibodies were incubated for 30 min at a 1:100 dilution in goat serum. A FITC labelled (495 nm excitation, 515 nm emission) secondary antibody was used for collagen type I and a Texas Red labelled (595 nm excitation, 615 nm emission) secondary antibody was used for collagen type III. Sections were then rinsed 3 times in 1X PBS for 5 min each.

Sections were coverslipped using Vectashield aqueous mounting media with DAPI (360 nm excitation, 460 nm emission) to stain the cell nuclei and then sealed with clear nail polish to prevent the sections from drying out. Negative controls were performed on the cyro-sections where the primary antibodies were replaced with goat serum. Sections of an acellular biomimetic scaffold were stained using the normal IHC procedure.

Histological Picrosirius Red staining was performed on native ligament sections to visualize the structure of the collagen fibrils. Intra-synovial bovine ligaments were dissected from the metacarpal joint above the hoof. The ligaments were trimmed of excess adipose tissue and fixed in 4 wt% paraformaldehyde solution for 1 week to ensure complete fixation. The fixed ligaments were washed 2-3 times with 1X PBS and stored in 70% ethanol. The fixed ligaments were then sent to the Department of Pathology in the Kingston General Hospital for paraffin embedding and sectioning (5-10 μm). The paraffin embedded sections were de-waxed by putting the slides through a series of toluene, ethanol (100%, 80% and 70%), and water washes 2X each for 5 min. The de-waxed slides were incubated in the Picrosirius Red stain for 1 hr at room temperature. The slides were then washed in 0.5% v/v aqueous acetic acid. Finally the slides were dehydrated by using the same de-waxing solutions but in the reverse order and coverslipped.

IHC and Live/Dead™ assay images were taken using a Leica TCS SP2 multi-photon confocal inverted microscope with Leica Image Pro Plus software. Images were processed using Leica Lite confocal software. An Axioplan 2 Imaging fluorescent

microscope equipped with an Axiocam High Resolution monochrome camera was used to capture additional images of the FITC, Texas Red and DAPI stained frozen IHC slides. Images were analyzed and modified using Axiovision LE version 4.5.0.0 software. A Nikon Eclipse E800 light microscope and digital camera with QCapture (verion 2.56) was used to capture images of the Picrosirius Red stained slides. Images were later enhanced using Microsoft Photo Editor.

4.4 Data Analysis

Unless otherwise noted, analysis techniques were only completed once. All quantitative results were averaged and are reported with a standard mean error value. No statistical analyses were completed on these results.

Chapter 5. Results & Discussion

5.1 Fibres

5.1.1 Electrospinning of Chitosan

Using the conventional electrospinning setup, the investigation of the chitosan and aqueous acetic acid electrospinning system started with a 1 wt% low molecular weight chitosan and a 1% v/v acetic acid solution. Appropriate changes were made based on these initial findings. A 1M NaOH bath was used to assist in producing fibres by precipitating them in solution due to the low volatility of the aqueous solvent. Without the precipitation bath only a chitosan solution was collected after electrospinning. Results indicated that the 1 wt% chitosan precipitate that was formed in the bath was not very fibrous in nature and was unable to remain intact during collection. Interactions of the chitosan molecules in solutions lower than 1 wt% were most likely not high enough which reduced the cohesiveness of the solution and led to a fine droplet spray from the needle tip to the collecting plate. Therefore, it was determined that the initial 1 wt% low molecular weight chitosan solution was below the minimum electrospinning weight percent.

The weight percent of chitosan was increased to overcome this problem. However, once the weight percent of chitosan was increased past 2 wt% the solution became too viscous resulting in an inconsistent electrospinning process. These inconsistencies were indicated by elongated droplets from the Taylor cone to the collecting plate. The high viscosity of chitosan observed in the aqueous acidic environment was a result of the positive free amino groups along the polymer backbone. These repulsive charges caused the chitosan

molecule to form a rod like conformation in solution leading to higher chitosan chain entanglements that increased the solution viscosity[92,156]. This high viscosity effect was noticeable with low molecular weight chitosan from 2 – 6 wt%, which made it difficult for the electric field to pull fibres from the Taylor cone. From the results it appeared that before a minimum electrospinning weight percent could be reached, high viscosity effects made the chitosan solutions unspinnable by conventional methods.

To overcome this viscosity effect, pH adjustments to the solution were attempted to de-protonate the positively charge amino groups and thereby reduce the repulsive charges along the chitosan backbone. Solutions of chitosan were adjusted with 1 M NaOH until the onset of precipitation, which was found to be at pH 5.5. However, only solutions up to 1 wt% chitosan (low molecular weight) were able to be pH-adjusted since higher weight percent solutions resulted in localized precipitation. Adjustments to the pH could be made to higher weight percent chitosan solutions by using a less concentrated NaOH solution but, a large volume was required to adjust the pH. The large increase in volume greatly reduced the weight percent of the solution leading to electrospinning problems previously mentioned. Therefore, pH adjustment of higher weight percent chitosan solutions in an attempt to reduce their viscosity was unsuccessful.

A heated co-axial air flow electrospinning method[93] was also used to decrease the viscosity of the previously unspinnable high weight percent chitosan solutions. Increasing the temperature of these solutions would increase the molecular interactions and reduce the inter-molecular cohesive forces, which, in theory, should help with their

electrospinning ability. This theory was confirmed from the results. With the aid of the heated co-axial air flow and 1 M NaOH precipitation bath, fibres were electrospun using 3.6, 3.8 and 4.0 wt% low molecular weight chitosan solutions with average fibre diameters of 94±7, 117±6 and 112±10 μm, respectively (n=50) (Figure 19). Diameter distributions for these fibres are shown in Figure 20.

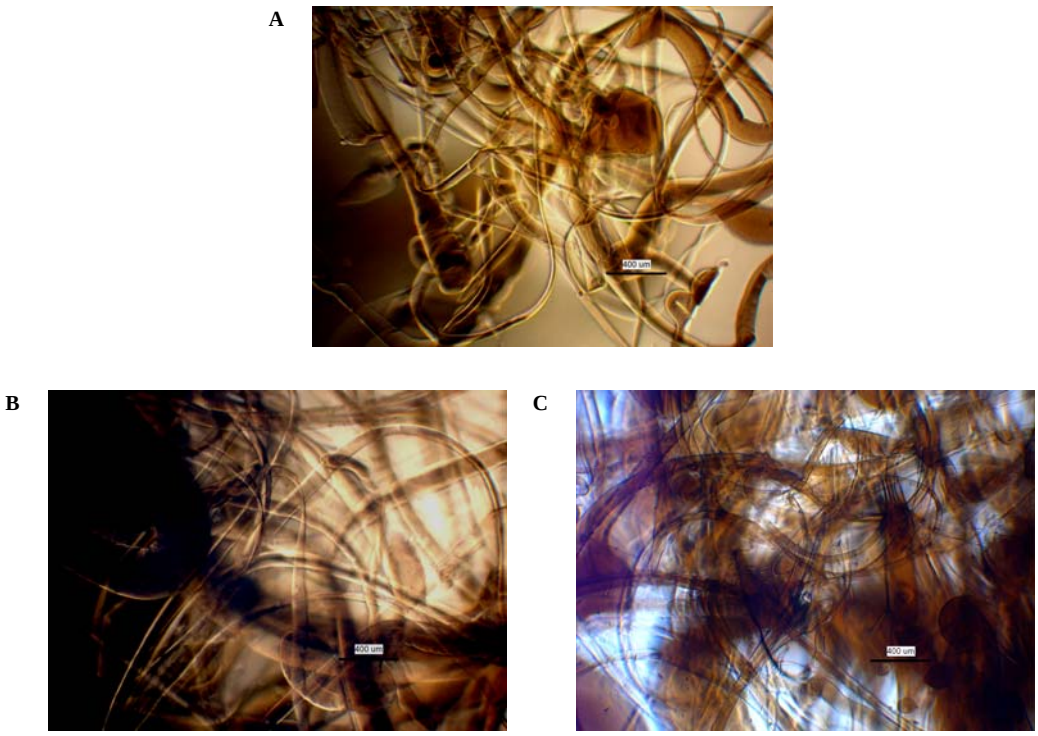

Figure 19: Brightfield images of electrospun low molecular weight chitosan with 1% v/v acetic acid in 1M NaOH precipitation bath
40x Magnification with 400 μm scale bar, A – 3.6 wt% low molecular weight chitosan, B – 3.8wt% low molecular weight chitosan and C – 4 wt% low molecular weight chitosan.

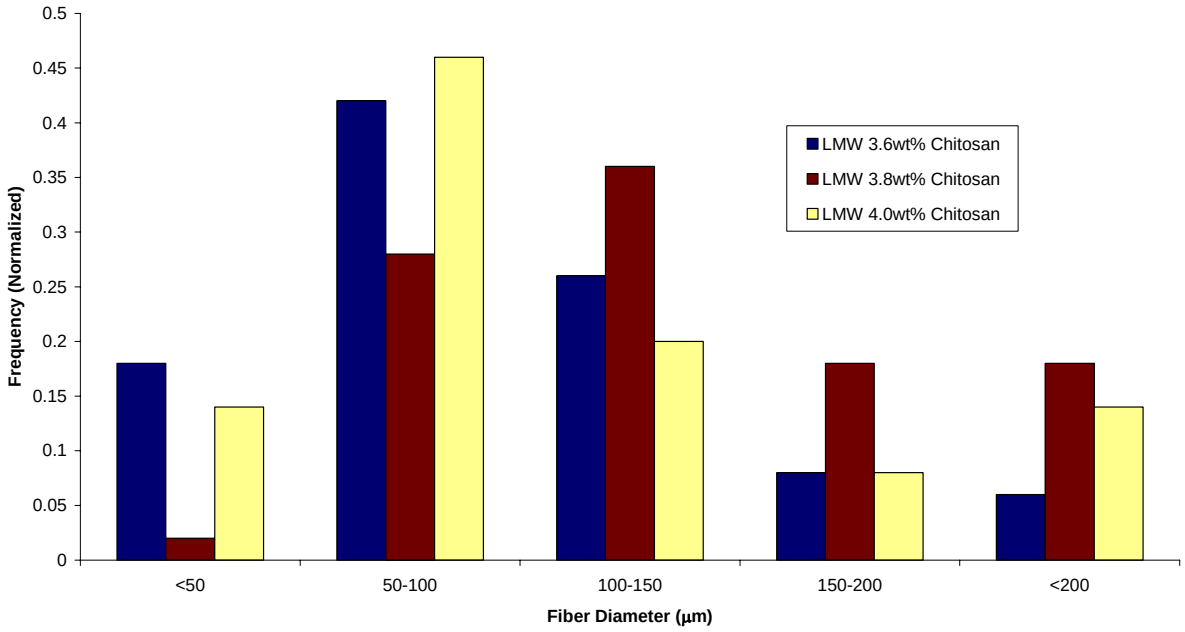

Figure 20: Low molecular weight chitosan in 1% v/v acetic acid electrospun fibre diameter distribution
Data was taken from a set of n=50

To reduce the fibre diameters, a small amount of high molecular weight chitosan was mixed with the low molecular weight chitosan. It was hypothesized that the high molecular weight chitosan would become the main structural molecule in the solution and the low molecular weight chitosan would act as filler. The main purpose of the low molecular weight filler was to increase the weight percent of the solution without greatly increasing its viscosity. To study this effect, a range of 4 wt% high to low molecular weight chitosan solutions (0.15, 7.5, 15 and 30 %, mass basis) were electrospun and compared to the 4 wt% low molecular weight chitosan previously mentioned (112±10 μm). Brightfield images of the electropun high/low molecular weight chitosan fibres are shown in Figure 21. The diameter results are shown in Table 5 along with the diameter distributions given in Figure 22.

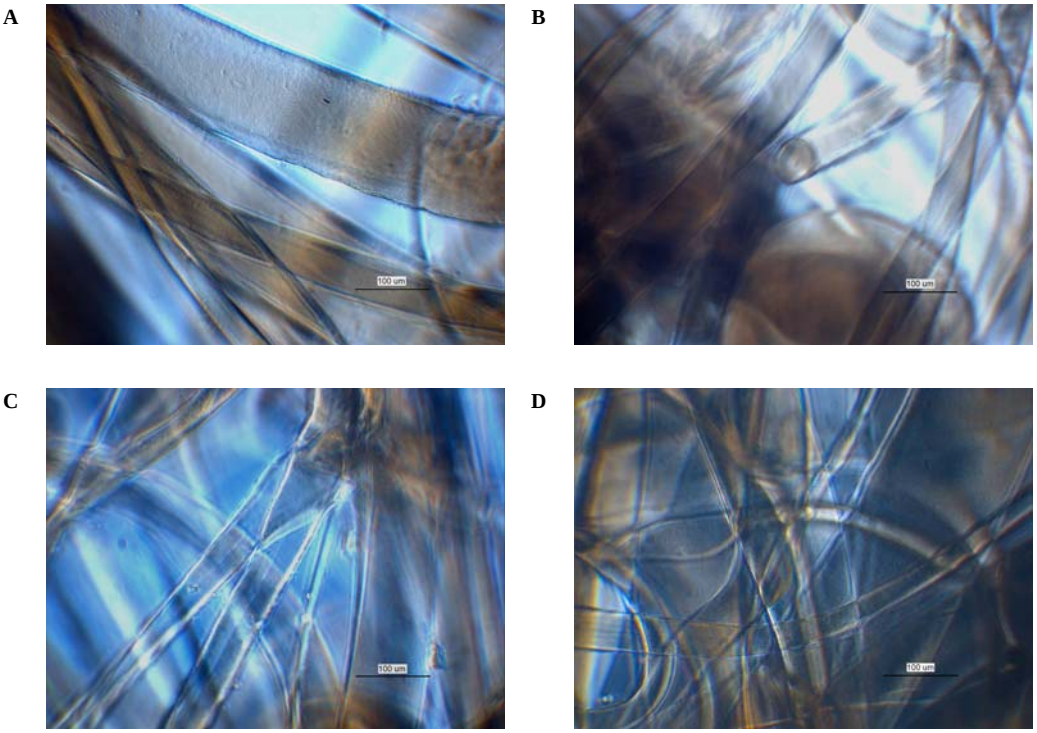

Figure 21: Brightfield images of electrospun high/low molecular weight chitosan blends with 1% v/v acetic acid in 1M NaOH precipitation bath
200x Magnification with 100μm scale bar, A – 0.15/99.85 High/Low ratio, B – 7.5/92.5 High/Low ratio, C – 15/85 High/Low ratio and D – 30/70 High/Low ratio.

Table 5: Average diameters for high:low chitosan fibres

High / Low Chitosan Mass Ratio	Average Fibre Diameter in microns (n=57)
0.15 / 99.85	81±6
7.5 / 92.5	54±5
15 / 85	85±7
30 / 70	115±8 (n=25)

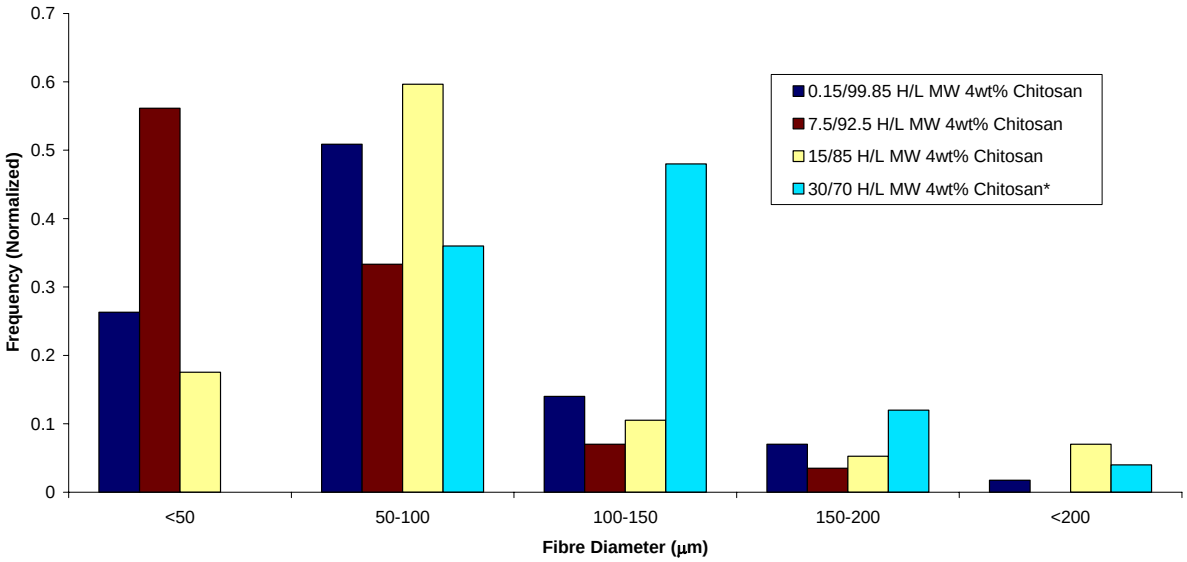

Figure 22: High/Low molecular weight (H/L MW) chitosan blends with 1% v/v acetic acid electrospun fibre diameter distributions
Data was taken from a set of n=57 (*n=25).

The results indicated that even at a low 0.15% of the high molecular weight chitosan, average fibre diameters were reduced when compared to the low molecular weight chitosan fibres. Fibre diameters were further reduced with the increase of high molecular weight component to 7.5%. However, an increase to 30% high molecular weight chitosan increased the fibre diameters to similar dimensions as the low molecular weight chitosan fibres. It seemed that high molecular weight chitosan below 30% was beneficial in reducing the fibre diameters of the 4 wt% low molecular weight chitosan solution. However, all the chitosan fibres electrospun under these conditions were well above the sub-cellular dimensions that were being sought (i.e. < 10 μm). Compared to these results, more consistent and continuous fibres with diameters of 20-40 μm can be produced using the wet spinning technique[163,164]. In addition, the low and high/low molecular weight chitosan fibres had poor mechanical properties after being dried. These

fibres were too brittle for use in a tissue engineering scaffold. Therefore, it was determined that electrospinning was not an ideal method to produce chitosan fibres using aqueous acetic acid as the solvent.

Recently, several reports were published stating that a variety of chitosan solutions were used to electrospin chitosan fibres with sub-cellular dimensions. For example, poly(ethylene oxide) (PEO) was used to aid in the electrospinning process of chitosan dissolved in dilute aqueous acetic acid[104,165,166]. PEO reportedly masked the positive charges on the backbone of chitosan through hydrogen bonding, thereby reducing the solution viscosity and making it spinable[104]. However, attempts to reproduce their results were unsuccessful, despite seeking assistance from the authors. Experiments were also conducted using a 7 wt% medium molecular weight chitosan in 90% aqueous acetic acid solution, which was also reported to have been successful[101]. However, the high viscosity of the spinning solution interfered with the electrospinning process and fibres could not be electrospun under these conditions. A study by Desbrieres[167] found that medium molecular weight chitosan in aqueous acetic acid solutions would become gel-like at concentrations between 4.0 – 4.5 wt%. This phenomenon could be a possible explanation for the poor results that were obtained from this approach. Another method suggested electrospinning chitin in hexafluoroisopropanol and afterwards de-acetylating the chitin fibres into chitosan[168]. However, the majority of the fibre morphology was lost during the de-acetylation process which decreased the usability of these fibres for tissue engineering applications. Therefore this method was not pursued further. In spite of the

previous failures, chitosan fibres were able to be reproduced using 6-8 wt% medium molecular weight chitosan in a 70:30 TFA:DCM solvent[102].

Similar solutions of 4, 6 and 8 wt% air dried low molecular weight chitosan were prepared in a 70:30 volume ratio of TFA to DCM. It was observed that the air dried chitosan required approximately 3 days to completely dissolve in the TFA:DCM solvent due to its very crystalline structure. However, chitosan dissolved in this solvent had solution properties that appeared promising for electrospinning since the solutions were not as viscous, yet more cohesive, than their aqueous-based counterparts. These improved solution conditions were observed in the 6 and 8 wt% solutions, which were able to electrospin fibres. The 6 and 8 wt% fibre mats were thick enough to be handled and were composed of individual fibres well within the sub-cellular diameter range. However, the 4 wt% chitosan/TFA:DCM solution was only able to produce droplets on the collecting mat. These results (Figure 23) possibly indicated that a minimum electrospinning weight percentage for the chitosan/TFA:DCM system was between 4 – 6 wt%. Figure 24 and Table 6 summarizes the average fibre diameters and their respective distributions for different conditions that were able to spin fibres.

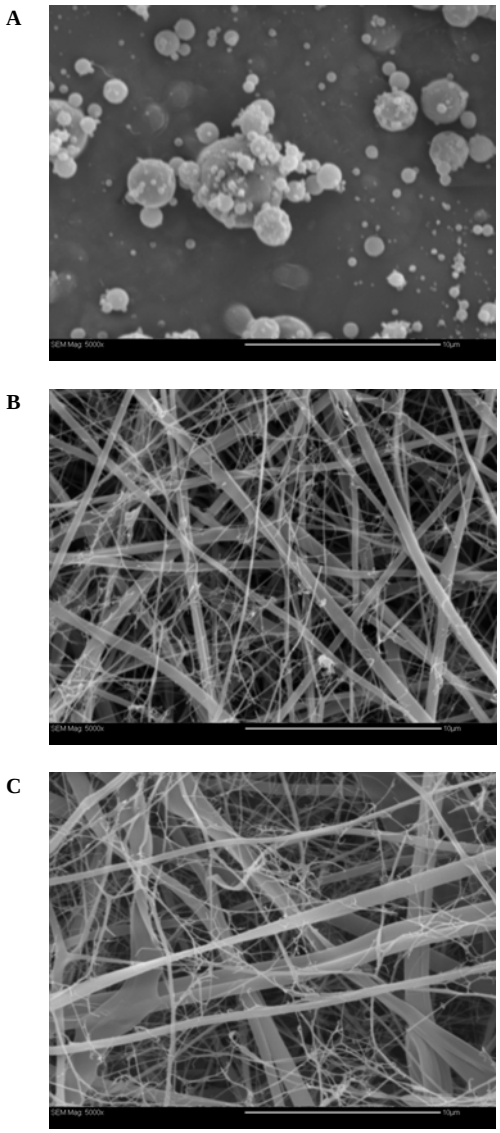

Figure 23: SEM images of electrospun low molecular weight chitosan with 70:30 TFA:DCM 10μm scale bar, A – chitosan spun at 6 wt% and 10 cm air gap, B – chitosan spun at 8 wt% at 6 cm

Table 6: Average diameters of electrospun chitosan in 70:30 TFA:DCM

Electrospinning Conditions	Average Fibre Diameter (nm), n=100
Air dried low molecular weight 6 wt%, 4% solution flow rate, 10 cm air gap, 20 kV	165±17
Air dried low molecular weight 6 wt%, 10% solution flow rate, 15 cm air gap, 20 kV	361±34
Air dried low molecular weight 8 wt%, < 10% solution flow rate, 6 cm air gap, 15-20 kV	218±26
Lyophilized medium molecular weight 8 wt%, 4% solution flow rate, 7-15cm air gap, 20-25 kV	188±10 (avg. from 133-243hrs) (330 avg, range between 210-650)[102]

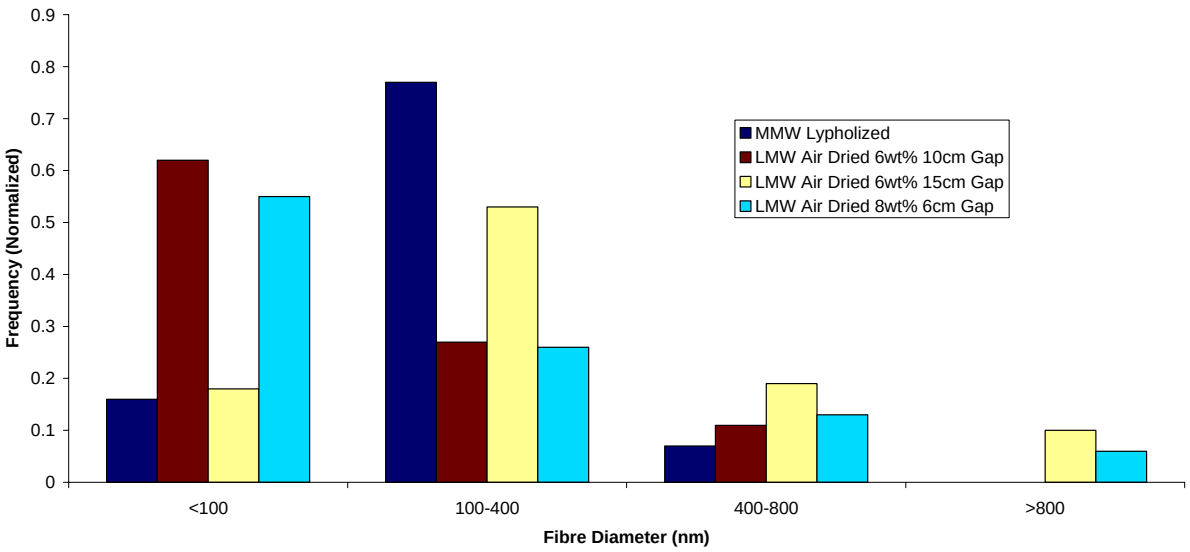

Figure 24: Low and medium molecular weight chitosan with 70:30 TFA:DCM electrospun fibre diameter distributions

The chitosan fibres produced from the 6 and 8 wt% solutions appeared suitable for use in the scaffold. However, during preparation of these fibres for cell culture they were found to dissolve in aqueous media (water and 70% ethanol). Moreover, the chitosan/TFA:DCM solutions were observed to rapidly change colour from yellow to a dark brown and dramatically decrease in viscosity. It was hypothesized that the molecular weight of chitosan was being reduced from the exposure to the acidic TFA (pKa = 0.23)[169] solvent. Therefore, the molecular weight was most likely degraded to such a degree that the dried chitosan fibres actually became soluble in neutral aqueous media. This was quite possible since concentrated acetic acid[170], hydrochloric acid[171] and nitric acid[172] have been use to fractionate chitosan.

To reduce the extent of chitosan degradation before it was electrospun and its solubility in aqueous media after spinning, a reduction in the dissolving time was required. A reduction in the time to dissolve chitosan was accomplished by increasing the porosity of the air dried chitosan. To increase the porosity of the dried chitosan material, chitosan solutions were lyophilized. A 6 wt% solution of the lyophilized low molecular weight chitosan was able to dissolve in TFA within 2.5 hrs. To confirm that the molecular weight of chitosan was being degraded, a viscosity versus time study of this solution was conducted. The results of this study confirmed that the chitosan was degraded immediately after being dissolved in the TFA:DCM solvent (Figure 25).

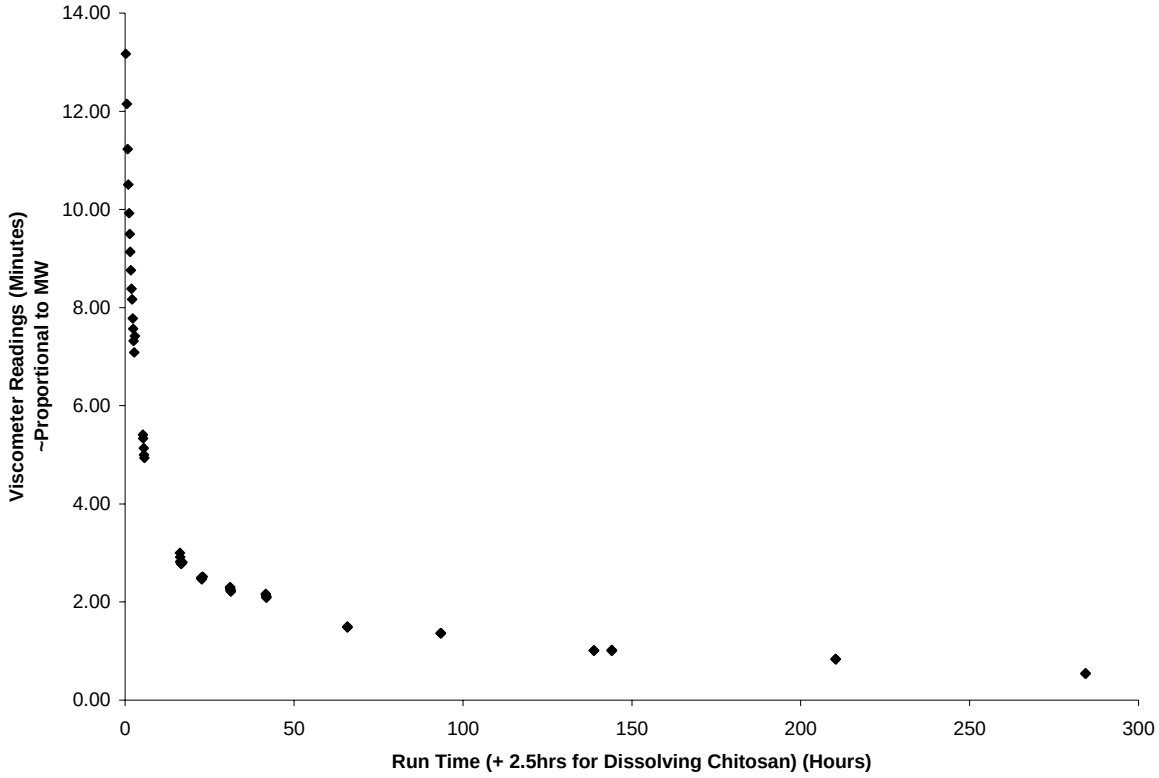

Figure 25: Low molecular weight chitosan and 70:30 TFA:DCM degradation study
6 wt% purified and lyophilized low molecular weight chitosan in 70:30 TFA:DCM solvent, viscosity was measured on a capillary viscometer and time was considered proportional to molecular weight of chitosan

An electrospinning experiment with respect to time was also conducted to determine when, and at relatively what molecular weight, the chitosan fibres were being spun. However, the 6 wt% lyophilized chitosan solution was unable to produce electrospun fibres during the 5 day experiment.

From the chitosan/TFA:DCM results, it was hypothesized that the 3 days required to dissolve the air dried chitosan resulted in a broader molecular weight distribution than the rapidly dissolved lyophilized chitosan. This was due to the fact that air dried chitosan was being dissolved and degraded in the TFA solvent at the same time. If all the chitosan had dissolved at the same time, as with the lypholized chitosan, then a narrower molecular weight distribution would be obtained. However, with the longer dissolving air dried chitosan the earliest dissolved chitosan would be severely degraded by the time the final mass of chitosan was dissolved. It appeared that the broader molecular weight distribution was beneficial to this electrospinning process, which was similar to earlier findings with the high/low molecular weight blends of chitosan in aqueous acetic acid. The effect of this molecular weight distribution on the electrospun fibres was evident from the large diameter distributions observed in the SEM images (Figure 23). These images show separate, larger fibres with consistent diameters in the sub-micron range along with a connected nanofibrous network between them.

In an attempt to improve the spinnability of the lyophilized chitosan solution, an 8 wt% lyophilized medium molecular weight chitosan solution was used. Ideally, the higher weight percent would allow fibres to be spun and the higher molecular weight would

prevent the fibres from dissolving in aqueous media. Therefore, another electrospinning versus time experiment was conducted after dissolving the chitosan for approximately 3.5 hours. It was found that more uniform chitosan fibres could be electrospun after 122hrs right up until the end of the experiment (243 hrs) (Figure 26a). However, if this solution followed similar degradation behaviour to the 6 wt% low molecular weight chitosan in TFA solution (Figure 25) then by 122 hrs the majority of the chitosan would have been severely degraded. This theory was confirmed by the fact that the medium molecular weight electrospun chitosan fibres could still be dissolved in aqueous media.

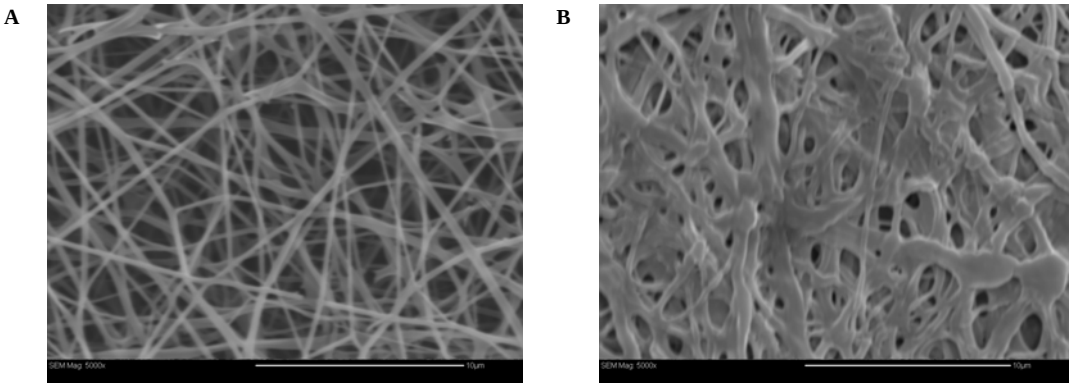

Figure 26: Lyophilized medium molecular weight chitosan with 70:30 TFA:DCM electrospun fibres
10μm scale bar, representative image at 169hrs, A – 8 wt% medium molecular weight chitosan, B – 8 wt% medium molecular weight chitosan after 1 M NaOH rinse (completely dissolved without base treatment)

To prevent the degraded chitosan fibres from dissolving in aqueous media, a 1 M NaOH solution was used to precipitate the chitosan by bringing the washing media up past its pK_a (6.5)[156]. Using this pre-treatment method, the fibres did not completely dissolve after rinsing in aqueous media. However, the chitosan in the fibres was degraded to such a

degree that even with a NaOH pre-treatment a fibrous morphology was not maintained (Figure 26). The loss of fibre morphology and inter-fibre spacing was not an ideal property for use in the biomimetic ligament scaffold. Therefore, the PCLDLLA copolymer was investigated for producing the fibres of the scaffold.

5.1.2 PCLDLLA copolymer

5.1.2.1 Electrospinning

Initially, a T_g close to or below physiological temperature (37°C) was chosen for the PCLDLLA copolymer. Ideally, having a T_g near or below 37°C should make the fibres flexible enough for manipulation during the electrospining process (room temperature) and tissue culture work (37°C). Therefore, two copolymer compositions were investigated: one near 37°C and one below (adjusted using a higher CL content). For a T_g of 37°C, Equation 1 determined that a 10:90 CL:DLLA mass ratio was required. For a copolymer with a T_g less then 37°C, a 40:60 copolymer was chosen since it had the lowest T_g out of the of other copolymers that were synthesized, which did not flow at room temperature.

DSC analysis of the methanol purified 10:90 and 40:60 copolymers revealed a T_g of 44°C and 11°C, respectively (Table 7). For the 10:90 copolymer, the actual CL:DLLA ratio calculated from the ^{1}H NMR spectra (using peak assignments from Figure 27) was 5:95, which explained the higher then expected T_g value. From Equation 1, the 5:95 ratio resulted in a T_g of 46°C, which was very similar to the experimental value obtained from the DSC thermogram. The 40:60 copolymer had a 34:66 CL:DLLA ratio calculated from

the ^{1}H NMR spectra. The difference in the CL:DLLA ratio for the 40:60 polymer was not of great concern due to the much lower T_g value.

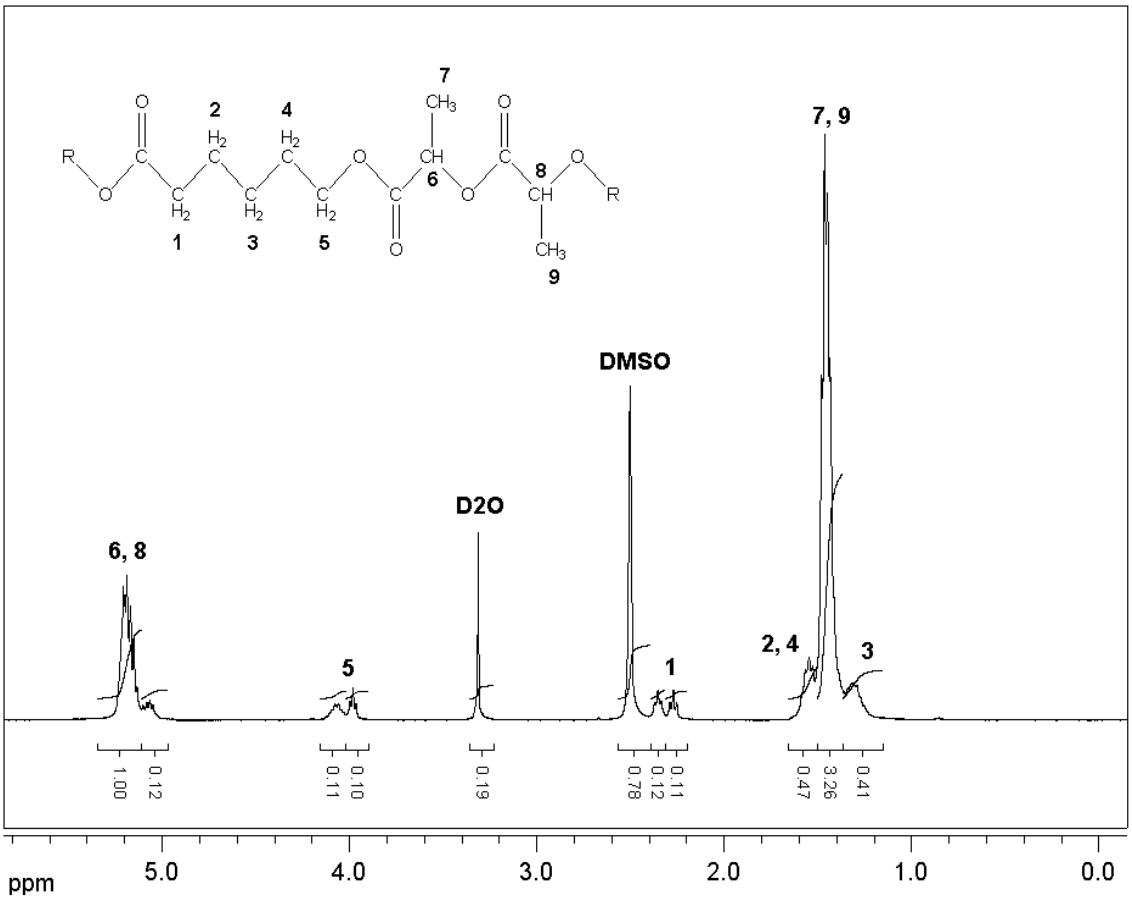

Figure 27: ^{1}H NMR of PCLDLLA polymer to determine peak assignment Ratios were calculated using peak integrations for 6, 8 (DLLA) and 5 (CL).

The 10:90 and 40:60 copolymers were electrospun in dichloromethane (DCM) to determine their fibre properties. A minimum electrospinning weight percent for the PCLDLLA copolymer occurred around 10 wt%. Optimum spinning conditions for this system were found between 20-35 wt%. However, the evaporation rate of DCM was found to be too high, which resulted in discontinuous fibre production and bead-on-fibre

defects. Therefore, DMF was added as a co-solvent to improve the spinning properties[103,105,106] of the PCLDLLA copolymer and DCM solutions. Further testing determined that a 35 wt% PCLDLLA solution with a 75:25 volume ratio of DCM:DMF solvent was ideal for producing continuous and defect free fibres. However, the fibres were not completely dry when collected due to the higher boiling point of DMF (153°C). DMF resulted in slightly wet fibres that would flow and stick to the surface of the collecting mat making it difficult to remove. To rectify this problem, a rotating wire mandrel was utilized. The mandrel acted as an infinite air gap that allowed the fibres to further dry without sticking to a planar surface. In addition to drying the fibres, the mandrel allowed for the collection of aligned fibres.

The 10:90 copolymer electrospun fibres were found to be too brittle after collection from the mandrel. Investigation of the electrospun 40:60 copolymer found that these fibres completely collapsed (no rigidity in the fibres) after removal from the mandrel and had flowed during long periods of storage (~1 month). From these results, it was determined that both the 10:90 and 40:60 copolymers did not have ideal properties for use in the biomimetic scaffold. Therefore, further modification to the copolymer was required to obtain a T_g close to 37°C.

Table 7: Physical properties of all CL:DLLA copolymers used

Copolymers	CL:DLLA Ratio (NMR)	Molecular Weight (M_n, kDa)	Polydispersity	T_g (°C)
10:90	8:92	27 RI	1.5 RI	33
10:90 (purified)	5:95	24 RI / 17 LS	1.4 RI / 1.2 LS	44
40:60	-	-	-	-2
40:60 (purified)	34:66	53 RI / 45 LS	1.84 RI / 1.49 LS	11
20:80 (purified)	16:84	52 RI / 44 LS	1.8 RI / 1.5 LS	36
20:80 blend (solvent)	-	-	-	43
20:80 blend (high temperature)	14:86	29 RI / 19 LS	1.9 RI / 1.8 LS	37

However, it was determined that the copolymerization was not going to completion since methanol purification removed most of the lower molecular weight impurities/monomers. Furthermore, viscosity limitations of the copolymerization system resulted in a wide variety of number averaged molecular weights for similar reactions. The combination of these limitations made it difficult to produce a copolymer with a desired T_g based on its theoretical CL:DLLA ratio. Therefore, to generate a PCLDLLA polymer with a T_g near 37°C, blending of the 10:90 and 40:60 copolymers was utilized. These purified copolymers had defined physical properties and if miscible would only require adjustment to their blends to produce the desired T_g. From Equation 1, and through additional experiments, it was determined that a 70:30 mass ratio of 10:90 to 40:60 copolymers was required to obtain a final T_g close to 37°C. However, DCM solvent blending resulted in an immiscible blend since a major T_g at 41°C and a broad transition from 10-30°C was observed in the DSC graph (Figure 28). Alternatively, the two copolymers were blended using high temperatures (~140°C) for 4-5 hrs to form a single T_g of 37°C.

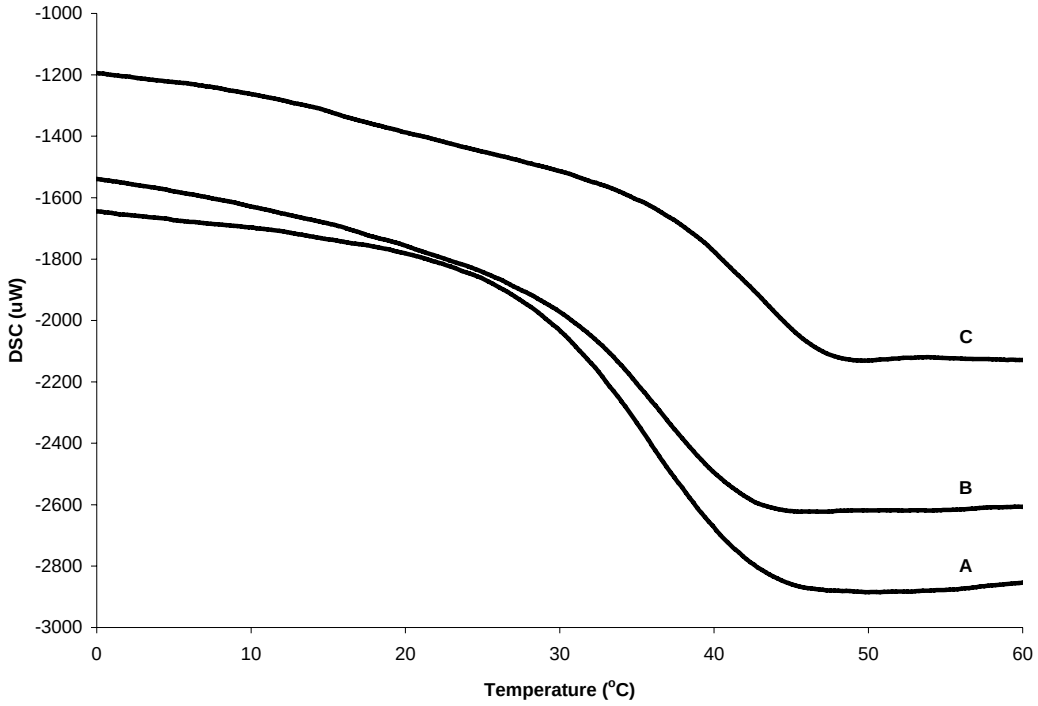

Figure 28: DSC versus temperature of 20:80 CL:DLLA polymers
20:80 copolymer (A) and 20:80 blends –high temperature blend (B) and solvent blend (C)

The 20:80 blended polymer, electrospun at the same conditions as the 10:90 and 40:60 copolymers, resulted in flexible fibres after removal from the mandrel. The electrospun fibres had an average diameter of 2.1±0.1 μm along with a fibre diameter distribution shown in Figure 29. The majority of the fibres were in the 0.8 – 1.3 μm range, which was important since one of the design criteria of the scaffold was to have fibres of sub-cellular dimensions (~ 10 μm).

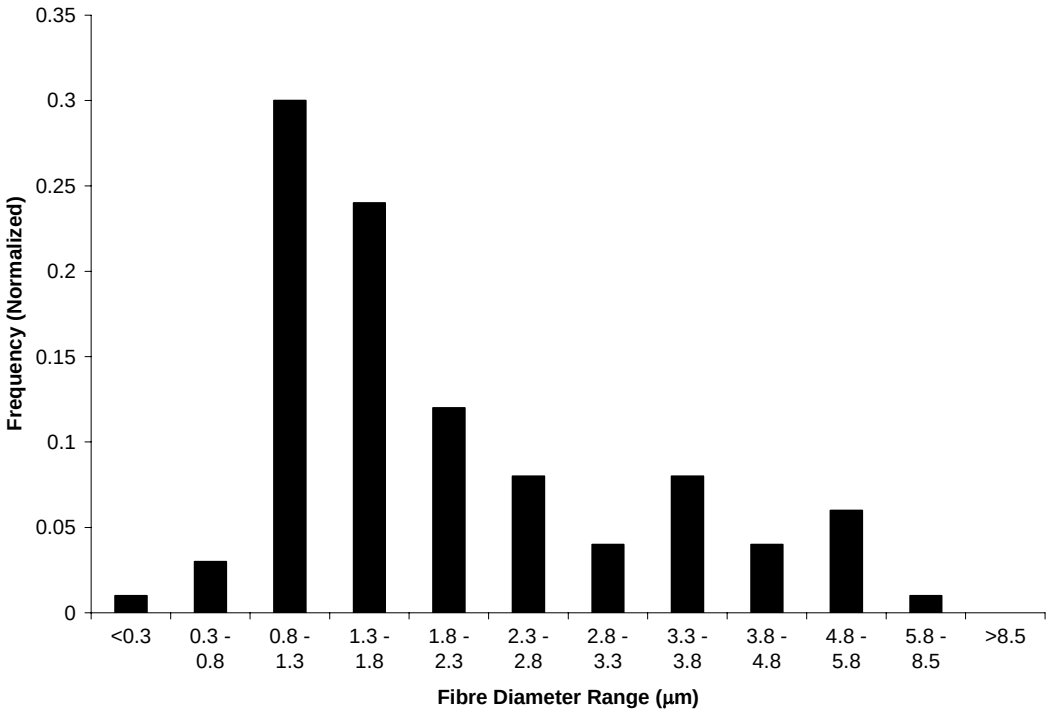

Figure 29: Electrospun PCLDLLA fibre diameter distribution
Data was taken from a set of n=100

The calculated density of 1.22g/cm^3 was used to find the cross sectional area for each fibre mat using the respective gauge length. The averaged stress-strain curve for the fibre mats are shown below in Figure 30. The number of fibres in each mat was calculated by a weighted average based on the fibre diameter distribution to then calculate an individual fibre stress-strain curve (Figure 31).

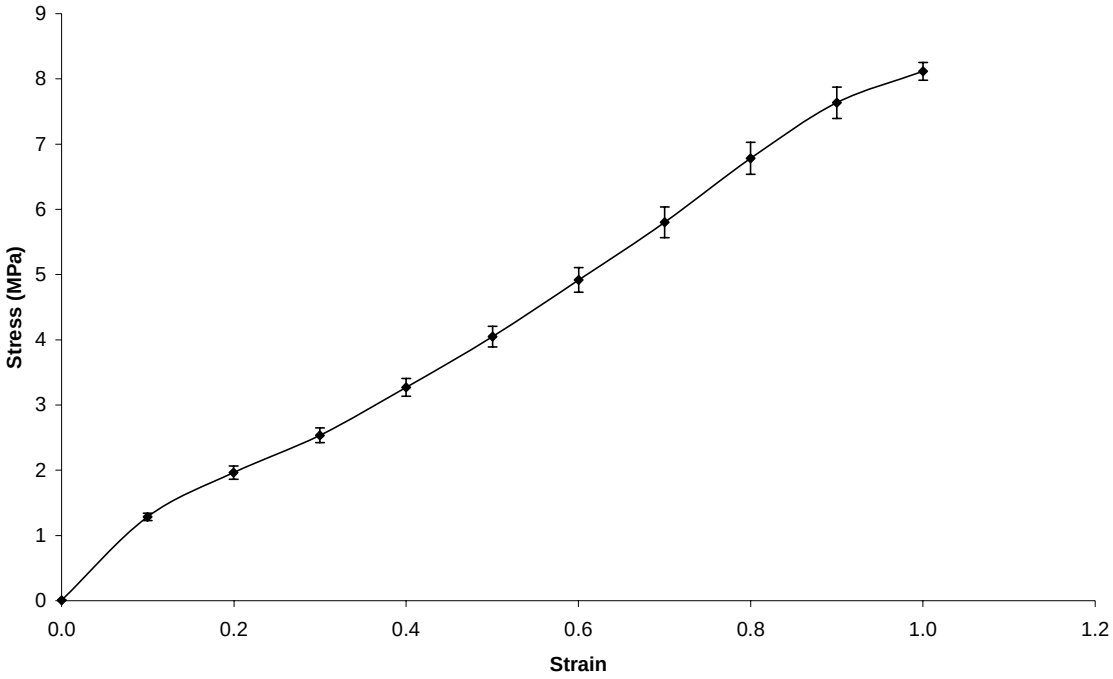

Figure 30: Averaged true stress-strain curve for PCLDLLA electrospun fibre mats
Data was compiled using an n=4

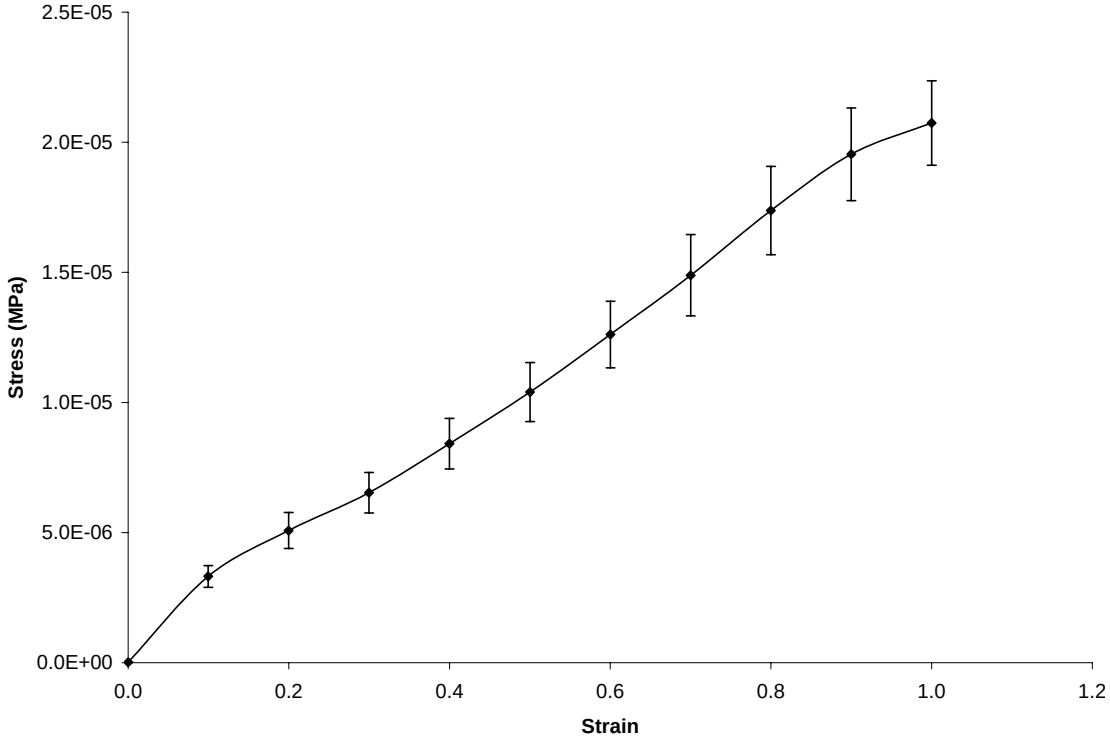

Figure 31: Averaged individual fibre true stress-strain curve
Average calculated using a weighted diameter distribution and an n=4

From the stress-strain curves it was observed that the behaviour of the mats and individual fibres did not resemble that of the native ligament. However, the goal of this thesis was not to produce fibres to mimic the function of the collagen fibrils but, to mimic the collagen fibrils in structure and dimension. The stress-strain curves were only calculated to obtain a better understanding of the mechanical properties of the fibres. This data could then be used to calculate important design information if the fibres were to be used in a mechanically loaded situation.

5.1.2.2 Fibre Crimp

The electrospun 20:80 blended polymer fibres were aligned and collected in tension due to the design of the wire mandrel. Once the aligned fibres were removed from the mandrel, the fibres generated a crimped configuration/pattern. These compressive forces that were generated in the individual electrospun fibres were measured and are shown below in Figure 32.

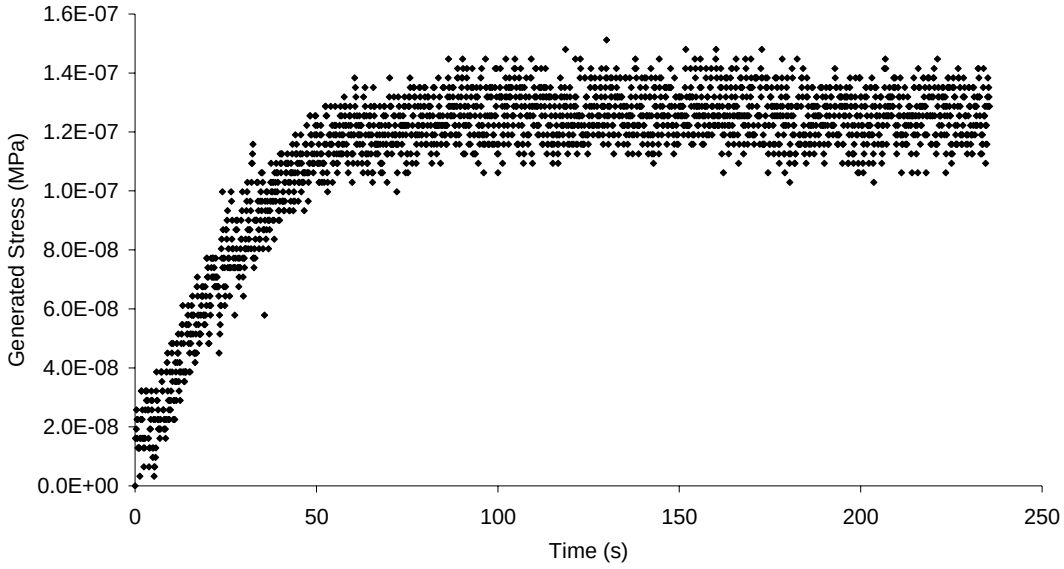

Figure 32: Generated stress over time in a single PCLDLLA fibre
Average calculated based a weighted diameter distribution

A

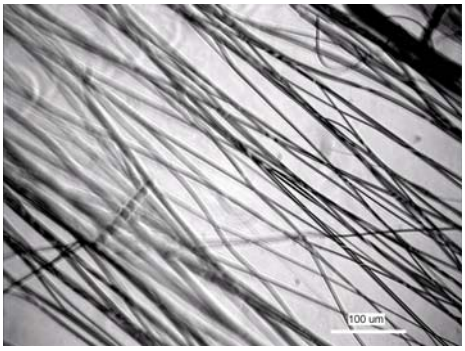

B

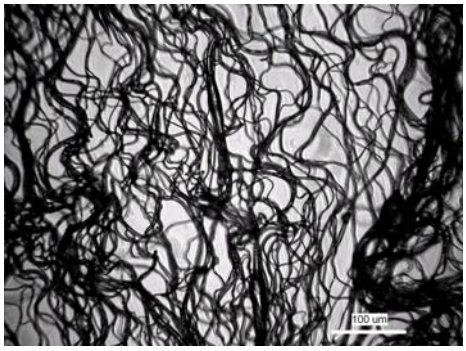

Figure 33: Electrospun 20:80 blend PCLDLLA fibres aligned and with crimp pattern 100 μm scale bar, A – aligned blended fibres collected in tension from the mandrel and B – blended fibres after base etching in 0.5 M NaOH (dried)

The production of the crimp pattern was accelerated and enhanced during the aqueous base-etching process (Figure 33). Further experiments revealed that this acceleration effect was most likely due to the hydrophobic nature of the fibres. Fibres that were tested with the same etching protocol but with water in place of the NaOH solution produced a similar crimp pattern to the base-etched fibres (Figure 34).

A

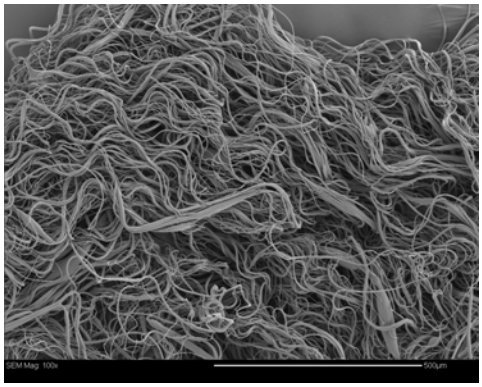

B

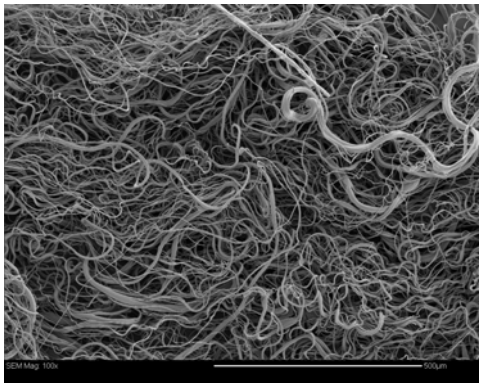

Figure 34: SEM images of crimped and dried electrospun 20:80 blend PCLDLLA fibres 500 μm scale bar, A – water control and B – 15 min base etch in 0.5M NaOH

The crimp parameters of the electrospun 20:80 blended polymer fibres was found to be very similar to the crimp parameters found in the native ligament (Table 8). Figure 35 compares the dimensions of the crimp in the Picrosirius Red stained bovine ligament and the crimped PCLDLLA electrospun fibres.

Table 8: Comparison of crimp wavelength and amplitude values

Source	Crimp Wavelength (μm)	Crimp Amplitude (μm)
Amiel *et al.*[1]	45-60	5-10
Native Bovine Ligament (n=50)	51± 1	-
20:80 Blended Fibres (n=100)	55±3	10±1
20:80 Copolymer Fibres (n=100)	151±6	23±1

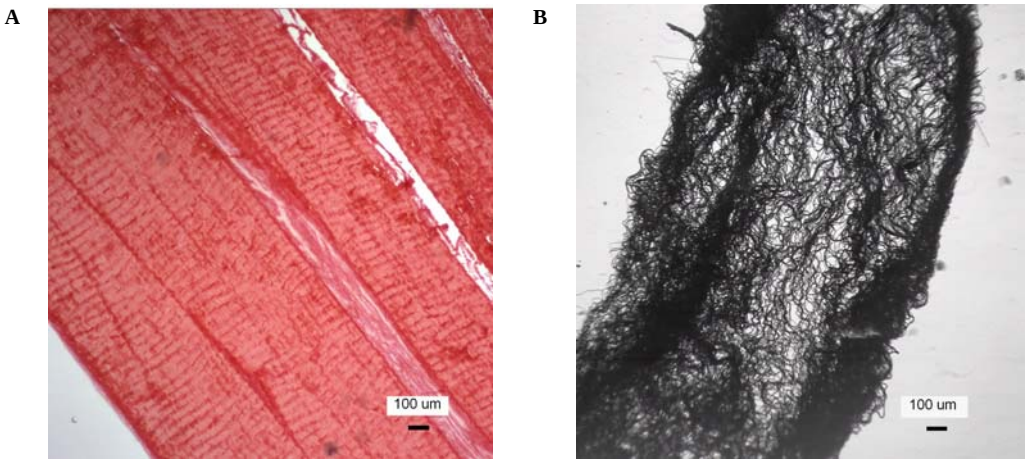

Figure 35: Comparison of native ligament and crimped 20:80 blend PCLDLLA fibres
100 μm scale bar, A – native bovine ligament stained with Picrosirius Red and B – 0.5 M NaOH base-etched blended fibres (dried)

To understand why the fibers were crimping, additional experiments were conducted on the 20:80 blended polymer fibres. Initially, it was thought that the mismatched physical

properties between the 10:90 and 40:60 copolymers were the cause for the crimp pattern[173]. However, a single T_g value indicated that these blends were completely miscible (Figure 28) and therefore comparable to unblended copolymers of the same CL:DLLA ratio. To confirm this fact, a 20:80 copolymer was synthesized (see Table 7 for properties) and electrospun. After base-etching, the 20:80 copolymer also produced a crimp pattern (Figure 36).

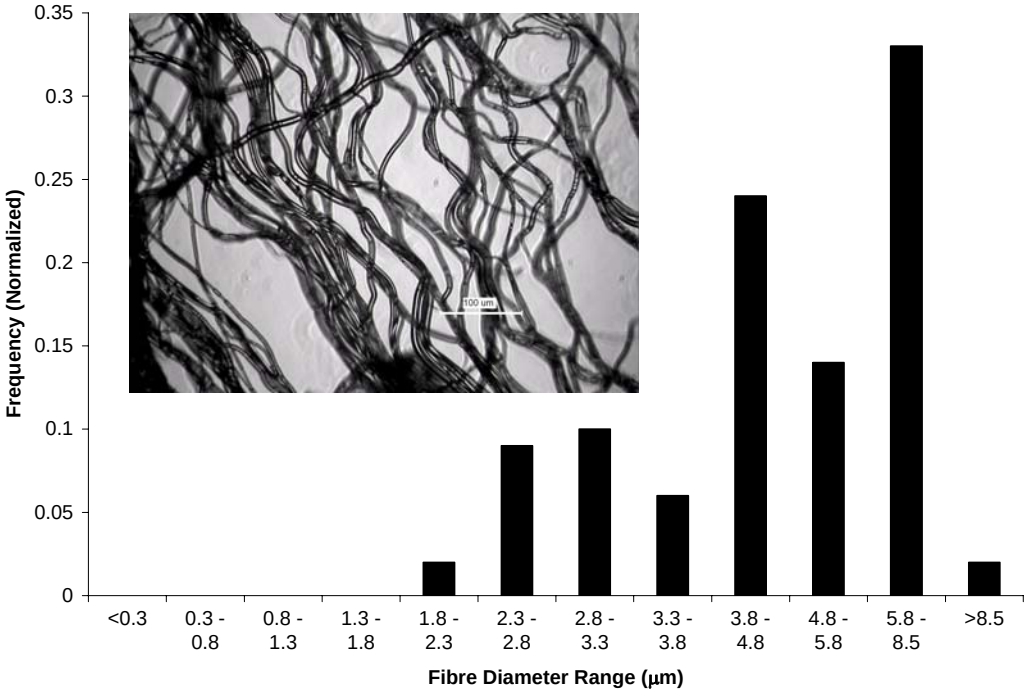

Figure 36: 20:80 copolymer - diameter distribution and image of base-etched fibres

The newly synthesized 20:80 copolymer had a higher molecular weight compared to the 20:80 blended polymers (Table 7). These results, as well as the previous chitosan findings, indicated that molecular weight had an effect on the fibre diameters under the

same electrospinning conditions. The higher molecular weight of the 20:80 copolymer led to an increase in the average fibre diameter to 5.0±0.2 μm. This was an increase of approximately 2.5 times that of the 20:80 blended polymer fibres. Interestingly, the magnitude of the crimp pattern (wavelength and amplitude, data shown in Table 8) for the electrospun 20:80 copolymer fibres were also approximately 2.5 times greater then the 20:80 blended fibres.

The system examined here consisted of copolymerized phases with different material properties: an elastic CL component and a stiff and glassy DLLA component. It was possible that the stiffer DLLA components were resisting the stress relaxation of the elastic CL components once the fibres were removed from the mandrel. From the results, it appeared that fibre crimping was facilitated by the aqueous wetting and drying process of the base etching procedure. In addition, the crimp pattern may be based on the CL:DLLA ratios (controlled through the copolymerization reaction or blending) and fibre diameter (controlled through the electrospinning process). This knowledge could be used to tailor the crimp pattern for certain applications and scaffold designs for tissue engineering.

5.1.2.3 Surface Modification

To observe the effect of the base-etching process on the 20:80 blended polymers, the fibres were base-etched in 0.5 M NaOH from 5 min – 3 hrs. Surface roughening and pitting were observed from the SEM pictures (Figure 37). The onset of surface roughness was detected at 15 min with major defects noticed at 3 hrs.

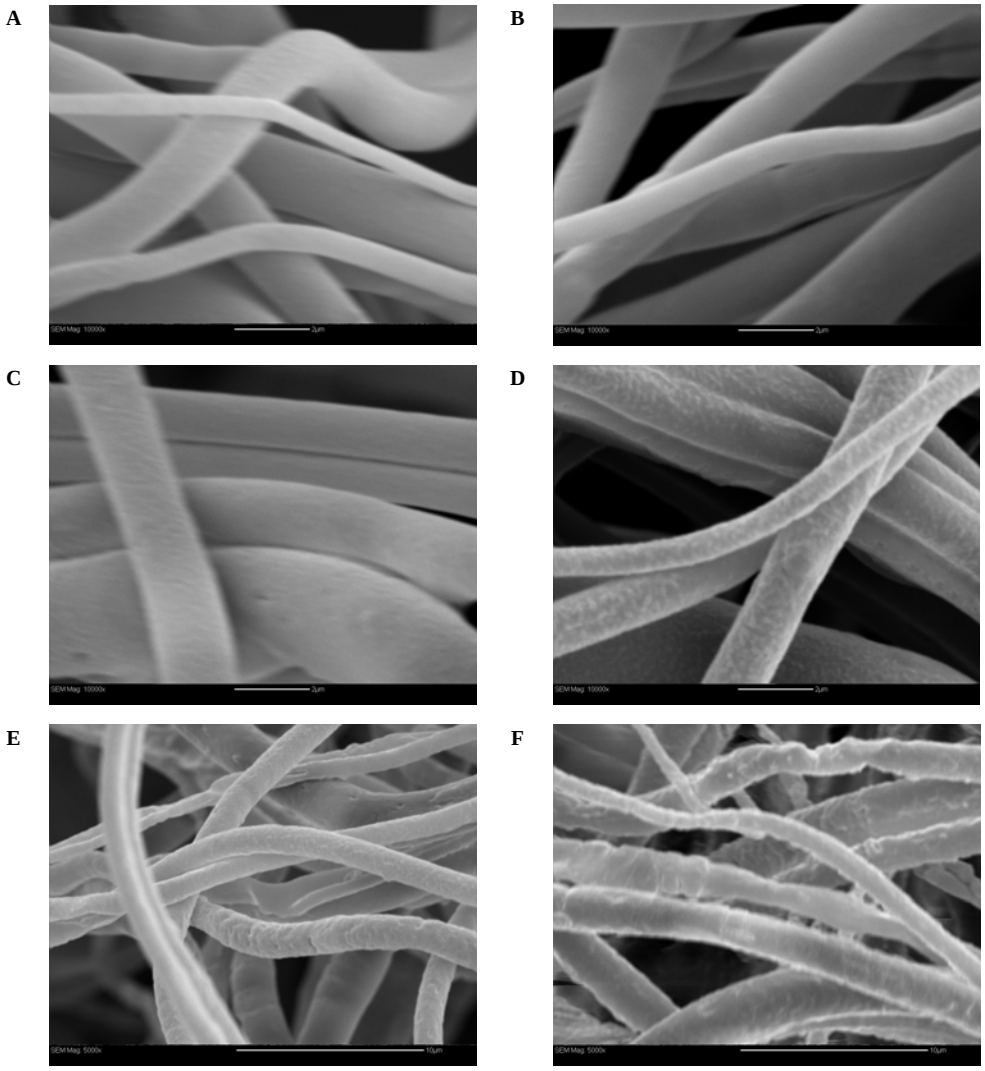

Figure 37: SEM images of 0.5M NaOH base-etched electrospun 20:80 blend PCLDLLA fibres Images A-D (2 μm scale bar) and for images E and F (10 μm scale bar), A – original fibres, B – 5 min, C – 15 min, D – 45 min, C – 90 min and D – 180 min

From the SEM pictures the surfaces were obviously being altered. In addition to the changes in surface roughness, reaction with the OH^- ions in solution and the carboxylate esters present in the polymer should have produced carboxylic acid and hydroxyl functional groups on the surface. ^1H NMR and ATR-FTIR were used to detect the presence of these groups on the surface of the PCLDLLA polymer.

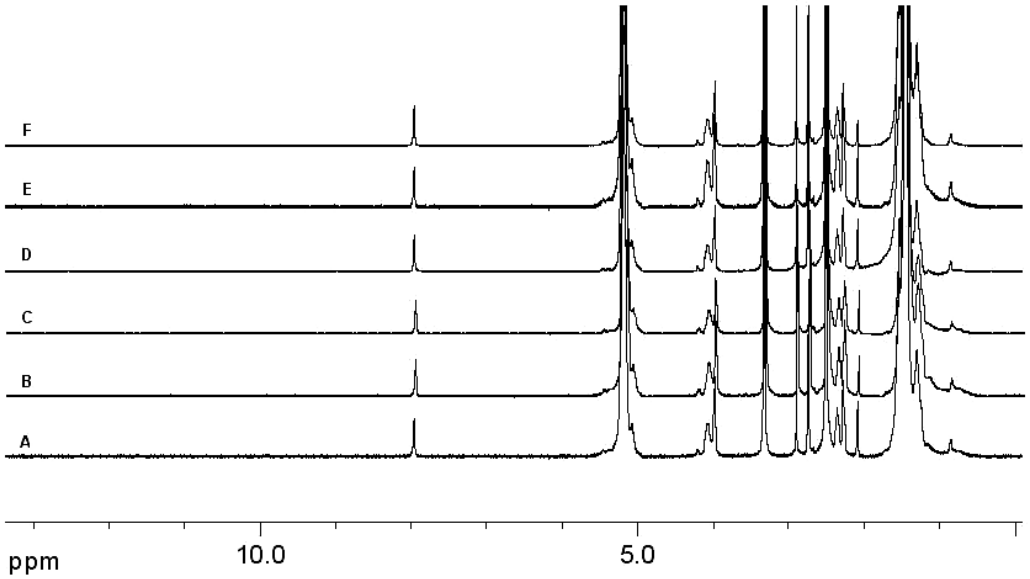

Figure 38: ^{1}H NMR spectra base-etched electrospun 20:80 blend PCLDLLA fibres to detect change in surface chemistry after base etching process
A – original electrospun fibres, B – 0.5M NaOH 5min base etch, C – 0.5M NaOH 15min base etch, D – 0.5M NaOH 45min base etch, E – 0.5M NaOH 1.5hr base etch, F – 0.5M NaOH 3hr base etch. DMSO was used as the solvent

However, no peaks were observed in the characteristic 10-12 ppm range for carboxylic acid in the ^{1}H NMR spectra for the variety of etching times tested (Figure 38). These results indicated that either no functional groups or only a very small amount below the detection limit were generated on the polymer surface. ATR-FTIR results on the base-etched thin films (Figure 39) were similar to those of the ^{1}H NMR results in that no changes were detected from the original thin films. If sufficient concentrations of carboxylic acid and hydroxyl groups were formed on the surface, ATR-FTIR would have detected a fairly board peak in the 3000-3700 cm^{-1} range due to hydrogen bonding and dimer formation with the carboxylic acid groups.

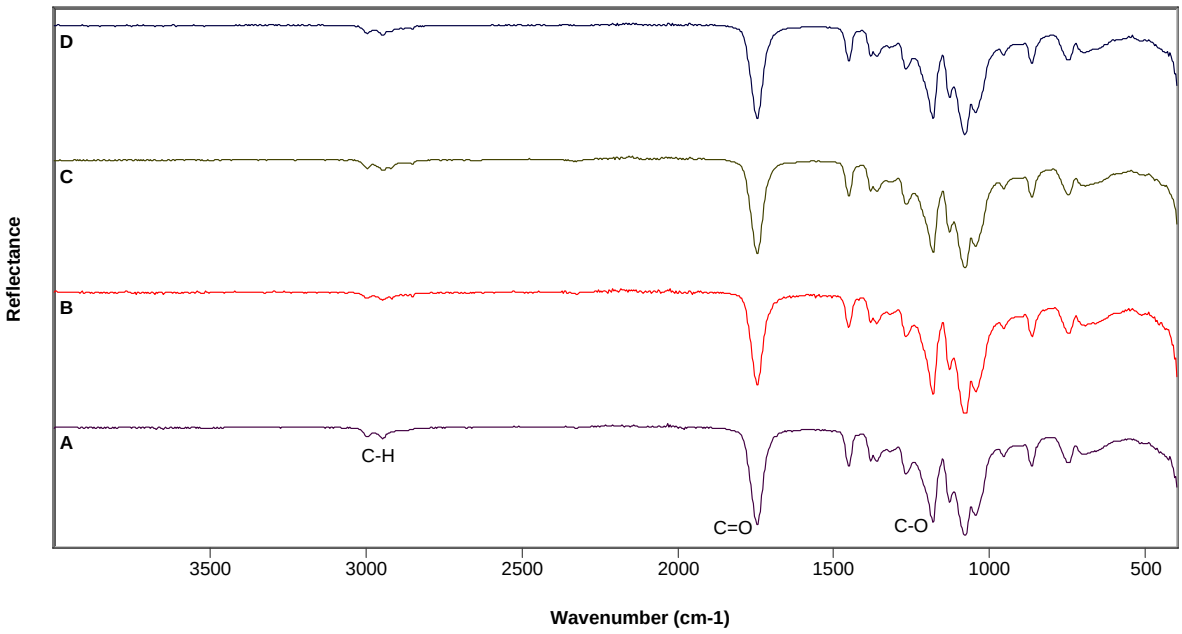

Figure 39: ATR-FTIR of base-etched 20:80 blend PCLDLLA thin films to determine change in surface chemistry
A – Original thin film, B – 0.5 M NaOH base-etched for 30 min, C – 0.5 M NaOH base etch for 1.5 hr and D – 1 M NaOH base etch for 1.5 hr.

Since the base etching technique only modifies the surface[127,174], the amount of functional groups produced is relatively small compared to the larger bulk of the material. Therefore, if surface functional groups were being produced on the polymer surface, it was possible that the ^{1}H NMR and ATR-FTIR analysis techniques were not sensitive enough to detect them. To determine if the base-etching process had enhanced the hydrophilicity of the polymer surface through the production of hydrophilic carboxyl and hydroxyl groups[175], water contact angle measurements were measured. The results indicated a change in contact angles between the original and base-etched PCLDLLA thin films. Original thin films had a contact angle of 90±1° compared to the base-etched surface with a contact angle of 82±1° (Figure 40). These contact angles were higher than those found in literature for similar polymer thin films. Ishaug-Riley *et al.*[176] reported

static water contact angles of 79±3°, 78±2° and 75±1° for spin cast PDLLA, PCL and 10:90 PCLDLLA unmodified thin films. It was possible that the solvent evaporation technique was not ideal for manufacturing the most uniform thin film surfaces. The roughening of the surface through the thin film manufacturing and base-etching processes (Figure 37) could be a reason for the higher then normal contact angles[177]. However, regardless of the higher contact angles, a change was observed between the original and base-etched PCLDLLA films. Therefore, the water contact angle results demonstrated that the base-etching process was most likely producing some functional groups on the PCLDLLA surface.

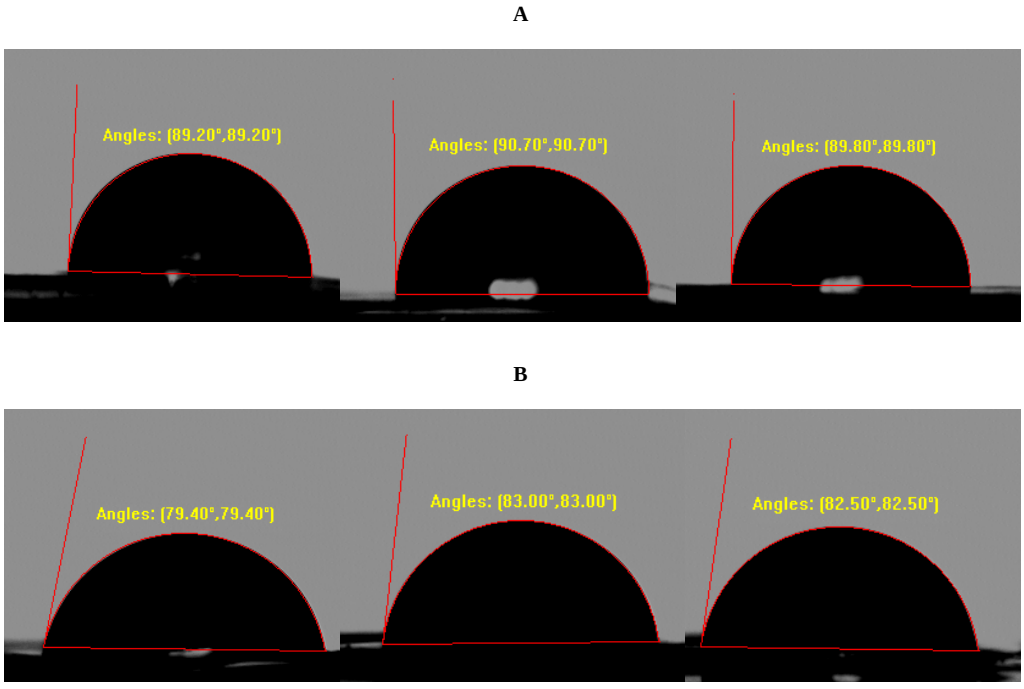

Figure 40: Water contact angle measurements for 20:80 blend PCLDLLA thin films Base etching was done with 0.5 M NaOH for 1.5 hrs, A – original and B – base-etched

A cell growth study was performed on the base-etched PCLDLLA thin films to visualize if these surface changes were beneficial to cell attachment and proliferation. The assay was performed on the original and base-etched 20:80 blended thin films with TCP surface as a control. From the results, the original thin films showed a much lower cell density and a less spread out cell morphology than the base-etched thin films and TCP surface after two weeks in culture (Figure 41). It appeared that this combination of increased surface roughness and enhanced surface chemistry was advantageous for cell attachment and proliferation.

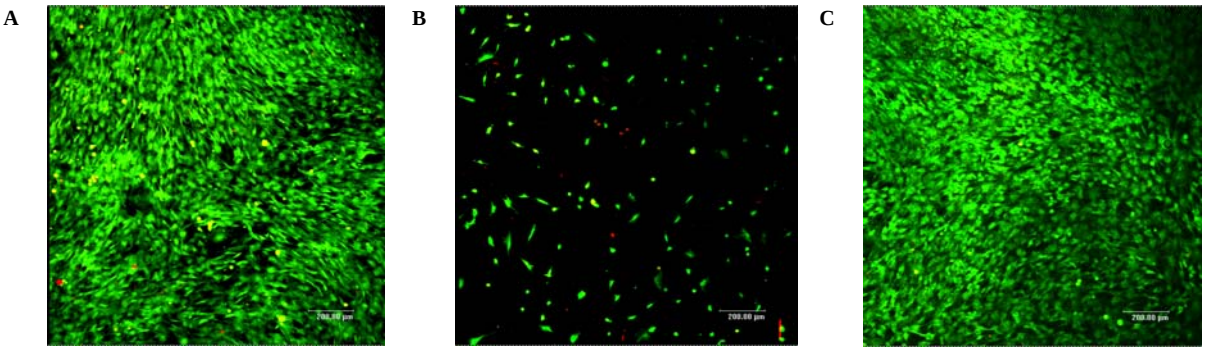

Figure 41: Cell attachment assay of original and modified 20:80 blend PCLDLLA thin films Representative confocal images after 2 weeks in static culture of A – control, B – Original thin film and C – 1.5 hr 0.5 M NaOH base-etched thin films, 200 μm scale bar

5.2 Hydrogels

5.2.1 Genipin and Glycol Chitosan

The genipin crosslinked glycol chitosan (GC) hydrogel was investigated first, since it was already established and shown to have acceptable viability levels after crosslinking[142,143,146]. Experimental results indicated that genipin was able to crosslink GC and create a hydrogel within 2-3 hrs at 37°C. However, the hydrogels were crosslinked to such an extent that they were brittle and broke apart when handled. Mi *et al.*[178] showed that chitosan crosslinked with genipin at neutral pH had the lowest degree of swelling when compared to hydrogels formed at pH 5, 9 and 13.6 due to the formation of tetramer crosslinks. The formation of these tetramer crosslinks would explain the brittle properties observed for the genipin crosslinked hydrogels. Performing the genipin crosslinking reaction at pH 13.6 has been shown to improve the mechanical properties of the chitosan hydrogel[147]. However, the long gelation times at conditions other than physiological pH could have adverse effects on the encapsulated cells. Therefore, the genipin-GC gelation system was not pursued further.

5.2.2 Poly(ethylene glycol) Diacrylate and Glycol Chitosan

The next hydrogel system investigated was the 1-4 Michael-type reaction with 700 g/mol poly(ethylene glycol) diacrylate (PEGD700). The advantage of using a 1-4 Michael type addition system was that the reaction between the free amino group on the glycol chitosan backbone and the carbon-carbon double bonds on PEGD700 is spontaneous at room temperature. However, hydrogels formed through a 1-4 Michael-type addition reaction require fairly long gelation times for complete conversion and their network

formation and degradation behaviors are not well established[132]. The network and the degradation properties of the hydrogel are important as they influence the diffusion of nutrients, metabolic waste products and immune molecules that could potentially lead to adverse effects on the encapsulated cells[129,148,150]. Long gelation periods are also undesirable as they could lead to cell nutrient deprivation or overexposure to unreacted crosslinking agents. Therefore, a variety of experiments were conducted to determine if cell encapsulation was feasible with a PEGD700 crosslinker and GC using a 1-4 Michael-type reaction.

To determine the working weight percent of GC, the highest weight percent with a solution viscosity that was still workable with a pipette or syringe was used. A higher weight percent of GC allowed for faster gel times because of the higher concentration of molecules present for reaction with PEGD700. The maximum workable GC concentration was found to be 6 wt% in 1X PBS. From the five 6 wt% GC:PEGD700 molar ratios that were tested (1:15, 1:30, 1:45, 1:60 and 1:80), the 1:45 molar ratio was the lowest concentration of PEGD700 (0.7% v/v PEGD) that resulted in acceptable crosslinking times (useable gels within 4-6 hrs). Sol fraction and equilibrium water content results for the 1:45 molar ratio gel were 16.9±1.1% and 89.0±0.3%, respectively. A gel stability study was also conducted and found that the gels completely degraded within 2-3 days in 1X PBS at 37°C with agitation. However, the degradation time was not considered a disadvantage for gel selection, since the main purpose of the hydrogel was to mimic the viscous proteoglycan matrix of the ligament and act as a cell delivery vehicle.

To determine if the cells would be able to survive the 4-6 hr gelation period without culture medium, a nutrient deprivation study was conducted. Cells were grown to confluence and the culture medium was replaced with 1X PBS for 1 to 24 hrs and cell viability was assessed using a Live/Dead™ assay (Figure 42). By 4 hrs the majority of the cells were still attached to the TCP surface but cellular condensation and loss of cellular striation was observed in a number of the cells. Similar results were observed at 6 hrs with the cells expressing a more intense yellow stain indicating an unhealthier state. By 24 hrs, the cells were completely condensed and showed limited coverage on the TCP surface. There were still some signs of cell viability, but a higher overlap with a red staining (dead cells) was observed in the confocal images.

The condensation of cells and increase in red staining could be a sign that the cells were possibly in a stage of programmed cell death (apoptosis) or necrosis[179]. Regardless, the majority of the fibroblasts were shown to be able to survive nutrient deprivation within the length of time required for gelation (4-6 hrs). These findings were within the range reported by Izuishi *et al*.[180] where 60% fibroblast viability was demonstrated after 12 hrs of nutrient deprivation.

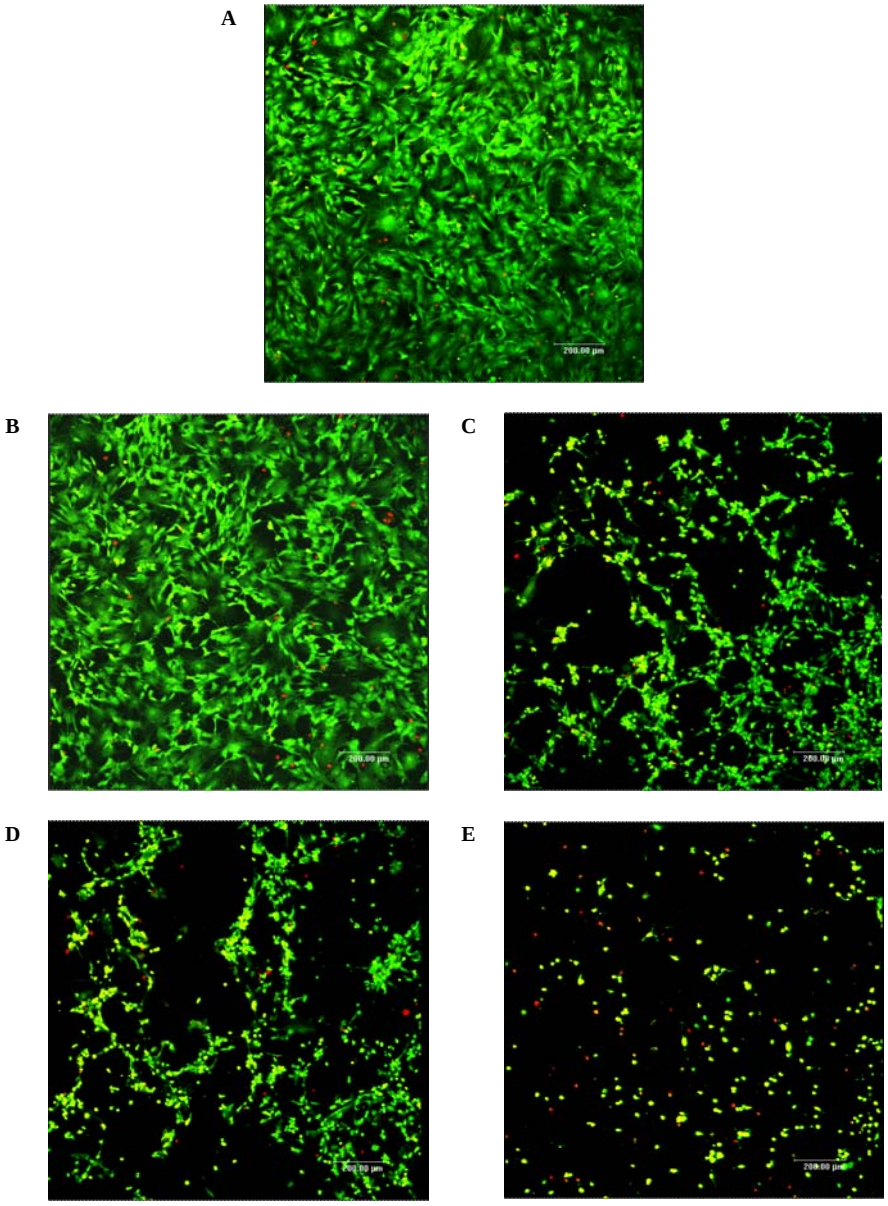

Figure 42: Nutrient deprivation study
200 μm scale bar, media was replaced with 1X PBS and cultured for respective times, A – TCP control, B – 1hr, C – 4hr, D – 6hr and E – 24hr

To test the cytotoxicity of PEGD and GC, these components were individually added to the culture media for a 24 hr period (Figures 43 and 44). Cell viability was assessed using the Live/Dead™ assay. Lower concentrations of chitosan (1.5wt%) than those in

the hydrogels (6wt%) were used for the cytotoxicity testing. The reason for the lower concentration was that the high molecular weight of the chitosan caused the culture media to become too viscous at higher concentrations that could lead to adverse side effects. Crosslinker cytotoxicity testing was done using concentrations in the range close to the actual amount used in the hydrogels. This was done as there was more concern of the cytotoxic effects of the crosslinkers then the hydrogel materials.

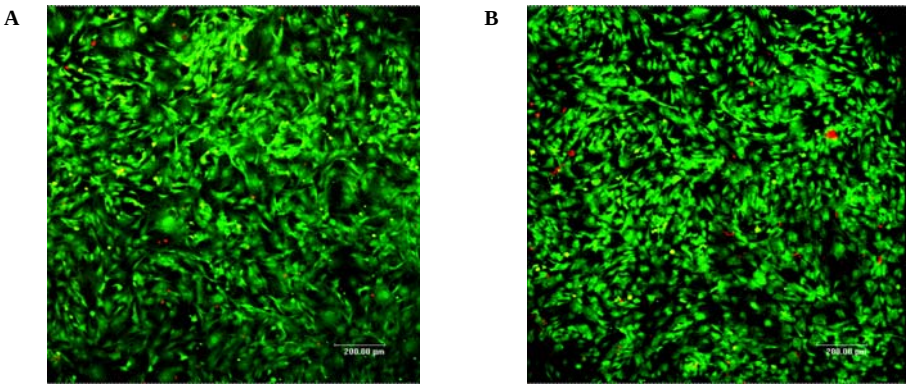

Figure 43: 24 hr cytotoxicity testing with 1.5wt% GC in 5% FBS culture media 200 μm scale bar, A – TCP control and B – after 24hr exposure

A 24 hr exposure of 1.5 wt% GC did not seem to have any adverse effects on the cells (Figure 43). On the other hand, 0.2% v/v PEGD700 was observed to have an effect on the cells within 10 min and this effect was more obvious after 30 min of exposure (Figure 44). By this time, cells started to condense and turn yellow indicating higher staining for the EthD-1 and possibly an early indication of cell necrosis/apoptosis as previously described. Cell viability was approximately 50% by 6 hrs and by 24hrs the majority of the cells were dead.

This toxicity occurred at lower concentrations (0.2% v/v) than those used in preparing the hydrogels (0.7% v/v) (Figure 44). However, similar results were also observed with a higher concentration of 5% v/v PEGD700 (data not shown) which indicated that the cytotoxicity of the PEGD700 was a result of exposure time rather than concentration. Shin *et al*.[136] reported that low molecular weight PEGD (575 Da) was cytotoxic within 2 hrs. Similarly, from these experiments PEGD700 resulted in poor cell viability with noticeable cytotoxic effects by 6 hrs. It was speculated that the acrylate groups on the PEGD molecules caused the cytotoxic effect. Therefore, the GC:PEGD700 and 1-4 Michael-type crosslinking method was not pursued further.

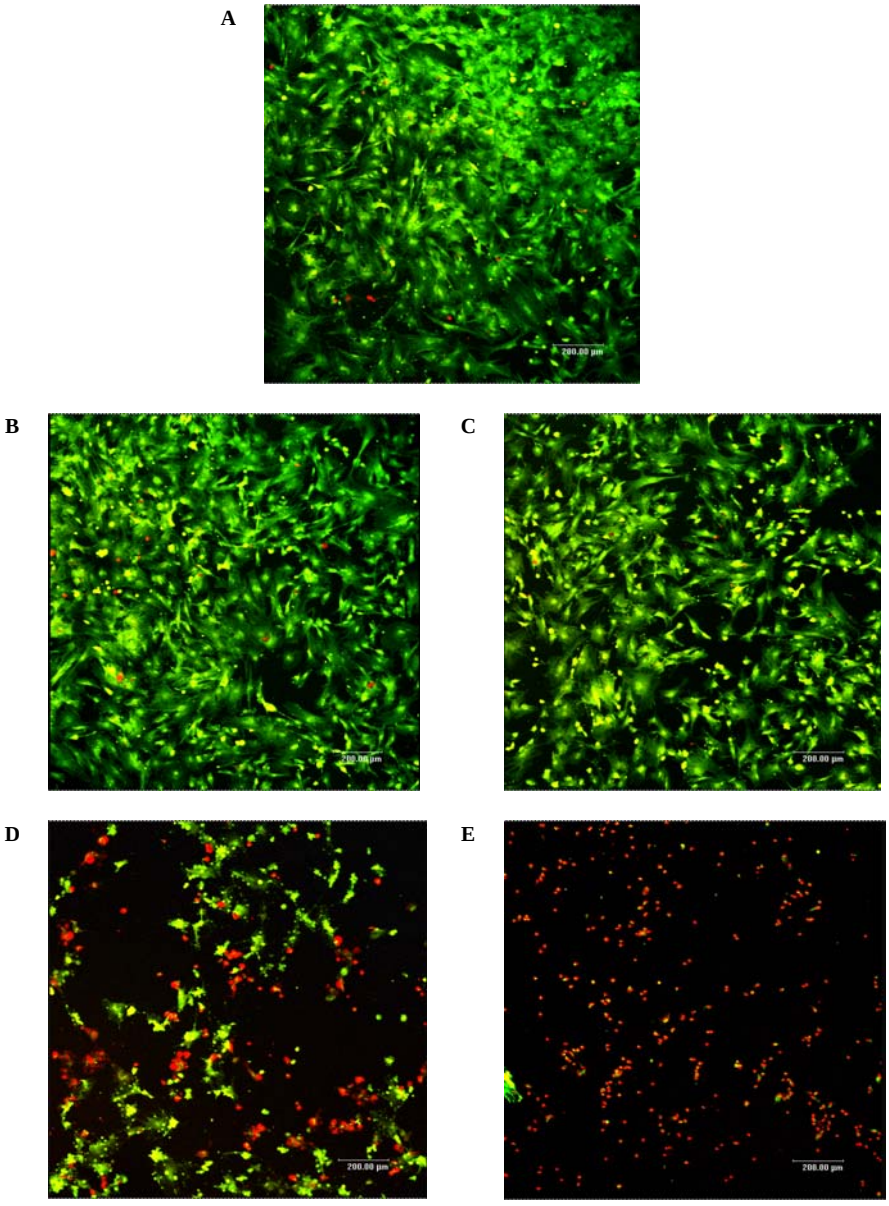

Figure 44: 24 hr cytotoxicity testing with PEGD700 in 5% FBS DMEM
200 μm scale bar, various exposure times with 0.2% v/v PEGD, A – 10 min, B – 30 min, C – 1 hr, D – 6 hr and E – 24 hr, (TCP control same as figure 45A)

5.2.3 Irgacure 2959 and Methacylated Glycol Chitosan

After the poor results observed with the other crosslinking systems, a photoinitiated system was investigated. A variety of water soluble photoinitiators and UV light sources have been shown to have some degree of toxicity towards cells, depending on their concentration and UV exposure times[149]. However, the rapid rate of the photocrosslinking reaction leads to relatively short exposure times (seconds to a few minutes)[150] to the harmful UV light source and chemical crosslinkers, and so cytotoxicity was expected to be low within this system.

Photocrosslinked hydrogels were prepared using methacrylated glycol chitosan possessing a degree of methacrylation of 4% (4M-GC). A 3 wt% 4M-GC solution was determined to be an optimum weight percent for use in the photocrosslinked hydrogels. The solution viscosity of the 3 wt% M-GC solution was low enough to prevent bubbles from being trapped in the solution after mixing and was high enough to produce a usable gel with good mechanical properties. Typically, UV light intensities of less than 10 mW/cm^2 and exposure times of 5-10 mins[149,152] are utilized. However, the lowest possible reading from the UV light source was 24 mW/cm^2. Therefore, the shortest exposure time was utilized to crosslink the hydrogel to minimize any adverse effects on the cells. It was found that the minimum exposure time that resulted in a gel that could be physically handled was 1 minute with 0.02% w/v I2959. These gels were found to have sol fractions and equilibrium water contents of 5.4±3.6% and 95±1%, respectively after 48hrs in 1X PBS. Based on these results, the 4M-GC/I2959 gels were considered suitable for *in vitro* culture testing.

To test the cytocompatibility of the photoinitiator, confluent cells were cultured with 0.04% w/v I2959 (double the concentration to be used to create the 4M-GC hydrogels) for 24 hrs and assessed using the Live/Dead™ assay (Figure 45). After the 24 hr culture period, the cells appeared to be slightly more yellow when compared with the controls (regular culture media), which could be an indication of cell death as previously mentioned. However, cells encapsulated in the gel would not be exposed to the photoinitiator for that length of time since the initiator would be rapidly consumed upon exposure to the UV light source. A potential problem was the cytotoxicity of the methacrylate groups present on M-GC. Therefore, M-GC with different degrees of methacrylate substitution (1, 4 and 8 %) was tested to determine any cytotoxicity effects. From these results, the methacrylate groups did not appear to have a large effect on cell viability. The majority of cells remained viable after the 24hr cytotoxicity testing with cell viabilities of 84±3%, 78±5% and 77±7% for 1, 4 and 8 % methacrylation M-GC, respectively. There was no noticeable difference between the different degrees of methacrylate substitution (concentration), which was similar to the finding with PEGD700.

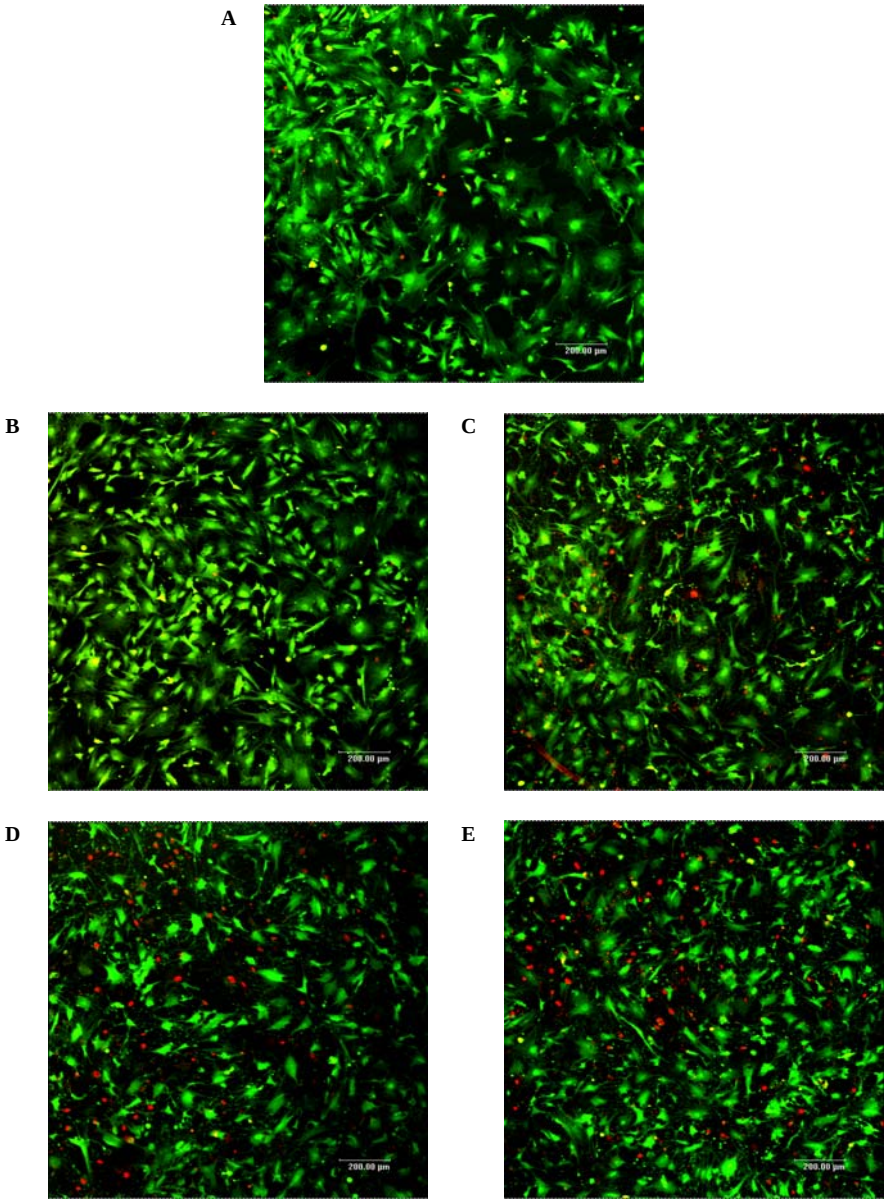

Figure 45: 24 hr cytotoxicity testing with M-GC and I2929 hydrogel components
200 μm scale bar, A – Control, B – D2959 (0.04 %w/v), C – 1M-GC, D – 4M-GC, E – 8M-GC.
(concentration of 1.5 wt% M-GC in 5% FBS/DMEM was used)

As all of the hydrogel components had acceptable cytotoxicity, a 24hr cytocompatibility test with passaged (P1) bovine ligament cells encapsulated in the 4M-GC hydrogels was conducted. Viability was assessed using the Live/Dead™ assay and results indicated that

there was approximately 57±3% cell viability after 24 hrs (Figure 46). The photocrosslinking process resulted in a noticeable decrease in cell viability either from the crosslinking process or the UV light source.

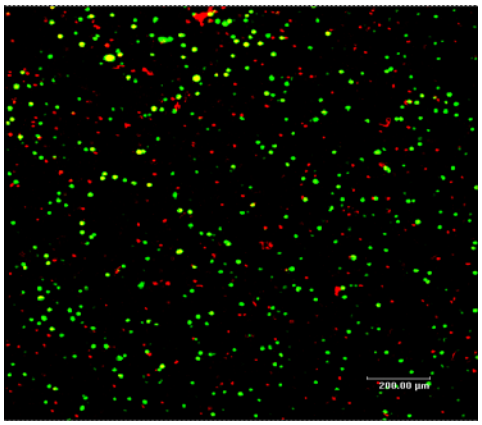

Figure 46: 24 hr 4M-GC/I2959 hydrogel cytotoxicity test with P1 bovine ligament cells 200 µm scale bar, cell viability was not tested with primary cells due to a higher occurrence of cell clumping in the gels, which made it difficult to determine an accurate live/dead cell ratio.

However, of the three gelation methods examined, the 4M-GC/I2959 photocrosslinking system was found to be the only one suitable for cell encapsulation studies. The other methods were not acceptable to be used in the biomimetic scaffold design either due to poor mechanical properties or poor cytocompatibility results. Results from the 4M-GC/I2959 hydrogel cytotoxicity study indicated that there were enough viable cells after the photocrosslinking process that it was feasible to be used as a cell delivery matrix.

5.3 Biomimetic Scaffolds

Approximately half of the maximum fibre content was used (4 mg) in the biomimetic scaffolds to give the cells adequate space between the fibres. To determine the effectiveness of these biomimetic scaffolds, two control scaffolds were also examined: a gel-only and a fibre-only scaffold. Analysis of the gel-only scaffold was used to determine if the hydrogel cell delivery system was effective for the entire culture period. By analysing the results of the gel-only and biomimetic scaffold, conclusions could also be made about cell growth behaviour between the two systems. The use of the fibre-only scaffold was to determine if the conventional (non-gel) cell seeding method was an effective means of delivering cells throughout the scaffold. A comparison of the three scaffolds could be used to determine how effective the biomimetic scaffold was for this particular tissue engineering application.

During the entire culture period, a gel-only construct was taken for analysis at 24 hrs and 1, 2 and 4 weeks using a Live/Dead™ assay to determine cell viability. This analysis was used as an in-progress monitoring system for the other scaffolds as they were opaque and could not be imaged with confocal microscopy. Results indicated that the cells remained viable throughout the entire culture period (Figure 47). However, upon closer inspection, the cells appeared to be growing in enlarged clusters and were seen thriving near or on the surface of the gels by the fourth week in culture (Figure 48 and 49).

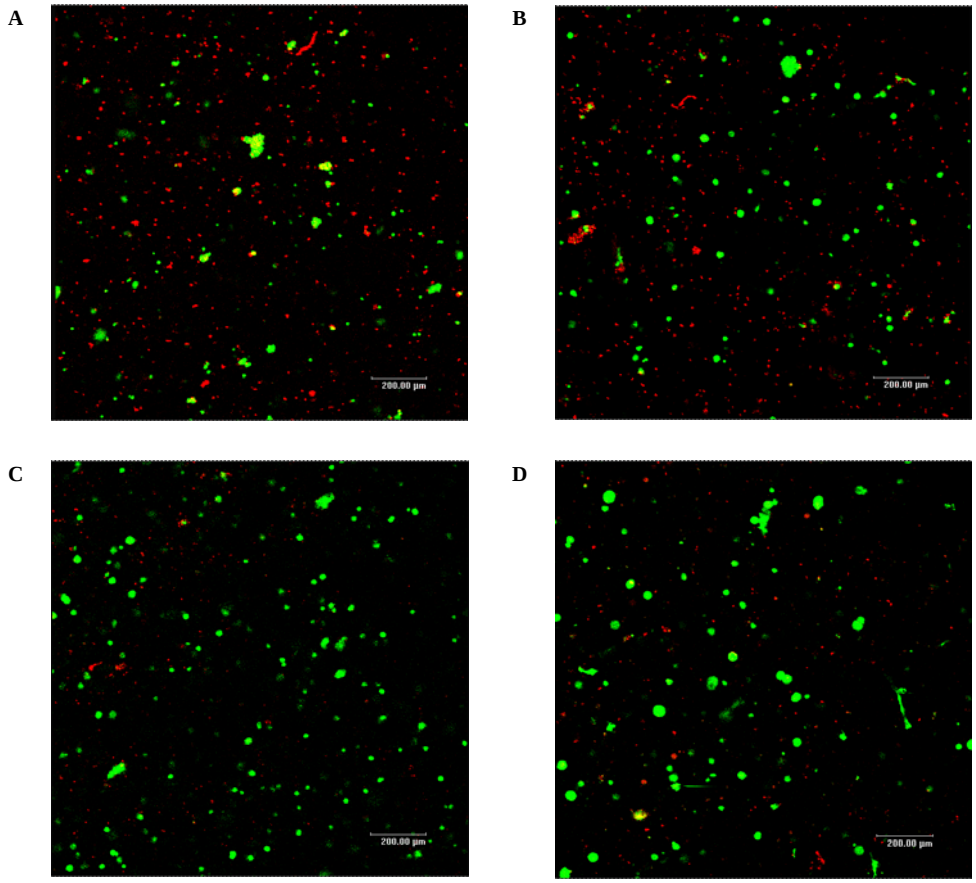

Figure 47: Primary ligament cells grown in M-GC/I2959 hydrogels for various times 200 µm scale bar, A – 24 hr, B – 1 week, C – 2 weeks, D – 4 weeks.

Higher magnification brightfield and confocal images gave a better understanding of the cell behavior in these cell clusters after 4 weeks in culture. Figure 49 showed that there was a fairly even mixture of live and dead cells within the clusters. There was also a large amount of space in the cluster that was not stained, which could indicate possible tissue production.

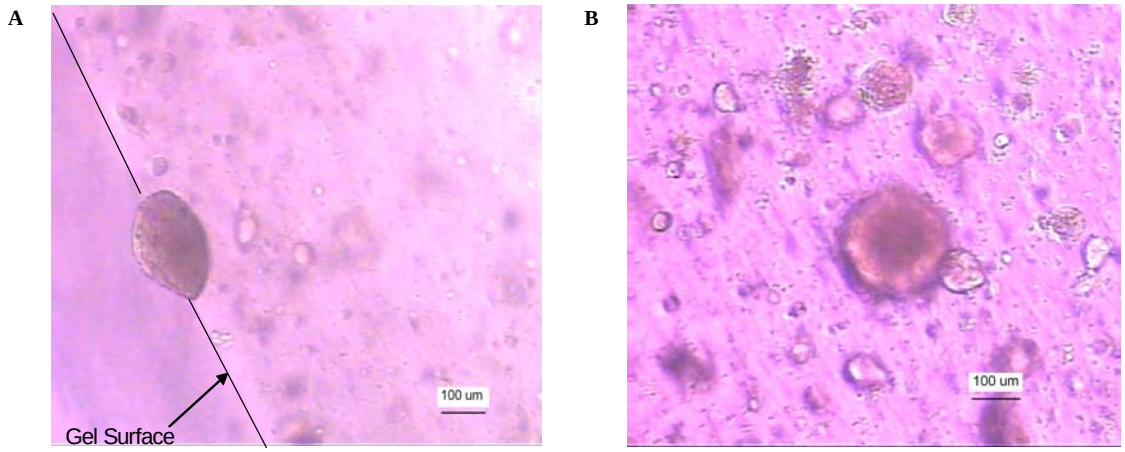

Figure 48: High magnification brightfield images of cell clusters
100 μm scale bar, A – on hydrogel surface and B - near gel surface after 4 weeks

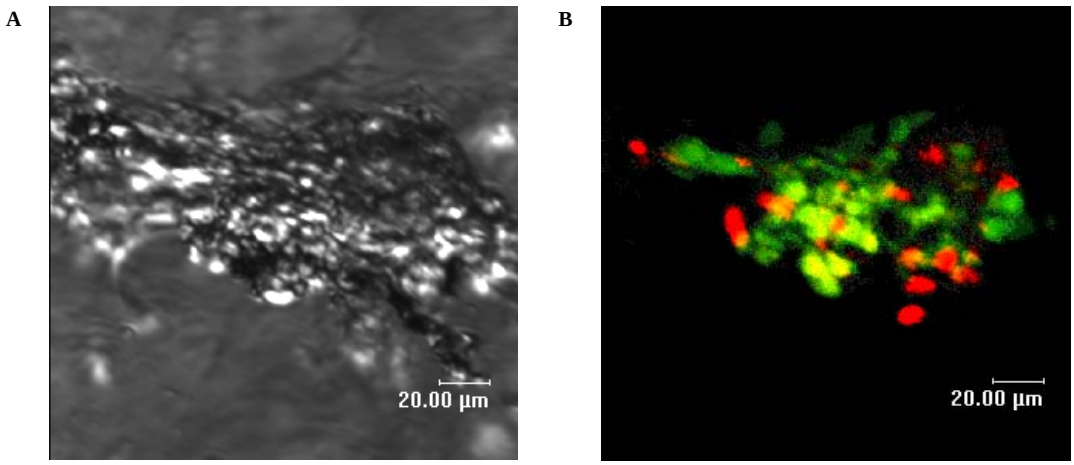

Figure 49: High magnification confocal images of cell clusters near gel surface after 4 weeks in culture
20 μm scale bar, A – Brightfield, B – Live/Dead™ assay confocal red/green channel overlay

In addition to the Live/Dead™ assay for the gel-only scaffolds, immunohistochemistry (IHC) with fluorescent secondary antibodies was performed on all of the scaffolds. IHC allowed for the visual identification, localization and organization of any tissue produced within the scaffolds. Negative controls, where the primary antibody was replaced with

goat serum, indicated that non-specific binding of the secondary antibody was not present in any of the scaffolds (Figure 50).

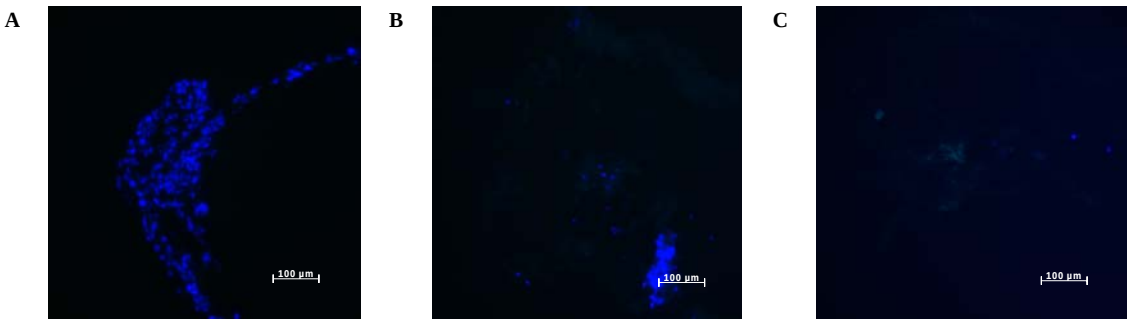

Figure 50: Negative controls performed on 28 day scaffolds omitting primary antibody 100 µm scale bar, A – Fibre-only scaffold, B – Gel-only scaffold, C – Biomimetic scaffold (blue nucleus staining DAPI)

To determine if any false-positive staining occurred due to with the scaffold materials, an acellular biomimetic scaffold was sectioned and stained using the normal IHC protocol. The results indicate that the PCLDLLA fibres and M-GC hydrogel did not produce any false staining (Figure 51).

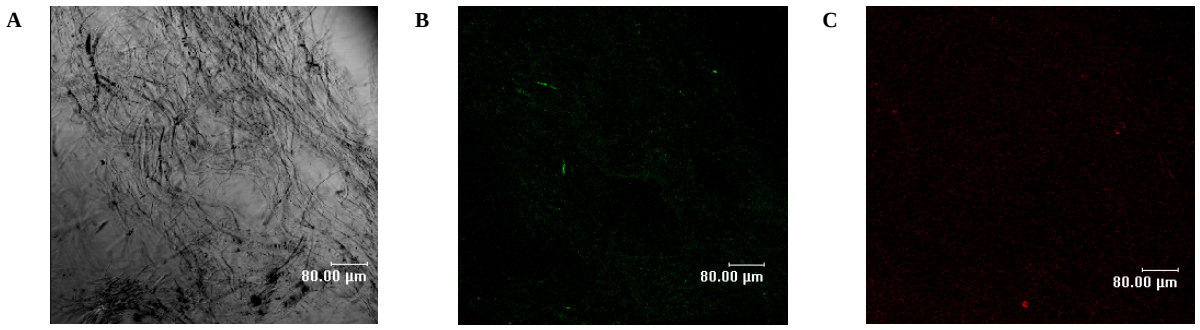

Figure 51: Acellular biomimetic scaffold stained using the normal IHC protocol 80 µm scale bar, to determine if false staining from the scaffold materials was occurring, A – Brightfield, B – stained with collagen type I 1° (FITC 2°), C – stained with collagen type III 1° (Texas Red 2°)

While preparing the fibre-only scaffold for tissue culture work it was discovered that the fibres collapsed upon themselves due to hydrophobic interactions with the aqueous media. After 4 weeks in culture, the fibres had completely collapsed and visual identification of fibre alignment along the long axis of the scaffold was no longer possible. This effect produced a planar cell culture surface that did not allow for cell or tissue integration into the scaffold. Therefore, over the 4 week culture period, cells produced a tissue capsule around the collapsed fibres. This phenomenon was evident in the cryo-cut fibre-only sections (Figure 52). Since not enough tissue was produced within the fibre-only scaffolds, the compacted PCLDLLA fibres detached from the slides during the IHC staining process. After IHC staining, only the tissue capsule surrounding the compacted fibres remained attached to the slides.

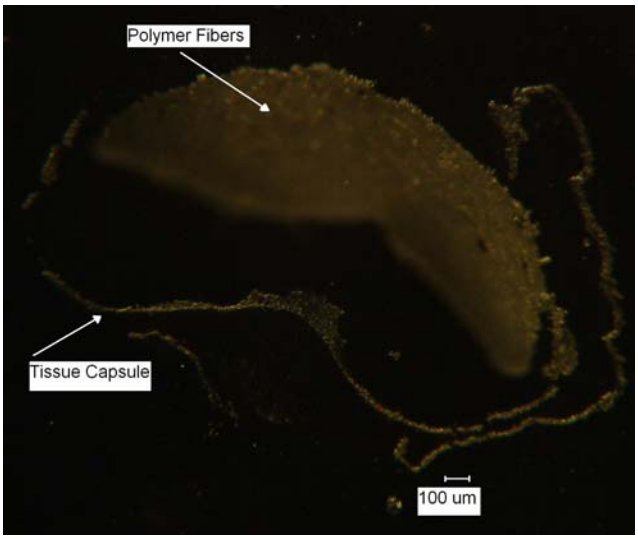

Figure 52: 28 day Fibre-only scaffold with tissue capsule encapsulating fibres 100μm scale bar, showing collapse of fibre scaffold and tissue encapsulation

Observations from the IHC images (Figure 53) of the fibre-only scaffold showed that the tissue capsules surrounding the collapsed fibres became more developed, and thicker, throughout the 4 week culture period. DAPI staining in the IHC images also indicated an increase in cell proliferation throughout the culture period. As well, there was the production of ligament-specific collagen type I and type III. During the first and second week, a higher amount of collagen type I than type III was observed whereas by the fourth week comparable amounts were observed. The results obtained from the fibre-only scaffolds were similar to previous reports on fibrous scaffolds using conventional seeding methods. The previous reports also demonstrated poor tissue integration due low porosity between the fibres[46,45,47,53,55,64].

An interesting result obtained with the fibre-only scaffold was that the primary fibroblasts grown on the planar surface of the collapsed PCLDLLA fibres were capable of producing similar collagen types to that in the native ligament. However, the tissue was not as highly organized and was much more cellular compared to that of the native ligament. The fact that ligament-specific tissue could be produced on a planar *in vitro* culture system could be useful to improve on future scaffold designs.

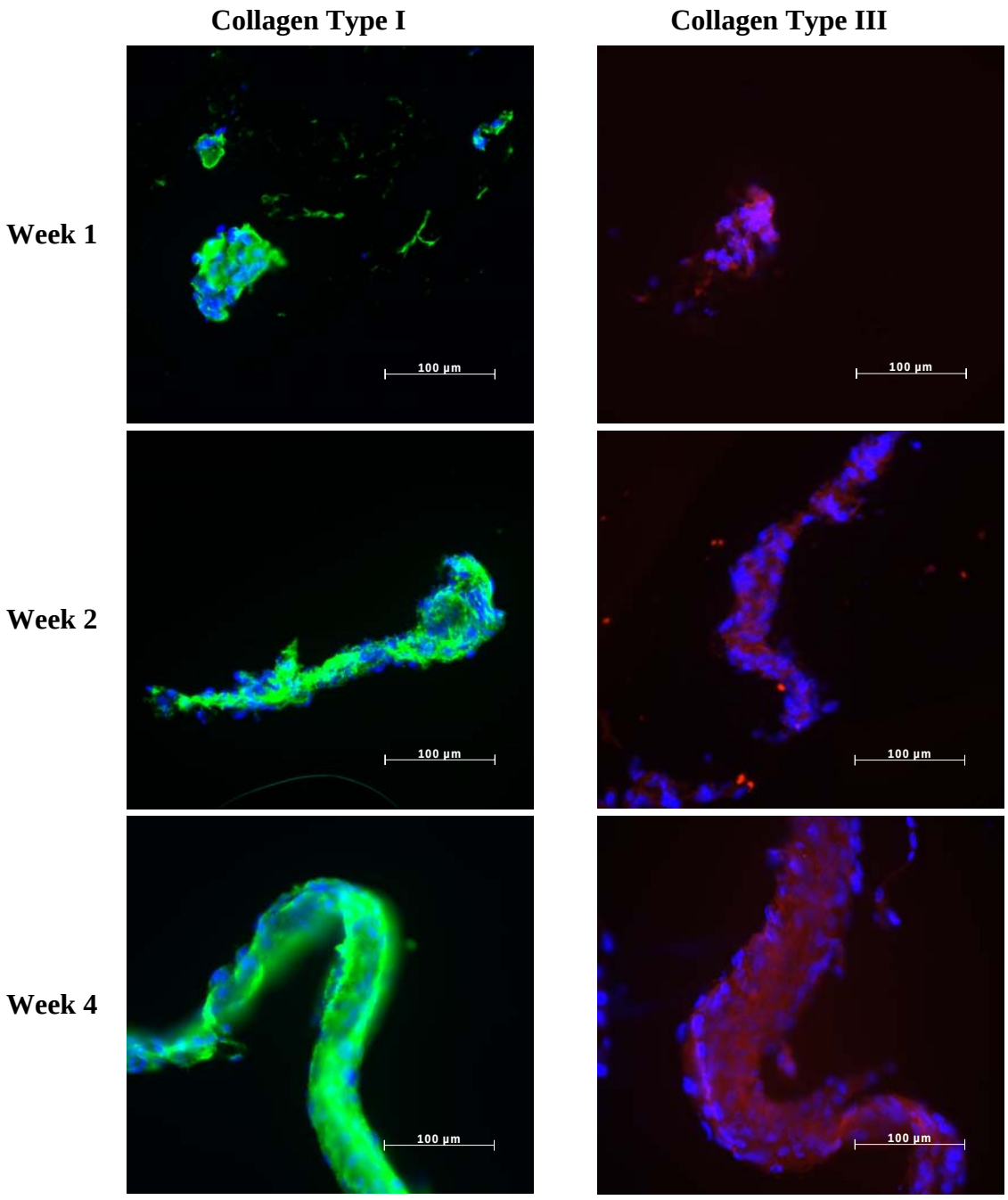

Figure 53: Fluorescent microscope images of fibre-only scaffold IHC staining on remaining tissue capsule for collagen types I and III
100 µm scale bar

IHC results for the gel-only control scaffold showed a decrease in cellularity over the entire culture period (Figure 54). However, the spherical cell clusters present throughout the hydrogel were observed to enlarge over time. These cell clusters also stained positive for both collagen types I and III, which increased over the 4 week culture period. By the fourth week, along with the cell clusters, smaller localized regions of collagen type I and III tissue appeared throughout the gel. These smaller regions within the gel-only scaffold were more evident with collagen type III staining. A low intensity stain was observed throughout the gel material by the fourth week, for both collagen types I and III. It was possible that higher amounts of collagen types I and III were being synthesized by the cells and accumulated throughout the gel matrix.

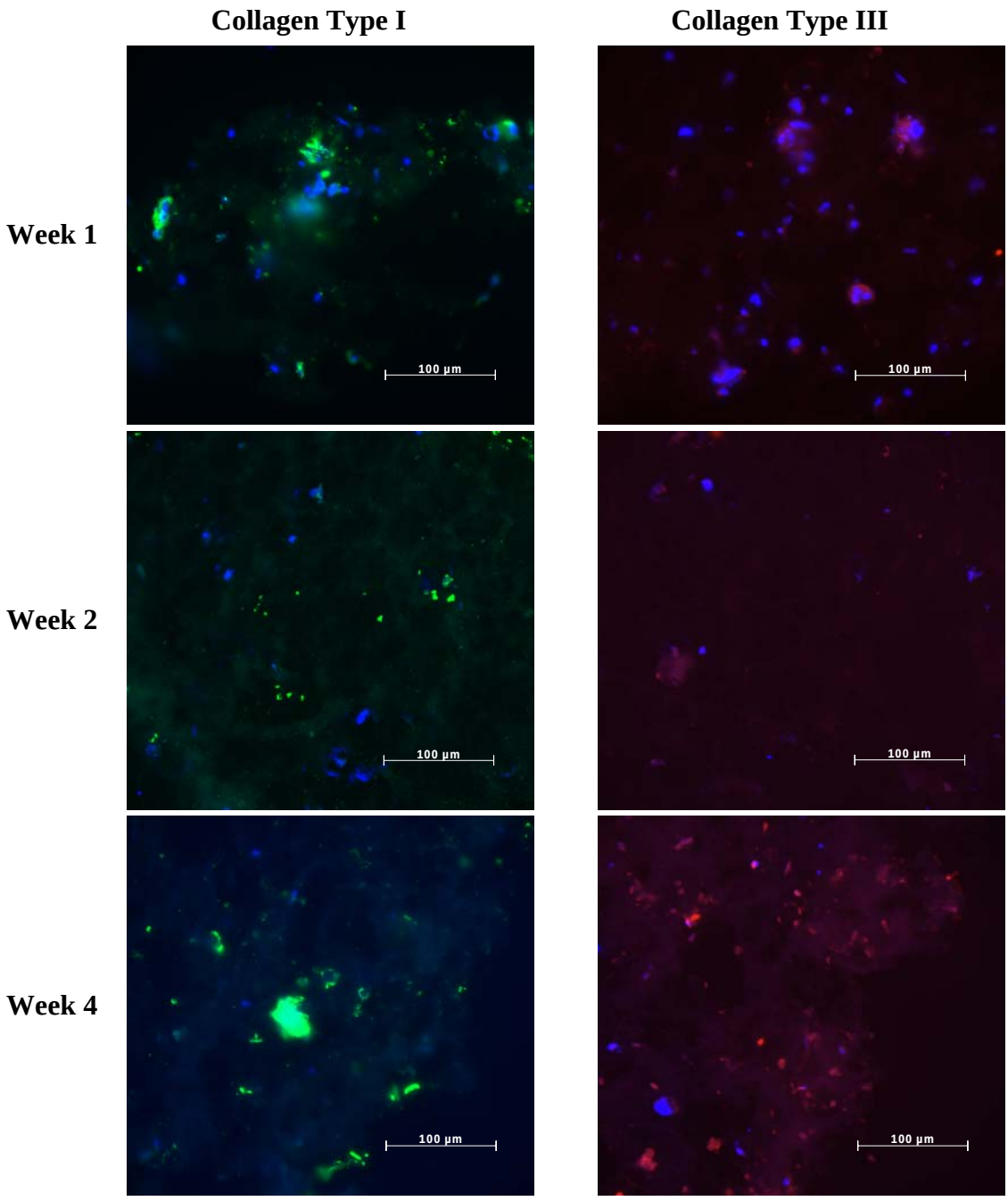

Figure 54: Fluorescent microscope images of gel-only scaffold IHC staining for collagen types I and III
100 µm scale bar

The biomimetic scaffolds showed similar results to the gel-only scaffolds in regards to ECM accumulation and cellularity within the scaffold. The fibroblasts appeared to be well distributed throughout the biomimetic scaffold. Over the four weeks of culture there was a slight decrease in the number of cells throughout the scaffold. By the fourth week, DAPI staining was only observed in the clusters and was slightly masked by the denser tissue staining from FITC and Texas Red. By comparing IHC fluorescent and confocal microscope images from the biomimetic scaffold it appeared that there was an increase in collagen type I production over the 4 week culture period (Figures 55 and 56). From the IHC images it appeared that a minimal amount of collagen type III was produced by the first week with a noticeable increase by the fourth week. In addition to the high intensity stained tissue clusters a non-specific, low intensity collagen type I and III fluorescence was observed throughout the gels and on the fibres by the fourth week. As previously mentioned, this fluorescence could be a result of an increase in tissue accumulation in/on the materials from the remaining cells producing new tissue and turning over the older tissue. This behaviour would be similar to ligamentum fibroblasts cells, which mainly perform ECM maintenance on the collagen fibril structure[13].

Similar cell/tissue clusters as in the gel-only scaffold were also observed in the biomimetic scaffold. However, one key difference between the clusters was that collagen types I and III attached and spread on the PCLDLLA fibres in the biomimetic scaffolds. These results confirmed that the base-etched fibre surfaces had enhanced cell adhesion properties. The results also indicated that the fibres were acting as tissue growth guides within the biomimetic scaffolds (Figures 55 and 57).

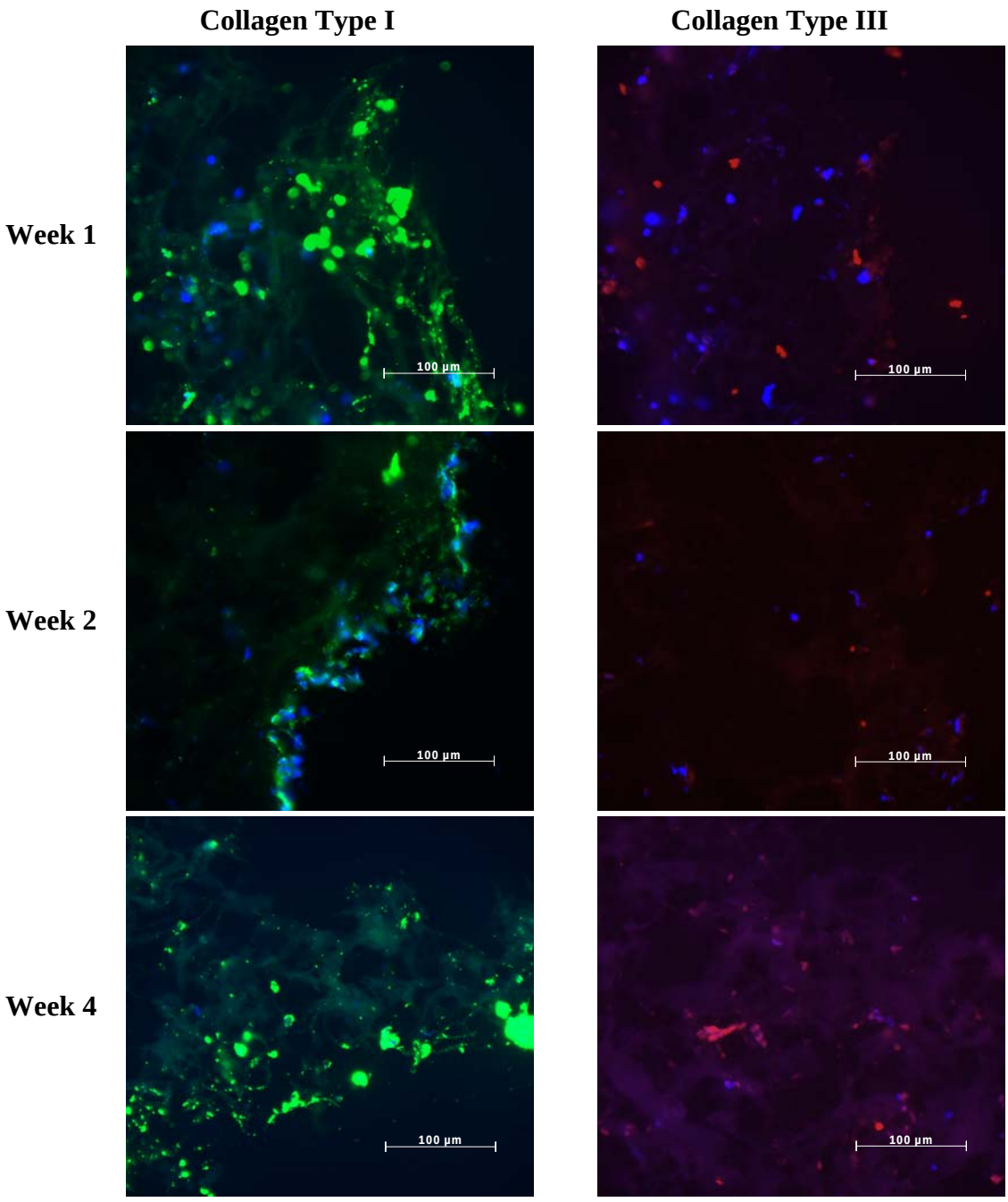

Figure 55: Fluorescent microscope images of biomimetic scaffold IHC staining for collagen types I and III
100 µm scale bar

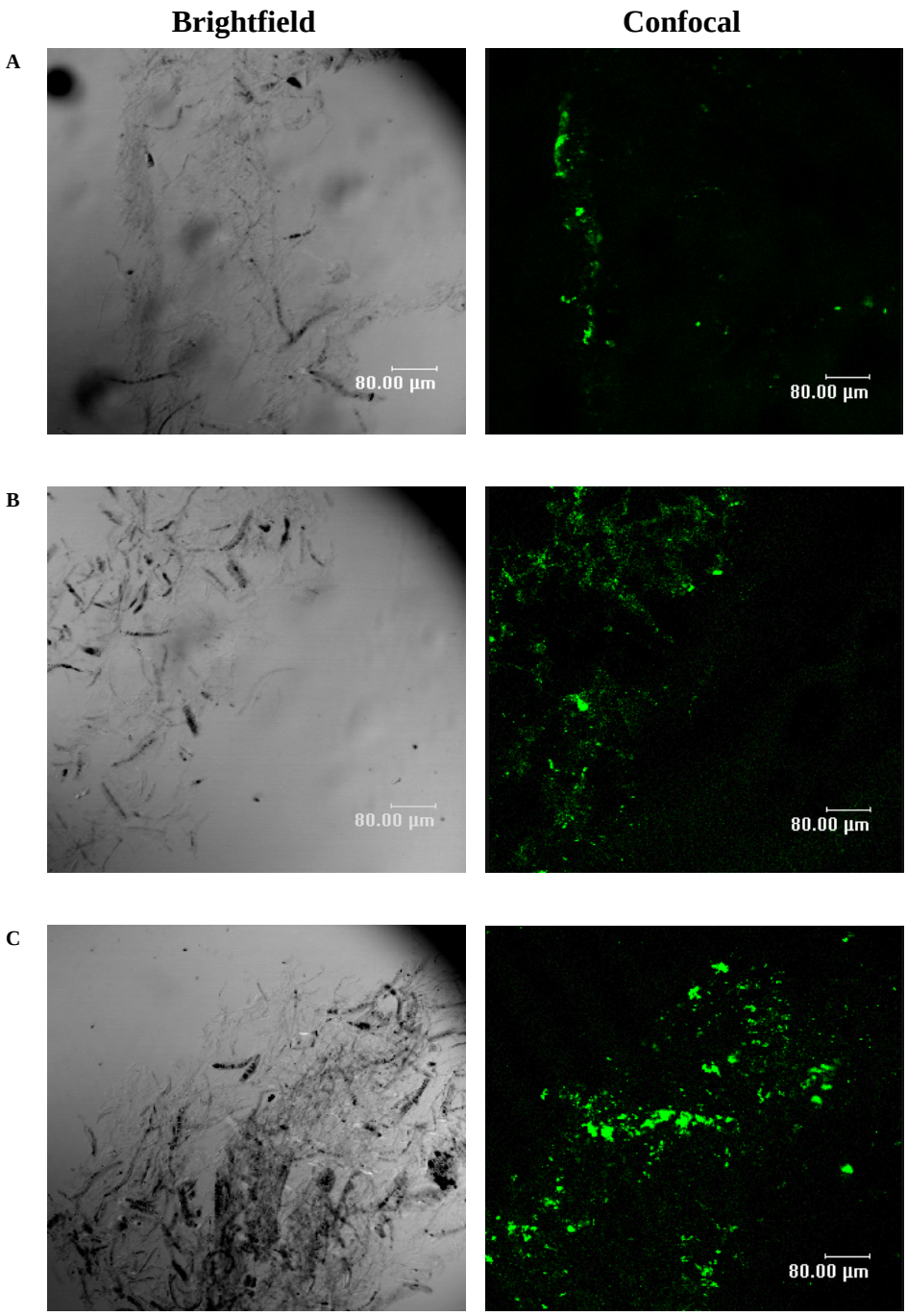

Figure 56: Confocal images of biomimetic Scaffold IHC staining for collagen type I (FITC) 80 µm scale bar, collagen type I staining with FITC, A – 1 week, B – 2 weeks and C – 4 weeks

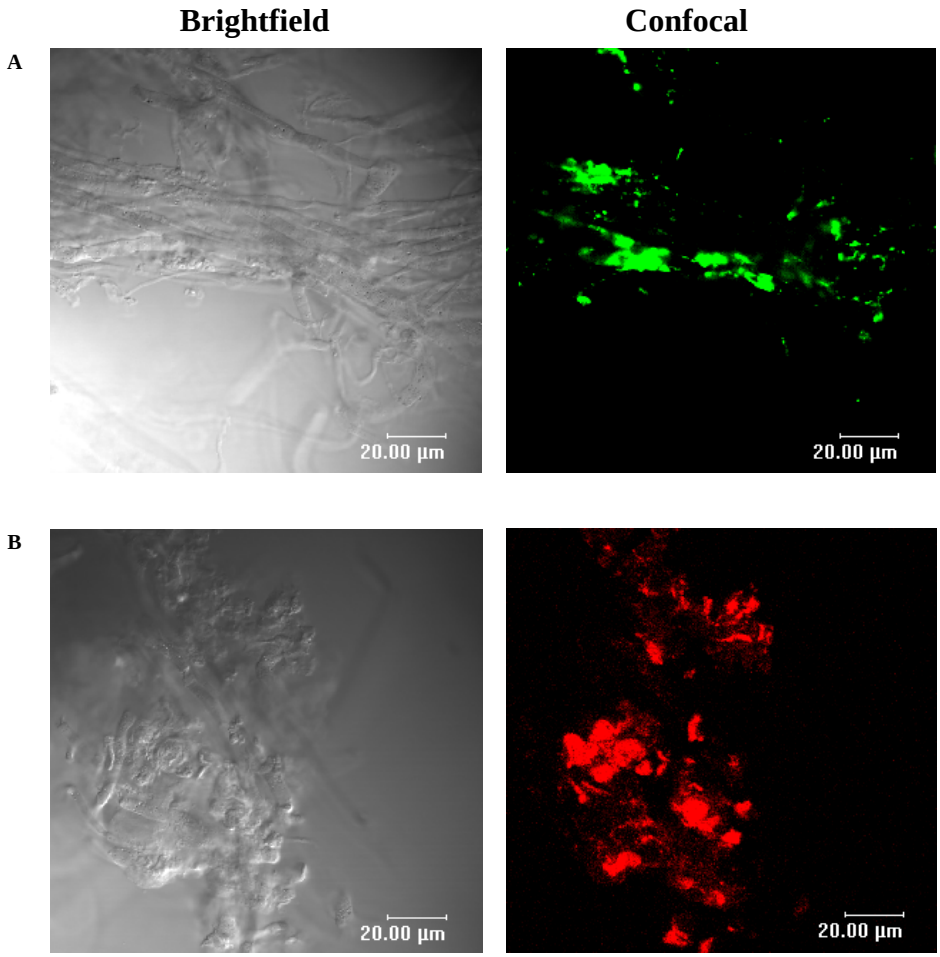

Figure 57: High magnification confocal images of biomimetic scaffold for collagen type I and III staining showing tissue growth along the 20:80 blend PCLDLLA fibres.
20 µm scale bar, A – Collagen type I staining with FITC, B – Collagen type III staining with Texas Red.

One possible issue that was observed within all the gel encapsulating (biomimetic and gel-only) systems was that cellularity decreased over the 4 week culture period. In contrast, the cellularity in the fibre-only scaffolds increased over the same period of time. The decrease in cellularity in the gel systems could be attributed to the static culture conditions that would limit the transport of nutrients to the cells as well as the removal of their waste products through the hydrogel material. However, there was the possibility

that the fibroblasts were switching from a proliferation/matrix production mode to maintenance mode similar to a wound healing response. Greenhalgh *et al*.[181] observed that after tissue was produced in healing ligaments and the remodelling phase was entered, cellular apoptosis resulted in a decrease in cellularity without any tissue degradation. Due to the biomimetic nature of the scaffold, the transplanted primary ligament cells could have been induced into a similar wound healing/tissue remodelling phase.

Another potential issue was that the collagen produced in the gel systems was present in clusters throughout the scaffold. This result indicated that a higher initial cell seeding density was possibly required in order to have connected tissue throughout the entire scaffold. A higher seeding density was also necessary for the system due to the decrease in cell population during the photocrosslinking period. However, due to the large number of scaffolds required and the limited number of primary cells available, cell seeding densities were reserved for this preliminary study.

It has been shown, from the results presented in this section that ligament specific collagen type I and III proteins were produced in sufficient amounts within the biomimetic scaffolds over a 4 week period. Other studies have also reported IHC localized collagen types I and III within their fibrous ligament scaffolds[45,46,61,62]. The most noteworthy of these studies was conducted by Sato *et al*.[46] who examined chitin, PCL, PLA and chitin/PCL braided fibre scaffolds. This study was able to demonstrate that chitin and chitin/PCL scaffolds were more efficient at integrating collagen type I and

III proteins into the center of the scaffold. However, the tissue that was produced did not attach directly to the fibres and was limited to a capsule that surrounded the fibres. Therefore, the fibres in these scaffolds were not acting as tissue growth guides but were potentially repelling the *de novo* tissue growth. Also, the tissue that was stained did not appear organized, which could result in poor mechanical properties of the scaffold once the fibres were fully degraded.

Current methods of ligament tissue engineering have reported collagen type I:III ratios, which are not typically observed in the native ligament (~ 8). For example, Garvin *et al.*[182] and Kim *et al.*[72] observed that cells cultured with mechanical stimulation produced higher levels of collagen type III than type I for both planar and three dimensional cultures. Hankemeier *et al.*[78] and Funakoshi *et al.*[61] found similar amounts of collagen type I and III produced from human BMSCs supplemented with various amounts of FGF-2 (fibroblasts growth factor 2) on HA coated and uncoated chitosan fibres, respectively. Moreau *et al.*[64] observed fairly low collagen type I:III ratios of (2.0 – 3.5):1 for BMSCs grown on silk matrices with various growth factors. Altman *et al.*[65] found higher than average collagen type I:III ratios of 16:1 in mechanically stressed hydrogels, indicating that not enough type III was being produced. Type III collagen levels are also observed to increase in healing ligaments leading to a higher degree of disorganization in the healed ligament[25,183]. The results for these studies were obtained using techniques such as reverse transcriptase polymerase chain reaction to determine whether the specific genes for collagen types I and III were being expressed. However, even though the genes were expressed, that did not necessarily imply that the proteins were secreted from the

cells and accumulating within the scaffold. Therefore, techniques such as IHC allow for a visual understanding of the actual tissue production within the scaffold

In summary, the biomimetic scaffolds were shown to be superior in design to the fibre-only and gel-only control scaffolds. The gel-only results indicate that the M-GC and I2959 photocrosslinking system was an acceptable method for cell delivery. The hydrogels were able to deliver cells evenly throughout the scaffold and were also able to maintain cell viability throughout the 4 week culture period. The hydrogel was also found to be essential in providing a usable scaffold since the fibres required the gel to maintain their structure. The fibres within the biomimetic scaffolds were required for cell and tissue attachment points and appeared to act as tissue growth guides. All scaffolds were shown to produce both collagen types I and III, whose concentrations increased throughout the 4 weeks.

Chapter 6. Conclusions

In order to produce an ideal biomimetic scaffold, the choice of materials and methods of manufacture are a very important aspect of the design. Sound decision making went into the material choices and processing methods for the production of the scaffold. However, after much work in producing electrospun chitosan fibres with sub-cellular dimensions they were found to be unusable in an aqueous environment. Therefore, PCLDLLA copolymers that had a better ability to adjust mechanical and electrospinning properties, were used. The material properties of the PCLDLLA copolymer were easily modified to suit the design needs of the biomimetic scaffold. As a result of the specific physical properties of the 20:80 copolymer, and collecting the electrospun fibres in tension, relaxation forces were generated in the fibres. The force generating property of the 20:80 copolymer resulted in the electrospun fibres having a crimp pattern. The process was found to be accelerated after the aqueous base-etching process and the magnitude of the crimp pattern was controllable through the fibre diameter. Surface modification of the PCLDLLA fibres by base-etching was shown to improve cell and protein adsorption.

Despite the marginal cytotoxic effects of the photo-initiator and UV light source, photocrosslinking to form a hydrogel was better when compared to the PEGD and genipin approaches that were also investigated. The final M-GC and I2959 hydrogel system that was used for cell delivery was an effective method for distributing cells evenly throughout the entire scaffold. Live/Dead™ assay results confirmed that the biomimetic scaffold was able to support the growth of primary ligament cells throughout a four week culture period. IHC results indicated that the primary bovine ligament cells

were able to produce collagen types I and III proteins within the biomimetic scaffold without the use of chemical or physical inputs. Therefore, it was assumed that the biomimetic environment of the scaffold did not allow the cells to de-differentiate into other cell lineages since ligament specific ECM was produced. The overall results indicated that the biomimetic design was an acceptable approach to ligament tissue engineering. Overall, these results demonstrate a wide-ranging potential for the biomimetic scaffold to be used for ligament tissue engineering; if not to make functional ligament tissue, then to better understand the factors affecting the growth of ligament tissue in a biomimetic environment.

Chapter 7. Recommendations and Future Work

A comprehensive understanding of the crimping mechanism to control the crimp pattern would be useful if the design or use of the scaffold is to be modified. Therefore, continued study with different PCLDLLA copolymers is required to obtain a better understanding between the effects the CL:DLLA ratio and the final physical properties (crimp) of the polymer fibres. An in-depth study of the mechanical properties of the fibres during wetting (aqueous) would allow for more insight into the crimping mechanism. Investigation with different monomer components would also be beneficial in controlling and/or modifying the fibre crimp pattern.

Additional work should be done to gain a better understanding of the cell behaviour within the biomimetic scaffold at the earlier times in culture. A longer culture period could be used to study the affects of the biomimetic scaffold on cell growth and tissue production. The degradation properties of the PCLDLLA fibres and M-GC hydrogel within those settings could also be investigated at the same time. An investigation into the fibre content (porosity between the fibres) may be beneficial for improving cell behaviour in the biomimetic scaffolds. Future work should also investigate whether the improved cell adhesion on the base-etched PCLDLLA polymer surfaces was due to changes in surface chemistry, increased surface roughness or a combination of both.

The decrease in cellularity within the gel encapsulating scaffolds could be remedied with the use of a bioreactor to give the cells a more controlled and maintained *in vitro* environment[184]. Other inputs such as mechanical stimulation and chemical growth

factors might also be beneficial. The modification of the gel properties such as crosslinking density and molecular weight of the M-GC may help to improve the conditions necessary for increased cellularity in the hydrogels. An investigation with a higher cell seeding density would also be beneficial to improve upon these initial findings. It may also be possible to produce connected tissue throughout the scaffold with a higher cell seeding density. The decrease in cellularity would be attributed to the cells natural tendency to maintain ligament tissue.

The same factors (growth factors, mechanical stimulation, use of a bioreactor) previously mentioned to potentially control the cellularity could also be used to try and enhance the ligament-specific tissue production and organization within the biomimetic scaffolds. Future work could also include additional IHC markers other than collagens types I and III to further confirm that ligament-like tissue was being produced in the scaffold, such as: tenascin-C, decorin and biglycan.

There are many possible applications for the use of the crimped and surface modified PCLDLLA fibres of sub-cellular dimensions as well as the M-GC hydrogel cell delivery system within the general field of tissue engineering. Research into the requirements from this general field could lead to many more possible uses for either the biomimetic scaffold design or its individual components.

References

[1] Amiel, D., Billings, E., and Akeson, W. Ligament structure, chemistry and physiology. In: Daniel, D., Akeson, W., and O'Connor, J., eds. Knee Ligaments: Structure, Function, Injury and Repair. New York, Raven Press, 1990, pp. 77-90.

[2] Venturoni, M., Gutsmann, T., Fantner, G., Kindt, J., and Hansma, P. Investigations into the polymorphism of rat tail tendon fibrils using atomic force microscopy. Biochemical and Biophysical Research Communications 303, 508, 2003.

[3] Watanabe, T., Hosaka, Y., Yamamoto, E., Ueda, H., Sugawara, K., Takahashi, H., and Takehana, K. Control of the collagen fibril diameter in the equine superficial digital flexor tendon in horses by decorin. Journal of Veterinary Medical Science 67, 855, 2005.

[4] Kastelic, J., and Baer, E. Deformation in tendon collagen. Symposia of the Society for Experimental Biology 34, 397, 1980.

[5] Sellaro, T. Effects of collagen orientation on the medium-term fatigue response of heart valve biomaterials [M.Sc. thesis]. School of Engineering, University of Pittsburgh, Pittsburgh, PA, 2003.

[6] Hirokawa, S., and Tsuruno, R. Three-dimensional deformation and stress distribution in an analytical/computational model of the anterior cruciate ligament. Journal of Biomechanics 33, 1069, 2000.

[7] Vesentini, S., Redaelli, A., and Montevecchi, F. Molecular analysis of interaction energies of the decorin proteoglycan – collagen complex in tendon fibrils. Abstract presented at the Bioengineering Conference, Florida, 2003

[8] Hakkinen, L., Strassburger, S., Kahari, V., Scott, P.G., Eichstetter, I., Iozzo, R.V., and Larjava, H. A role for decorin in the structural organization of periodontal ligament. Laboratory Investigation 80, 1869, 2000.

[9] Campbell, M., Tester, A.M., Handley, C.J., Checkley, G.J., Chow, G.L., Cant, A.E., Winter, A.D., and Cain, W.E. Charactization of a large chondrotin sulphate proteoglycan present in the bovine collateral ligament. Archives of Biochemistry and Biophysics 329, 181, 1996.

[10] Cuppone, M., and seedhom, B. Effect of implant lengthening and mode of fixation on knee laxity after ACL reconstruction with an artificial ligament: A cadaveric study. Journal of Orthopaedic Science 6, 253, 2001.

[11] Yamamoto, E., Hayashi, K., and Yamamoto, N. Effects of stress shielding on the transverse mechanical properties of rabbit patellar tendons. Journal of Biomechanical Engineering 122, 608, 2000.

[12] Yamamoto, E., Hayashi, K., and Yamamoto, N. Mechanical properties of collagen fascicles from stress-shielded patellar tendons in the rabbit. Clinical Biomechanics 14, 418, 1999.

[13] Everts, V., Van Der Zee, E., Creemers, L., and Beertsen, W. Phagocytosis and intracellular digestion of collagen, its role in turnover and remodelling. Histochemical Journal 28, 229, 1996.

[14] Miyasaka, K., Daniel, D., and Hirschman, P. The incidence of knee ligament injuries in the general population. American Journal of Knee Surgery 4, 3, 1991.

[15] Albright, J., Carpenter, J., Graf, B., and Richmond, J. Knee and leg: Soft-tissue trauma. In: Betty, J., eds. Orthopaedic Knowledge Update 6, American Academy of Orthopaedic Surgeons, Rosemont, IL, 1999.

[16] Fritz, S., Paholsky, M., and Grosenbach, J. The Joints. In: Mosby's Basic Science for Soft Tissues and Movement Therapies, St. Louis, Mosby, 1999, pp. 281.

[17] Fetto, J. Knee lesions I. In: Jenkins, D., eds. Ligament Injuries and their Treatment, London, Chapman and Hall, 1985, pp. 113-143.

[18] Guidoin, M.F., Marois, Y., Bejui, J., Poddevin, N., King, M., and Guidoin, R. Analysis of retrieved polymer fibre based replacements for the ACL. Biomaterials 21, 2461, 2000.

[19] Johnson, R., Pope, M., Weisman, G., White, B., and Ettlinger, C. Knee injury in skiing: A multifaceted approach. American Journal of Sports Medicine 7, 321, 1979.

[20] Malek, M., Fanelli, G., and Golden, M. Combined intraarticular and extraarticular anterior cruciate ligament reconstruction. In: Scott, W., eds. Ligament and Extensor Mechanism Injuries of the Knee, St. Louis, Mosby, 1991, pp. 267-300.

[21] Chick, R., and Jackson, D. Tears of the anterior cruciate ligament in young athletes. Journal of Bone and Joint Surgery 60, 970, 1978.

[22] Jacobsen, K. Osteoarthritis following insufficiency of the cruciate ligament in man. Acta Orthopaedica Scandinavica 48, 520, 1977.

[23] McDaniel, W., and Dameron, T. The untreated anterior cruciate ligament rupture. Clinical Orthopaedics 172, 158, 1983.

[24] Carpenter, J., and Hankenson, K. Animal models of tendon and ligament injuries for tissue engineering applications. Biomaterials 25, 1715, 2004.

[25] Woo, S., Jia, F., Zou, L., and Gabriel, M. Functional tissue engineering for ligament healing: Potential of antisense gene therapy. Annals of Biomedical Engineering 32, 342, 2004.

[26] Woo, S., Horibe, S., Ohland, K., and Amiel, D. The response of ligaments to injury: Healing of the collateral ligaments. In: Daniel, D., Akeson, W., and O'Connor, J., eds. Knee Ligaments: Structure, Function, Injury and Repair. New York, Raven Press, 1990, pp. 351-364.

[27] Amiel, D., Abel, M., Kleiner, J., Lieber, R. and Akeson, W. Synovial-fluid nutrient delivery in the diathrial joint – an analysis of rabbit knee ligaments. Journal of Orthopaedic research 4, 90, 1986.

[28] Amiel, D., Kuiper, S., and Akeson, W. Cruciate ligaments: Response to injury. In: Daniel, D., Akeson, W., and O'Connor, J., eds. Knee Ligaments: Structure, Function, Injury and Repair. New York, Raven Press, 1990, pp. 365-376.

[29] Salman, L., Russell, V., Refshauge, K., Kader, D., Connolly, C., Linklater, J., and Pinczewski, L. Long-term outcome of endoscopic anterior cruciate ligament reconstruction with patellar tendon autograft. The American Journal of Sports Medicine 34, 721, 2006.

[30] Denti, M., Lo Vetere, D., Bandi, M., and Volpi, P. Comparative evaluation of knee stability following reconstruction of the anterior cruciate ligament with the bone-patellar tendon-bone and the double semitendinosus-gracilis methods: 1- and 2- year prospective study. Knee Surgery, Sports Tramatology, Arthroscopy 14, 637, 2006.

[31] Marumo, K., Saito, M., Yamagishi, T., and Fuji, K. The "ligamentization" process in human anterior cruciate ligament reconstruction with autogenous patellar and hamstring tendons. The American Journal of Sports Medicine 33, 1166, 2005.

[32] Kartus, J., Stener, S., Lindahl, S., Engstrom, B., Eriksson, B., and Karlsson, J. Factors affecting donor-site morbidity after ACL reconstruction using bone-patellar tendon-bone autografts. Knee Surgery, Sports Traumatology, Arthroscopy 5, 222, 1997.

[33] Kartus, J., Movin, T., and Karlsson, J. Donar site morbidity and anterior knee problems after ACL reconstruction using autografts. Anthroscopy: The Journal of Arthroscopic and Related Surgery 17, 971, 2001.

[34] Breitfuss, H., Frohlich, R., Povacz, P., Resch, H., and Wicker, A. The tendon defect after ACL reconstruction using the mid-third patellar tendon – a problem for the patellofemoral joint? Knee Surgery, Sports Traumatology, Arthroscopy 3, 194, 1996.

[35] Scranton, P., Lanzer, W., Ferguson, M., Kirkman, T., and Pflaster, D. Mechanisms of anterior cruciate ligament neovascularization and ligamentization. Arthroscopy: The Journal of Arthroscopic and Related Surgery 14, 702, 1998.

[36] Falconiero, R., DiStefano, V., and Cook, T. Revascularization and ligamentization of autogenous anterior cruciate ligament grafts in humans. Arthroscopy: The Journal of Arthroscopic and Related Surgery 14, 197, 1998.

[37] Lane, J., Mcfadden, P., Bowden, K., and Amiel, D. The ligamentization process - a 4 year case-study following ACL reconstruction with semitendinosus graft. Arthroscopy 9, 149, 1993.

[38] Elmlinger, B., Nyland, J., and Tillett, E. Knee floxor function 2 years after anterior cruciate ligament reconstruction with semitendinosus-gracilis autografts. Arhroscopy 22, 650, 2006.

[39] Barbour, S., and King, W. Basic science update. The safe and effective use of allograft tissue- an update. American Journal of Sports Medicine 31, 791, 2003.

[40] Berg, E. Tibial bone plug nonunion: A cause of anterior cruciate ligament reconstructive failure. Arhroscopy 8, 380, 1992.

[41] Douglas, J., and Simon, T. Donar cell survival and repopulation after intraarticular transplantation of tendon and ligament allografts. Microscopy Research and Technique 58, 25, 2002.

[42] Harris, L., Indelicato, P., Bloomberg, M., Meister, K., and Wheeler, D. Radiographic and histologic analysis of the tibial tunnel after allograft anterior cruciate ligament reconstruction in goats. The American Journal of Sports Medicine 30, 368, 2002.

[43] Kanazawa, T., Soejima, T., Murakami, H., Inoue, T., Katouda, M., and Nagata, K. An immunohistological study of the integration at the bone-tendon interface after reconstruction of the anterior cruciate ligament in rabbits. The Journal of Bone and Joint Surgery 88, 682, 2006.

[44] Bell, E. Tissue Engineering in Perspective. In: Lanza, R., Langer, R., and Vacanti, J., eds. Principles of Tissue Engineering, San Diego, Academic Press, 2000, pp. xxxv- xxxvi.

[45] Cristino, S., Grassi, F., Toneguzzi, S., Piacentini, A., Grigolo, B., Santi, S., Riccio, M., Tognana, E., Facchini, A., and Lisignoli, G. Analysis of mesenchymal stem cells grown on a three-dimensional HYAFF 11®-based prototype ligament scaffold. Journal of Biomedical Material Research 73, 275, 2005.

[46] Sato, M., Maeda, M., Kurosawa, H., Inoue, Y., and Yamauchi, Y. Reconstruction of rabbit Achilles tendon with three bioabsorable materials: histological and biomechanical studies. Journal of Orthopaedic Science 5, 256, 2000.

[47] Altman, G., Horan, R., Lu, H., Moreau, J., Martin, I., Richmond, J., and Kaplan, D. Silk Matrix for tissue engineering anterior cruciate ligaments. Biomaterials 23, 4131, 2002.

[48] Gentleman, E., Lay, A., Dickerson, D., Nauman, E., Liversay, G., and Dee, K. Mechanical characterization of collagen fibres and scaffolds for tissue engineering. Biomaterials 24, 3805, 2003.

[49] Koob, T., Willis, T., Qiu, Y., and Hernandez, D. Biocompatibility of NDGA-polymerized collagen fibres. II. Attachment, proliferation, and migration of tendon fibroblasts *in vitro*. Journal of Biomedical Material Research 56, 40, 2001.

[50] Chvapil, M., Speer, D., Holubec, H., Chvapil, T., and King, D. Collagen fibres as a temporary scaffold for replacement of ACL in goats. Journal of Biomedical Materials Research 27, 313, 1993.

[51] Bourke, S., Kohn, J., and Dunn, M. Preliminary development of a novel restorable synthetic polymer fibre scaffold for anterior cruciate ligament reconstruction. Tissue Engineering 10, 43, 2004.

[52] Durselen, L., Dauner, M., Hierlemann, H., Planck, H., Ignatius, A., and Claes, L. Control of material stiffness during degradation for constructs made of absorbable polymer fibres. Journal of Biomedical Material Research Part B: Applied Biomaterials 67, 697, 2003.

[53] Cooper, J., Bailey, L., Carter, J., Castiglioni, C., Kofron, M., Ko, F., and Laurencin, C. Evaluation of the anterior cruciate ligament, medial collateral ligament, Achilles tendon and patellar tendon as cell sources for tissue engineered ligament. Biomaterials 27, 2747, 2006.

[54] Ouyang, H., Goh, J., Thambyah, A., Teoh, S., and Lee, E. Knitted poly-lactide-co-glycolide scaffold loaded with bone marrow stromal cells in repair and regeneration of rabbit Achilles tendon. Tissue Engineering 9, 431, 2003.

[55] Eijk, F. Saris, D., Riesle, J., Willems, W., Van Blitterswijk, C., Verbout, A., and Dhert, W. Tissue engineering of ligaments: A comparison of bone marrow stromal cells, anterior cruciate ligament, and skin fibroblasts as cell source. Tissue Engineering 10, 893, 2004.

[56] Cooper, J., Lu, H., Ko, F., Freeman, J., and Laurencin, C. Fibre-based tissue-engineered scaffold for ligament replacement design considerations and *in vitro* evaluation. Biomaterials 26, 1523, 2005.

[57] Sahoo, S., Ouyang, H., Goh, J., Tay, T., and Toh, S. Characterization of a novel polymeric scaffold for potential application in tendon/ligament tissue engineering. Tissue Engineering 12, 91, 2006.

[58] Cao, D., Liu, W., Wei, X., Xu, F., Cui, L., and Cao, Y. *In vitro* tendon engineering with avian tenocytes and polyglycolic acids: A preliminary report. Tissue Engineering 12, 1369, 2006.

[59] Ide, A., Sakane, M., Chen, G., Shimojo, H., Ushida, T., Tateishi, T., Wadano, Y., and Miyanaga, Y. Collagen hybridization with poly(L-lactic acid) braid promotes ligament cell migration. Materials Science and Engineering C 17, 95, 2001.

[60] Lu, H., Cooper, J., Manuel, S., Freeman, J., Attawia, M., Ko, F., and Laurencin, C. Anterior cruciate ligament regeneration using braided biodegradable scaffolds: *in vitro* optimization studies. Biomaterials 26, 4805, 2005.

[61] Funakoshi, T., Majima, T., Iwasaki, N., Yamane, S., Masuko, T., Minami, A., Harada, K., Tamura, H., Tokura, S., and Nishimura, S. Novel chitosan-based hyaluronan hybrid polymer fibres as a scaffold in ligament tissue engineering. Journal of biomedical Material Research 74, 338, 2005.

[62] Miajima, T., Funakosi, T., Iwasaki, N., Yamane, S., Harada, K., Nonaka, S., Minami, A., and Nishimura, S. Alginate and chitosan polyion complex hybride fibres for scaffolds in ligament and tendon engineering. Journal of Orthopaedic Science 10, 302, 2005.

[63] Chen, J., Altman, G., Karageorgiou, V., Horan, R., Collette, A., Volloch, V., Colabro, T., and Kaplan, D. Human bone marrow stromal cells and ligament fibroblast responses on RGD-modified silk fibres. Journal Biomedical Material Research 67, 559, 2003.

[64] Moreau, J., Chen, J., Horan, R., Kaplan, D., and Altman, G. Sequential growth factor application in bone marrow stromal cell ligament engineering. Tissue Engineering 11, 1887, 2005.

[65] Altman, G., Horan, R., Martin, I., Farhadi, J., Stark, P., Volloch, V., Richmond, J., Vunjak-Novakovic, G., and Kaplan, D. Cell differentiation by mechanical stress. The FASEB Journal 16, 270, 2002.

[66] Noth, U., Schupp, K., Heymer, A., Kall, S., Jakob, F., Schutze, N., Baumann, B., Barthel, T., Eulert, J., and Hendrich, C. Anterier cruciate ligament constructs fabricated from human mesenchymal stem cells in a collagen type I hydrogel. Cytotherapy 7, 447, 2005.

[67] Dunn, M., Bellinicampi, L., Tria, A., and Zawadsky, J. Preliminary development of a collagen-PLA composite for ACL reconstruction. Journal of Applied Polymer Science 63, 1423, 1997.

[68] Davis, P., Huang, S., Ambrosio, L., Ronca, D., and Nicolais, L. A biodegradable composite artificial tendon. Journal of Materials Science: Materials in Medicine 3, 359, 1992.

[69] Gentleman, E., Livesay, G., Dee, K., and Nauman, E. Development of ligament-like structural organization and properties in cell-seeded collagen scaffolds *in vitro*. Annals of Biomedical Engineering 34, 726, 2006.

[70] Takashi, T., Matsumoto, H., Fujikawa, K., Saito, S., and Inoue, K. Tensile load and the metabolism of anterior cruciate ligament cells. Clinical Orthopaedics and Related Research 1, 247, 1998.

[71] Lee, C., Shin, H., Cho, I., Kang, Y., Kim, I., Park, K., and Shin, J. Nanofibre alignment and direction of mechanical strain affects the ECM production of human ACL fibroblasts. Biomaterials 26, 1261, 2005.

[72] Kim, S., Akaike, T., Sasagawa, T., Atomi, Y., and Kurosawa, H. Gene expression of type I and type III collagen by mechanical stretch in anterior cruciate ligament cells. Cell Structure and Function 27, 139, 2002.

[73] Ozaki, S., Kaneko, S., Podyma-Inoue, K., Yanagishita, M., and Soma, K. Modulation of extracellular matrix synthesis and alkaline phosphatase activity of periodontal ligament cells by mechanical stress. Journal of Periodontal Research 40, 110, 2005.

[74] Miyaki, S., Ushida, T., Nemoto, K., Shimojo, H., Itabashi, A., Ochiai, N., Miyanaga, Y., and Tateishi, T. Mechanical stretch in anterior cruciate ligament derived cells regulates type I collagen and decorin expression through extracellular signal-regulated kinase ½ pathway. Materials Science and Engineering C 17, 91, 2001.

[75] Calve, S., Dennis, R., Kosnik, P., Barr, K., Grosh, K., and Arruda, E. Engineering of functional tendon. Tissue Engineering 10, 755, 2004.

[76] Goh, J., Ouyang, H., Teoh, S., Chan, C., and Lee, E. Tissue-engineering approach to the repair and regeneration of tendons and ligaments. Tissue Engineering 9, 31, 2003.

[77] Murray, M., Bennett, R., Zhang, X., and Spector, M. Cell outgrowth from the human ACL *in vitro*: Regional variation and response of TGF-β1. Journal of Orthopaedic Research 20, 875, 2002.

[78] Hankemeier, S., Keus, M., Zeichen, J., Jagodzinski, M., Barkausen, T., Bosch, U., Krettek, C., and Griensven, M. Modulation of proliferation and differentiation of human bone marrow stromal cells by fibroblast growth factor 2: Potential implication for tissue engineering of tendons and ligaments. Tissue Engineering 11, 41, 2005.

[79] Hildebrand, K., Deie, M., Allen, C., Smith, D., Georgescu, H., Evans, C., Robbins, P., and Woo, S. Early expression of marker genes in the rabbit medial collateral and anterior cruciate ligament: The use of different viral vectors and the effects of injury. Journal of Orthopaedic Research 17, 37, 1999.

[80] Pascher, A., Steinert, A., Palmer, G., Betz, O., Gouze, J., Gouze, E., Pilapil, C., Ghivizzani, S., Evans, C., and Murray, M. Enhanced repair of the anterior cruciate ligament by in situ gene transfer: Evaluation in an *in vitro* model. Molecular Therapy 10, 327, 2004.

[81] Nakamura, N., Hart, D., Boorman, R., Kaneda, Y., Shrive, N., Marchuk, L., Shino, K., Ochi, T., and Frank, C. Decorin antisense gene therapy improves functional healing of early rabbit ligament scar with enhanced collagen fibillogenesis *in vivo*. Journal of Orthopaedic Research 18, 517, 2000.

[82] Nakamura, N., Shino, K., Natsuume, T., Horibe, S., Matsumoto, N., Kaneda, Y., and Ochi, T. Early biological effects of *in vivo* gene transfer of platelet-derived growth factor (PDGF)-B into healing patellar ligament. Gene Therapy 5, 1165, 1998.

[83] Woo, S., Abramowitch, S., Kilger, R., and Liang, R. Biomechanics of knee ligament: Injury, healing, and repair. Journal of Biomechanics 39, 1, 2006.

[84] Deuel, T., and Zhang, N. Growth Factors. In: Lanza, R., Langer, R., and Vacanti, J., eds. Principles of Tissue Engineering, San Diego, Academic Press, 2000, pp. 129-141.

[85] Fradkin, L., Ropp, J., and Warner, J. Gene-based therapeutics. In: Lanza, R., Langer, R., and Vacanti, J., eds. Principles of Tissue Engineering, San Diego, Academic Press, 2000, pp. 385-405.

[86] Shin, H., Jo, S., and Mikos, A. Biomimetic materials for tissue engineering. Biomaterials 24, 4353, 2003.

[87] Palsson, B., and Bhatia, S. Tailoring Biomaterials. In: Tissue Engineering, New Jersey, Prentice Hall, 2003, pp. 270-287.

[88] Formhals, A. Process and apparatus for preparing artificial threads. United States Patent Office, No. 1975504, 1934.

[89] Theron, A., Zussman, E., and Yarin, A. Electrostatic field-assisted alignment of electrospun nanofibres. Nanotechnology 12, 384, 2001.

[90] Taylor, G. Disintegration of water drops in an electric field. Proceeding of the Royal Society of London. Series A, Mathematical and Physical Sciences 280, 383, 1964.

[91] Baumgarten, P. Electrostatic spinning of acrylic microfibres. Journal of Colloid and Interface Science 36, 71, 1971.

[92] McKee, M., Hunley, M., Layman, J., and Long, T. Solution rheological behavior and electrospinning of cationic polyelectrolytes. Macromolecules 39, 575, 2006.

[93] Um, I., Fang, D., Hsiao, B., Okamoto, A., and Chu, B. Electro-spinning and electro-blowing of hyaluronic acid. Biomacromolecules 5, 1428, 2004.

[94] Li, M., Mondrinos, M., Gandhi, M., Ko, F., Weiss, A., and Lelkes, P. Electrospun protein fibres as matrics for tissue engineering. Biomaterials 26, 5999, 2005.

[95] Boland, E., Wnek, G., Simpson, D., Pawlowski, K., and Bowlin, G. Tailoring tissue engineering scaffolds using electrosptatic processing techniques: A study of poly(glycolic acid) electrospinning. Journal of Macromolecular Science, Part A: Pure Applied Chemistry 38, 1231, 2001.

[96] Deitzel, J., Kleinmeyer, J., Harris, D., and Beck Tan, N. The effects of processing variables on the morphology of electrospun nanofibres and textiles. Polymer 42, 261, 2001.

[97] Huang, Z., Zhang, Y., Ramakrishna, S., and Lim, C. Electrospinning and mechanical characterization of gelatine nanofibres. Polymer 45, 5361, 2004.

[98] Son, W., Youk, J., Lee, T., and Park, W. The effects of solution properties and polyelectrolyte on electrospinning of ultrafine poly(ethylene oxide) fibres. Polymer 45,2959, 2004.

[99] Zong, X., Kim, K., Fang, D., Ran, S., Hsaio, B., and Chu, B. Structure and process relationship of electrospun bioabsorbable nanofibre membranes. Polymer 43, 4403, 2002.

[100] Liu, H. and Hsieh, Y. Ultrafine fibrous cellulose membranes from electrospinning of cellulose acetate. Journal of Polymer Science, Part B: Polymer Physics 40, 2119, 2002.

[101] Geng, X., Kwon, O., and Jang, J. Electrospinning of chitosan dissolved in concentrated acetic acid solution. Biomaterials 26, 5427, 2005.

[102] Ohkawa, K., Cha, D., Kim, H., Nishida, A., and Yamamoto, H. Electrospinning of Chitosan. Macromolecular Rapid Communications 25, 1600, 2004.

[103] Bhattarai, S., Bhattarai, N., Yi, H., Hwang, P., Cha, D., and Kim, H. Novel biodegradable electrospun membrane: Scaffold for tissue engineering. Biomaterials 25, 2595, 2004.

[104] Bhattarai, N., Edmondson, D., Veiseh, O., Matsen, F., and Zhang, M. Electrospinning chitosan-based nanofibres and their cellular compatibility. Biomaterials 26, 6176, 2005.

[105] Li, W., Laurencin, C., Caterson, E., Tuan, R., and Ko, F. Elecrospun nanofibrous structure: A novel scaffold for tissue engineering. Journal of Biomedical Materials Research 60, 613, 2002.

[106] Li, W., Danielson, K., Alexander, P., and Tuan, R. Biological response of chondrocytes cultured in three dimensional nanofibrous poly(ε-caprolactone) scaffolds. Journal of Biomedical Materials Research, Part A 67, 1105, 2003.

[107] Badami, A., Kreke, M., Shane Thompson, M., Riffle, J., and Goldstein, A. Effect of fibre diameter on spreading, proliferation and differentiation of osteoblastic cells on electrospun poly(lactic acid) substrates. Biomaterials 27, 596, 2006.

[108] Xu, C., Inai, R., Kotaki, M., and Ramakrishna, S. Aligned biodegradable nanofibrous structure: A potential scaffold for blood vessel engineering. Biomaterials 25, 877, 2004.

[109] Knaul, J., Hudson, S., and Creber, K. Crosslinking of chitosan fibres with dialdehydes: Proposal of a new reaction mechanism. Journal of Polymer Science, Part B: Polymer Physics 37, 1079, 1999.

[110] Muzzarelli, R., Baldassarre, V., Conti, F., Ferrara, P., and Biagini, G. Biological activity of chitosan: Ultrastructural study. Biomaterials 9, 247, 1988.

[111] Prudden, J., Migel, P., Hanson, P., Friedrich, L., and Balassa, L. The discovery of a potent pure chemical wound-healing accelerator. The American Journal of Surgery 119, 560, 1970.

[112] Prasitsilp, M., Jenwithisuk, R., Kongsuwan, K., Damrongchai, N., and Watts, P. Cellular responses to chitosan *in vitro*: The importance of deacetylation. Journal of Materials Science: Materials in Medicine 11, 773, 2000.

[113] Howling, G., Dettmar, P., Goddard, P., Hampson, F., Dornish, M., and Wood, E. The effect of chitin and chitosan on the proliferation of human skin fibroblasts and karinocytes *in vitro*. Biomaterials 22, 2959, 2001.

[114] Varum, K., Myhr, M., Hjerde, R., and Smidsrod, O. *In vitro* degradation rates of partially N-acetylated chitosans in human serum. Carbohydrate Research 299, 99, 1997.

[115] Tomihata, K., and Ikada, Y. *In vitro* and *in vivo* degradation of films of chitin and its deacetylated derivatives. Biomaterials 18, 567, 1997.

[116] Ren, D., Yi, H., Zhang, H., Xie, W., Wang, W., and Ma, X. A preliminary study of fabrication of nanoscale fibrous chitosan membranes in situ by biospecific degradation. Journal of Membrane Science 280, 99, 2006.

[117] An, Y., Woolf, S., and Friedman, R. Pre-clinical *in vivo* evaluation of orthopaedic bioabsorbable devices. Biomaterials 21, 2635, 2001.

[118] Griffith, L. Polymeric Biomaterials. Acta Materialia 48, 263, 2000.

[119] Yang, S., Leong, K., Du, Z., and Chua, C. The design of scaffolds for use in tissue engineering. Part I: Traditional factors. Tissue Engineering 7, 679, 2001.

[120] Kim, K., Yu, M., Zong, X., Chiu, J., Fang, D., Seo, Y., Hsiao, B., Chu, B., and Hadjiargyrou, M. Control of degradation rate and hydrophilicity in electrospun non-woven poly(D,L-lactide) nanofibre scaffold for biomedical applications. Biomaterials 24, 4977, 2003.

[121] Talyor, M., Daniels, A., Andriano, K., and Heller, J. Six bioabsorable polymers: *in vitro* acute toxicity of accumulated degradation products. Journal of Applied Biomaterials 5, 151, 1994.

[122] Ouyang, H., Goh, J., Mo, X., Teoh, S., and Lee, E. Characterization of anterior cruciate ligament cells and bone marrow stromal cells on various biodegradable polymeric films. Biomaterials 20, 63, 2002.

[123] Ikada, Y. Surface modification of polymers for medical applications. Biomaterials 15, 725, 1994.

[124] Yang, J., Wan, Y., Tu, C., Cai, Q., Bei, J., and Wang, S. Enhancing the cell affinity of macroporous poly(L-lactide) cell scaffold by a convenient surface modification method. Polymer International 52, 1892, 2003.

[125] Khang, G., Choee, J., Rhee, J., and Lee, H. Interaction of different types of cells on physicochemically treated poly(L-lactide-co-glycolide) surfaces. Journal of Applied Polymer Science 85, 1253, 2002.

[126] Perego, G., Preda, P., Pasquinelli, G., Curti, T., Freyrie, A., and Cenni, E. Functionalization of poly-L-lactic-co-e-caprolactone: Effects of surface modification on endothelial cell proliferation and hemocompatibility. Journal of Biomaterial Science, Polymer Edition 14, 1057, 2003.

[127] Gao, J., Niklason, L., and Langer, R. Surface hydrolysis of poly(glycolic acid) meshes increases the seeding density of vascular smooth muscle cells. Journal of Biomedical Materials Research 42, 417, 1998.

[128] Drury, J., and Mooney D. Hydrogels for tissue engineering: Scaffold design variables and applications. Biomaterials 24, 4337, 2003.

[129] Bryant, S., and Anseth, K. Hydrogel properties influence ECM production by chondrocytes photoencapsulated in poly(ethylene glycol) hydrogels. Journal of Biomedical Materials Reseach 59, 63, 2002.

[130] Burdick, J., and Anseth, K. Photoencapsulation of osteoblasts in injectable RGD-modified PEG hydrogels for bone tissue engineering. Biomaterials 23, 4315, 2002.

[131] Alhadlaq, A., Tang, M., and Mao, J. Engineered adipose tissue from human mesenchymal stem cells maintain predefined shape and dimension: Implications in soft tissue augmentation and reconstruction. Tissue Engineering 11, 556, 2005.

[132] Metters, A., and Hubbell, J. Network formation and degradation behavior of hydrogels formed by Michael-Type addition reactions. Biomacromolecules 6, 290, 2005.

[133] Bryant, S., and Anseth, K. The effects of scaffold thickness on tissue engineered cartilage in photochrosslinked poly(ethylene oxide) hydrogels. Biomaterials 22, 619, 2001.

[134] Desai, N., and Hubbell, J. Solution technique to incorporate polyethylene oxide and other water-soluble polymers into surfaces of polymeric biomaterials. Biomaterials 12, 144, 1991.

[135] Patel, P., Gobin, A., West, J., and Patrick, C. Poly(ethylene glycol) hydrogel system supports preadipocyte viability, adhesion and proliferation. Tissue Engineering 11, 1498, 2005.

[136] Shin, H., Temenoff, J., and Mikos, A. *In vitro* cytotoxicity of unsaturated oligo[poly(ethylene glycol) fumarate] macromers and their cross-linked hydrogels. Biomaterials 4, 552, 2003.

[137] Augst, A., Kong, H., and Mooney, D. Alginate hydrogels as biomaterials. Macromolecular Bioscience 6, 623, 2006.

[138] Rowley, J., Madlambayan, G., and Mooney, D. Alginate hydrogels as synthetic extracellular matrix materials. Biomaterials 20, 45, 1999.

[139] Rosa, M., Carteni, M., Petillo, O., Calarco, A., Margarucci, S., Rosso, F., Rosa, A., Farina, E., Grippo, P., and Peluso, G. Cationic polyelectrolyte hydrogel fosters fibroblast spreading, proliferation and extracellular matrix production: Implications for tissue engineering. Journal of Cellular Physiology 198, 133, 2004.

[140] Arimura, H., Ouchi, T., Kishida, A., and Ohya, Y. Preparation of a hyaluronic acid hydrogel through polyion complex formation using cationic polylactide-based microspheres as a biodegradable crosslinking agaent. Journal of Biomaterial Science: Polymer Edition 16, 1347, 2005.

[141] Chenite, A., Chaput, C., Wang, D., Combes, C., Buschmann, M., Hoemann, C., Leroux, J., Atkinson, B., Binette, F., and Selmani, A. Novel injectable neutral solutions of chitosan form biodegradable gels in situ. Biomaterials 21, 2155, 2000.

[142] Mwale, F., Iordanova, M., Demers, C., Steffen, T., Roughley, P., and Antoniou, J. Biological evaluation of chitosan salts cross-linked to genipin as a cell scaffold for disk tissue engineering. Tissue Engineering 11, 130, 2005.

[143] Roughley, P., Hoemann, C., DesRosiers, E., Mwale, F., Antoniou, J., and Alini, M. The potential of chitosan-based gels containing intervertebral disc cells for nucleus pulposus supplementation. Biomaterials 27, 388, 2005.

[144] Zielinski, B., and Aebischer, P. Chitosan as a matrix for mammalian cell encapsulation. Biomaterials 15, 1049, 1994.

[145] Berger, J., Reist, M., Felt, O., Peppas, N., and Gurny, R. Structure and interactions in covalently and ionically crosslinked chitosan hydrogels for biomedical applications. European, Journal of Pharmaceutics and Biopharmaceutics 57, 19, 2004.

[146] Mi, F., Tan, Y., Liang, H., and Sung, H. *In vivo* biocompatibility and degradation of a novel injectable-chitosan-based implant. Biomaterials 23, 181, 2002.

[147] Mi, F., Shyu, S., and Peng, C. Characterization of ring-opening polymerization of genipin and pH-dependent cross-linking reactions between chitosan and genipin. Journal of Polymer Science A: Polymer Chemistry 43, 1985, 2005.

[148] Bryant, S., Durand, K., and Anseth, K. Manipulations in hydrogel chemistry control photoencapsulated chondrocyte behavior and their extracellular matrix production. Journal of Biomedical Materials Research, Part A 67, 1430, 2003.

[149] Bryant, S., Nuttelman, C., and Anseth, K. Cytocompatibility of UV and visable light photoinitating systems on cultured NIH/3T3 fibroblasts *in vitro*. Journal of Biomaterial Science, Polymer Edition 11, 439, 2000.

[150] Nguyen, K., and West, J. Photopolymerizable hydrogels for tissue engineering applications. Biomaterials 23, 4307, 2002.

[151] Wang, D., Christopher, W., Li, Q., Sharman, B., and Elisseeff, J. Synthesis and characterization of a novel degradable phosphate-containing hydrogel. Biomaterials 24, 3969, 2003.

[152] Williams, C., Malik, A., Kim, T., Manson, P., and Elisseeff, J. Variable cytocompatibility of six cell lines with photoinitiators used for polymerizing hydrogels and cell encapsulation. Biomaterials 26, 1211, 2005.

[153] Knight, D. A chitosan-based hydrogel for the prevention of postsurgical adhesions [M.Sc.]. Department of Chemical Engineering, Queen's University, Kingston, ON, 2004.

[154] Nerem, R. The challenge of imitating nature. In: Lanza, R., Langer, R., and Vacanti, J., eds. Principles of Tissue Engineering, San Diego, Academic Press, 2000, pp. 9-15.

[155] Zimmermann, T., Kunisch, E., Pfeiffer, R., Hirth, A., Stahl, H., Sack, U., Laube, A., Liesaus, E., Roth, A., Palombo-Kinne, E., Emmrich, F., and Kinne, R. Isolation and characterization of rheumatoid arthritis synovial fibroblasts from primary culture – primary culture cells markedly differ from fourth-passage cells. Arthritis Research 3, 72, 2001.

[156] Lopez-Leon, T., Carvalho, E., Seijo, B., Ortega-Vinuesa, J., and Bastos-Gonzalex, D. Physiochemical characterization of chitosan nanoparticles electrokinetic and stability behavior. Journal of Colloid and Interface Science 283, 344, 2005.

[157] Turner, N. Surface modification of a biodegradable elastomer through the attachment of a hydrogel [M.Sc.]. Department of Chemical Engineering, Queen's Unversity, Kingston, ON, 2004.

[158] Shuster, M., and Narkis, M. Polymeric antiplasticization of polycarbonate with polycaprolactone. Polymer Engineering and Science 34, 1613, 1994.

[159] Fischer, E., Sterzel, H., and Wegner, G. Investigation of the structure of solution grown crystals of lactide copolymers by means of chemical reactions. Colloid and Polymer Science 251, 980, 1973.

[160] Geesin, J., Darr, D., Kaufman, R., Murad, S., and Pinnell, S. Ascorbic acid specifically increases type I and type III procollagen messenger RNA levels in human skin fibroblasts. Journal of Investigative Dermatology 90, 420, 1988.

[161] Bates, C., Prynne, C., and Levene, C. The synthesis of underhydroxylated collagen by 3T6 mouse fibroblasts in culture. Biochimica et Biophysica Acta 263, 397, 1972.

[162] Pinnel, S., Murad, S., and Darr, D. Induction of collagen synthesis by ascorbic acid. A possible mechanism. Archives of Dermatology 123, 1684, 1987.

[163] Knaul, J., Hooper, M., Chanyi, C., and Creber, K. Improvements in the drying process for wet-spun chitosan fibres. Journal of Applied Polymer Science 69, 1435, 1998.

[164] Agboh, O., and Qin, Y. Chitin and chitosan fibres. Polymers for Advanced Technologies 8, 355, 1997.

[165] Subramanian, A., Vu, D., Larsen, G., and Lin, H. Preparation and evaluation of the electrospun chitosan/PEO fibres for potential applications in cartilage tissue engineering. Journal of Biomaterial Science: Polymer Edition 16, 861, 2005.

[166] Duan, B., Dong, C., Yuan, X., and Yao, K. Electrospinning of chitosan solutions in acetic acid with poly(ethylene oxide). Journal of Biomaterial Science, Polymer Edition 15, 797, 2004.

[167] Desbrires, J. Viscosity of semiflexible chitosan solutions: Influence of concentration, temperature and role of intermolecular interactions. Biomacromolecules 3, 342, 2002.

[168] Min, B., Lee, S., Lim, J., You, Y., Lee, T., Kang, P., and Park, W. Chitin and chitosan nanofibres: Electrospinning of chitin and deacetylation of chitin nanofibres. Polymer 45, 7137, 2004.

[169] Boutonnet, J., Bingham, P., Calamari, D., Rooij, C., Franklin, J., Kawano, T., Libre, J., McCuloch, A., Malinverno, G., Odom, J., Rusch, G., Smythe, K., Sobolev, I., Thompson, R., and Tiedje, J. Environmental risk assessment of trifluoroacetic acid. Human and Ecological Risk Assessment 5, 59, 1999.

[170] Agnihotri, S., Kulkarni, V., Kulkarni, A., and Aminabhavi, T. Degradation of chitosan and chemically modified chitosan by viscosity measurements. Journal of Applied Polymer Science 102, 3255, 2006.

[171] Cabrera, J., and Cutsem, P. Preparation of chitooligosaccharides with degree of polymerization higher then 6 by acid or enzymatic degradation of chitosan. Biochemical Engineering Journal 25, 165, 2005.

[172] Knight, D., Shapka, S., and Amsden, B. Characterization of glycol chitosan: A potential material for use in biomedical and pharmaceutical applications. Polysaccharides for Drug Delivery and Pharmaceutical Applications ACS Symposium Series 934, 227, 2006.

[173] Rwei, S., Lin, Y., and Su, Y. Study of self-crimp polyester fibres. Polymer Engineering and Science 45, 838, 2005.

[174] Croll, T., O'Connor, A., Stevens, G., and Cooper, J. Controllable surface modification of poly(lactic-co-glycolic acid) (PLGA) by hydrolysis or aminolysis: Physical, chemical, and theoretical aspects. Biomacromolecules 5, 463, 2004.

[175] Tsuji, H., and Ishida, T. Poly(L-lactide). X. Enchanced surface hydrophilicity and chain-scission mechanisms of poly(L-lactide) film in enzymatic, alkaline, and phosphate-buffered solutions. Journal of Applied Polymer Science 87, 1628, 2002.

[176] Ishaug-Riley, S., Okun, L., Prado, G., Applegate, M., and Ratcliffe, A. Human articular chondrocyte adhesion and proliferation on synthetic biodegradable polymer films. Biomaterials 20, 2245, 1999.

[177] Miller, J., Veeramasuneni, S, Drelich, J., and Yalamanchili, M. Effect of roughness as determined by atomic force microscopy on the wetting properties of PTFE thin films. Polymer Engineering and Science 36, 1849, 1996.

[178] Mi, F. Characterization of ring-opening polymerization of genipin and pH-dependent cross-linking reactions between chitosan and genipin. Journal of Polymer Science Part A: Polymer Chemistry 43, 1985, 2005.

[179] Bialik, S., Cryns, V., Drincic, A., Miyata, S., Wollowick, A., Srinivasan, A., and Kitsis, R. The mitochondrial apoptotic pathway is activated by serum and glucose deprivation in cardiac myocytes. Circulation Research 85, 403, 1999.

[180] Izuishi, K., Kata, K., Ogura, T., Kinoshita, T., and Esumi, H. Remarkable tolerance of tumor cells to nutrient deprivation: Possible new biochemical target for cancer therapy. Cancer Research 60, 6201, 2000.

[181] Greenhalgh, D. The role of apoptosis in wound healing. International Journal of Biochemical Cell Biology 30, 1019, 1998.

[182] Garvin, J., Qi, J., Maloney, M., and Banes, A. Novel system for engineering bioartificial tendons and application to mechanical load. Tissue Engineering 9, 967, 2003.

[183] Laurencin, C., and Freeman, J. Ligament tissue engineering: An evolutionary materials science approach. Biomaterials 26, 7530, 2005.

[184] Altman, G., Lu, H., Horan, R., Calabro, T., Ryder, D., and Kaplan, D. Advanced bioreactor with controlled application of multi-dimensional strain for tissue engineering. Transactions of the ASME 124, 742, 2002.